The emission and scattering of L-band microwave radiation from rough ocean surfaces and wind speed measurements from the Aquarius sensor

Thomas Meissner, Frank J. Wentz and Lucrezia Ricciardulli

Remote Sensing Systems, Santa Rosa, California, USA.

Corresponding author: Thomas Meissner, Remote Sensing Systems, 444 Tenth Street, Suite 200, Santa Rosa, CA 95401, USA. (meissner@remss.com).

Key Points

- Geophysical model functions for L-band surface emission and radar backscatter
- Wind speed measurements with L-band sensors
- Surface roughness correction for ocean salinity retrievals

Abstract

In order to achieve the required accuracy in sea surface salinity (SSS) measurements from L-band radiometers such as the Aquarius/SAC-D or SMOS (Soil Moisture and Ocean Salinity) mission, it is crucial to accurately correct the radiation that is emitted from the ocean surface for roughness effects. We derive a geophysical model function (GMF) for the emission and backscatter of L-band microwave radiation from rough ocean surfaces. The analysis is based on radiometer brightness temperature and scatterometer backscatter observations both taken on board Aquarius. The data are temporally and spatially collocated with wind speeds from WindSat and F17 SSMIS (Special Sensor Microwave Imager Sounder) and wind directions from NCEP (National Center for Environmental Prediction) GDAS (Global Data Assimilation System). This GMF is the basis for retrieval of ocean surface wind speed combining L-band H-pol radiometer and HH-pol scatterometer observations. The accuracy of theses combined passive/active L-band wind speeds matches those of many other satellite microwave sensors. The L-band GMF together with the combined passive/active L-band wind speeds are utilized in the Aquarius SSS retrieval algorithm for the surface roughness correction. We demonstrate that using these L-band wind speeds instead of NCEP wind speeds leads to a significant improvement in the SSS accuracy. Further improvements in the roughness correction algorithm can be obtained by adding VV-pol scatterometer measurements and wave height (WH) data into the GMF.

Index Terms

- OCEANOGRAPHY GENERAL: Ocean observing systems
- OCEANOGRAPHY GENERAL: Remote sensing and electromagnetic processes
- RADIO SCIENCE: Remote sensing
- ELECTROMAGNETICS: Random media and rough surfaces

1 Introduction

The goal of the Aquarius mission is to provide the science community with monthly SSS maps at 150 km spatial scale to an accuracy of 0.2 psu [*Lagerloef et al.*, 2008]. The basis of the Aquarius SSS retrieval algorithm [*Wentz et al.*, 2012] is to match the observed surface emissivity of a flat ocean surface with the Fresnel emissivity, which is calculated from a model of the permittivity of sea water [*Meissner and Wentz*, 2004, 2012]. The sea water permittivity itself depends on SSS and this dependence is such that on a global scale the uncertainty in the surface brightness temperature (in Kelvin) translates into an SSS uncertainty (in psu) roughly as 1:2. That means that the 0.2 psu SSS accuracy requirement corresponds to a radiometric accuracy of about 0.1 K, which poses a very challenging task for the SSS retrieval algorithm.

One of the major drivers in the error budget of the SSS retrieval is the change of the ocean surface emission due to surface roughness. This roughness signal has to be removed from the Aquarius observation in order to obtain the emissivity of a specular ocean surface. The roughening is mainly caused by surface winds that result in large gravity waves, small capillary waves and, at higher wind speeds, foam coverage of the ocean surface.

The functional dependence of emissivity on wind speed is called geophysical model function (GMF). Numerous empirical studies using various instruments and observation techniques have been performed to derive the GMF of this wind-induced surface emissivity signal, which is also known as excess emissivity. The first measurement of the L-band emissivity as function of wind speed was performed by *Hollinger* [1971], who used a microwave radiometer that was mounted on a fixed ocean platform. Subsequent studies and experiments include a 2-scale scattering model [*Dinnat et al.*, 2003], the Wind and Salinity Experiment (WISE), which was part of the pre-launch campaign for SMOS [*Camps et al.*, 2004; *Etcheto et al.*, 2004] and the airborne Passive-Active L-band Sensor (PALS), which was part of the Aquarius pre-launch efforts [*Yueh et al.*, 2010]. More recently, the L-band emissivity was analyzed using brightness temperature observations from the SMOS sensor [*Guimbard et al.*, 2012; *Yin et al.*, 2012] and for the Aquarius instrument using the Combined Active – Passive (CAP) approach [*Yueh et al*., 2013; *Fore et al.*, 2014]. Our study should be regarded as complementary to those earlier analyses. All of our results are based on actual Aquarius observations. Several components of our L-band emissivity

model functions based on preliminary data analyses have been presented in [*Meissner et al.*, 2012a, 2012b].

Most studies agree that an uncertainty in surface wind speed of 1 m/s translates at the Aquarius Earth incidence angles into an uncertainty in the surface brightness temperature of roughly 1/3 K for both vertical and horizontal polarizations. This, in turn, would correspond to an error in the retrieved Aquarius SSS of roughly 2/3 psu for average surface temperatures. This poses a very stringent requirement not only for the accuracy of the wind speed that is used in calculating the roughness signal, but it also requires an accurate knowledge of the GMF itself.

In order to aid the performance of the removal of the surface roughness emissivity signal, it was decided to combine the Aquarius radiometer with an L-band scatterometer that takes observations at 1.26 GHz simultaneously with the passive instrument [*Yueh et al.*, 2012]. The idea is that the active radar observations can provide a characterization of the rough ocean surface at L-band, which is sufficiently accurate to be used in removing the roughness signal from the passive emissivity signal [*Isoguchi et al.*, 2009; *Yueh et al.*, 2010]. As we will show, the L-band scatterometer observations does not only serve as an accurate proxy for the ocean surface wind speed at the instance and location of the radiometer observation but can also give information on surface roughness that goes beyond wind speed.

The goal of our study is twofold: First we want to develop an active and passive L-band GMF, which allow an accurate measurement of the ocean surface wind speed. This wind speed will then serve as crucial input for removing the roughness effect in the passive emissivity signal. We will show that in order to do that it is not only essential to have simultaneous active and passive observations but it is also necessary to combine the various channels of the radiometer and scatterometer in an optimal way during the multiple stages of the roughness correction algorithm. We will demonstrate that the wind speed product that we derive for our roughness correction is of excellent quality itself, its accuracy being comparable to wind speeds from validated space-borne microwave sensor, such as WindSat or SSMIS.

Our analysis is based on a global match-up set of Aquarius brightness temperature (TB) and backscatter (σ_0) measurements that are collocated with wind speed measurements from WindSat and F17 SSMIS.

The GMF for the wind induced surface emissivity and the form of the surface roughness correction is used in the salinity retrieval algorithm of the Aquarius Version 3.0 data, which has been released by the Aquarius Data Processing System (ADPS) on June 9, 2014, (http://aquarius.nasa.gov/).

Our paper is organized as follow: Section 2 describes the features of the matchup data consisting of Aquarius TB and σ_0 observations and WindSat and F17 SSMIS wind speeds and discusses the quality checks that were used to obtain it. We also list and briefly describe the major ancillary fields that we need in our analysis. In section 3 we derive the GMF for the radar backscatter σ_0 and in section 4 we develop the GMF of the wind induced ocean surface emissivity for the Aquarius channels. Both GMF are functions of surface wind speed and surface wind direction. Section 5 discusses the retrieval and validation of the L-band wind speeds including high wind speeds in tropical and extratropical cyclones. In section 6 we develop the full surface roughness correction model, which is based on this L-band wind speed. We also give an estimate of the accuracy of this roughness correction. In section 7 we compare our model function and wind speed retrievals with the results of other approaches, in particular the SMOS GMF and the GMF and wind speeds of the CAP algorithm. A summary and conclusions are presented in section 8.

2 Data Sets and Analysis Method

2.1 Aquarius Radiometer and Scatterometer Observations

Our analysis and derivation of the GMF are based on the Aquarius Level 2 (L2) product. It consists of radiometer antenna temperatures (T_A) and radar backscatter measurements σ_0 at the top of the atmosphere (TOA) that are both sampled into 1.44 sec time intervals. The Aquarius instrument has three separate feedhorns, each of which taking Earth observations at fixed off-nadir and azimuthal looks. This is known as pushbroom design [*Lagerloef et al.*, 2008]. The nominal Earth incidence angles (EIA) of these three horns are 29.36° (horn 1), 38.44° (horn 2) and 46.29° (horn 3). These values are slightly different from the pre-launch values [*Dinnat and LeVine*, 2007] because of pointing adjustments that were made post-launch. The 3dB footprint averages of along and cross track directions are 84 km (horn 1), 102 km (horn 2) and 126 km (horn 3). The Aquarius radiometer measure vertical (V-pol) and horizontal (H-pol) polarization as well as

the 3rd Stokes parameter (U). The Aquarius scatterometer measures the backscatter σ_0 for co-pol (VV and HH) and cross-pol (VH and HV) channels.

In order to obtain the brightness temperature $T_{B\,surf}$ and radar backscatter σ_0 at the Earth's surface many spurious signals have to be removed. This is part of the L2 processing algorithms for the radiometer [*LeVine et al.*, 2011; *Wentz et al.*, 2012] and the scatterometer [*Yueh et al.*, 2012]. The most important of these signals are:

1. Radio frequency interference (RFI) [*Misra and Ruf*, 2008].
2. Cross polarization contamination in the antenna.
3. Intruding radiation from cold space (spillover).
4. Intruding radiation from celestial sources (galaxy, moon, sun), which can enter the antenna directly from the backlobes or through reflection at the Earth's surface
5. Faraday rotation in the Earth's ionosphere.
6. For the radiometer measurement we also need to correct for attenuation in the Earth's atmosphere. For the scatterometer measurements the atmospheric attenuation can be neglected at L-band frequencies.

The passive GMF will be given in terms of ocean surface emissivity E, which is related to ocean surface brightness temperature by $T_{B\,surf} = E \cdot T_S$ where T_S denotes the sea surface temperature (SST). In this paper all emissivity values are multiplied by a typical value of $T_S = 290$ K and therefore have units of Kelvin.

The L2 processing for the radiometer is complicated by the fact that the internal Aquarius calibration system exhibits a temporal drift that needs to be corrected before meaningful TB measurements can be obtained [*Piepmeier et al.,* 2013]. The basic idea in performing this calibration drift correction is to match the Aquarius salinity product on a global, weekly average with the reference salinity field from the Hybrid Coordinate Ocean Model HYCOM (c.f. section 2.4). This matching is done at the TB level. The TB measured from Aquarius are globally matched to the TB that are computed from the geophysical model using the HYCOM SSS.

2.2 Aquarius – Imager Match-up Data Set: Collocation and Quality Control

For the derivation of the radar backscatter and surface emissivity GMF we have created a match-up data set of Aquarius $T_{B\,surf}$ and σ_0 observations and microwave imager wind speeds W from the Level 3 (L3) Remote Sensing Systems (RSS) Version 7 climate data record (www.remss.com). For a valid match-up we demand that there exists a wind speed measurement from either WindSat or F17 SSMIS no more than 1 hour from the Aquarius observation and that the center of the Aquarius footprint falls within the 1/4° by 1/4° cell of the L3 imager wind speed map. Because all three sensors (Aquarius, WindSat, F17 SSMIS) have approximately the same ascending node times (18:00), the choice of this time window guarantees good global coverage at both low and high latitudes. The mismatch between observation time and resolution of the three sensors will show up in a random sampling mismatch error, which will be part of our validation and error analysis (section 5.3). Decreasing the time window will compromise the global coverage. Increasing the time window will lead to increased mismatch errors.

An observation is discarded if any of the following quality control (Q/C) conditions applies:

1. The land or ice fraction within the Aquarius footprint weighted by the antenna pattern exceeds 0.001. The corresponding estimated uncertainty of land contamination on TA is 0.1 - 0.15 K if no land correction was included. A first order land correction is applied in the Level 2 processing.
2. The L2 Aquarius data product flags the scatterometer observation for RFI [*Yueh et al.*, 2012].
3. The L2 Aquarius data product indicates possible RFI contamination of the radiometer [*Misra and Ruf*, 2008]. This is the case if the difference between RFI filtered and non-filtered TA exceeds 0.3 K.
4. The radiometer observation falls within an area for which data analysis indicates that they are likely contaminated by undetected RFI entering through the antenna sidelobes.
5. The L2 Aquarius data product indicates degraded navigation accuracy, or if there is an ongoing spacecraft cold space maneuver or a maintenance maneuver.
6. The RSS L3 map of the imager indicates rain within the 1/4° by 1/4° grid cell or any of its 8 surrounding 1/4° by 1/4° grid cells.
7. For the wind speed validation study (section 5.3), we also exclude events if the Ku-band microwave radiometer (MWR) on board the SAC-D spacecraft [*Biswas et al.,* 2012] shows rain

at the instance of the Aquarius observation. For doing this check the MWR measurements have been collocated with Aquarius.

8. The value for the average of V-pol and H-pol of the galactic radiation that is reflected from a specular ocean surface exceeds 1.8 K if the wind speed is less than 3 m/s or 2.8 K for any wind speed.

The thresholds that were chosen for items 1, 3, 8 and the regions of suspected undetected RFI (item 4) are based on the results of the degradation study by [*Meissner*, 2014]. The V3.0 Aquarius L2 files contain explicit Q/C flags, which indicate to the user that the performance starts to degrade in these cases.

Following this match-up procedure, we can create an Aquarius – WindSat and an Aquarius – F17 SSMIS data set. For the derivation of the GMF (sections 3, 4, 6) we have combined the WindSat and SSMIS sets. If there is a valid match-up wind speed for both WindSat and F17 SSMIS, then we include only the WindSat observation in the match-up set. The time frame that is used in creating this match-up set comprises the full calendar year 2012. The total number of match-ups is about 5 million for each of the three Aquarius horns. For the validation of the Aquarius wind speed product in section 5.3 we have used 2 years' worth of data comprising September 2011 – August 2013 and we use the Aquarius – WindSat match-up set only. The WindSat wind speeds are slightly more accurate than the F17 SSMIS wind speeds.

Both, passive and active GMF depend on wind direction $\varphi_r = \varphi_w - \alpha$ relative to the azimuthal look α, where φ_w is the geographical wind direction relative to North. An upwind observation has $\varphi_r = 0°$, a downwind observation has $\varphi_r = 180°$ and crosswind observations have $\varphi_r = +/-90°$. The value for φ_w comes from the ancillary NCEP GDAS field (c.f. section 2.4).

For the derivation of the GMF we have averaged the values of E and σ_0 of match-up data set into 2-dimensional intervals (W, φ_r), whose sizes are 1 m/s for W and 10° for φ_r.

2.3 Aquarius – Buoy Match-ups

For the wind speed validation in section 5.3 we have created a match-up set of Aquarius observations with wind speed measurements from a global data set of about 200 moored buoys. The data sources for the buoys are the U.S. National Data Buoy Center (NDBC), the Canadian Marine

Environmental Data Service (MEDS), the Tropical Atmospheric Ocean TAO/TRITON array (Pacific Ocean), the Pilot Research Moored Array in the Tropical Atlantic PIRATA (Atlantic Ocean) and the Research Moored Array for African-Asian-Australian Monsoon Analysis RAMA (Indian Ocean). The buoy wind speed measurements were referenced to 10 m above the ocean surface. For creating a match-up a buoy observation is used if it is located within the Aquarius 3dB footprint and if the time of the buoy measurement falls within 60 minutes of the Aquarius observation.

Most of these buoys are in the tropics but the NDBC and Canadian MEDS buoys guarantee sufficient coverage also at higher Northern latitudes reaching up to 55N. Unfortunately, there are no buoy observations at mid and high Southern latitudes and the wind speed range in the buoy match-up set with sufficient valid observations is limited to below 15 m/s.

2.4 Ancillary Geophysical Fields

At various stages of our study we will use a variety of ancillary fields. These are:

1. Wind speed W_{NCEP} and wind direction $\varphi_{w,NCEP}$ from NCEP GDAS given at a 1° spatial and 6 hour temporal resolution. Our data source is ftpprd.ncep.noaa.gov/pub/data/nccf/com/gfs/prod/gdas.YYYYMMDD/ gdas1.tHHz.pgrbf00, where YYYY, MM, DD, HH stand for year, month, day of month and hour, respectively.
2. Daily SSS from the Hybrid Coordinate Ocean Model HYCOM (www.hycom.org) that were resampled on a 1/4° by 1/4° map. Our data source is: ftp.podaac.jpl.nasa.gov, user: aqst, directory /Ancillary/HYCOM/.
3. Daily SST analysis maps from the National Oceanic Atmospheric Administration (NOAA), which are based on measurements from the infrared AVHRR (Advanced Very High Resolution Radiometer) instrument and in-situ measurements and which were optimally interpolated onto a 1/4° by 1/4° Earth grid [*Reynolds et al.*, 1994]. Our data source is ftp://eclipse.ncdc.noaa.gov/pub/OI-daily-v2/IEEE/YYYY/AVHRR-AMSR, where YYYY is the year 2002 to present.
4. Significant wave height (WH) data from the NOAA/NCEP Wave Watch III model. Our data source is http://polar.ncep.noaa.gov/waves/download.shtml.

5. The monthly SSS climatology from the 1998 World Ocean Atlas (WOA98, N.O.D.C., CD-ROM).

All of these ancillary fields are linearly interpolated in space and time to the center of the Aquarius footprint and its measurement time. The auxiliary fields 1 - 4 in the list above are all contained in the Aquarius V3.0 L2 files.

For the validation of Aquarius wind speeds in storms in section 5.4 we also use wind speed analysis fields from NOAA's Hurricane Research Division of Atlantic Oceanographic and Meteorological Laboratory (HRD) [*Powell et al.*, 1998]. The data source is http://www.aoml.noaa.gov/hrd/index.html. The HRD wind speed fields have been shifted along the storm track to the time of the Aquarius pass over the storm and resampled to the Aquarius footprint resolution.

2.5 Ionospheric Electron Content and Faraday Rotation

The derivation of the 3rd Stokes ocean surface emissivity signal U in section 4.3 is largely based on maps for the total electron content (TEC) and Faraday rotation in the Earth's ionosphere [*Rybicki and Lightman*, 1979; *Yueh,* 2000; *LeVine and Abraham*, 2002]. We use TEC maps from the International GPS Service for Geodynamics (IGS). Our data source for this product is ftp://cddis.gsfc.nasa.gov/pub/gps/products/ionex. It contains the vertically integrated electron content between the Earth's surface and an altitude of about 20,200 km. This value needs to be scaled to the altitude of the SAC-D spacecraft, whose average value is 657 km. Our scaling factor is 0.75, which is an average global value based on a model of vertical ionospheric electron density profiles (International Reference Ionosphere IRI 2012, http://irimodel.org/). Using the small-shell approximation [*Klobuchar,* 1987; *Mannucci et al.*, 1998], which assumes that the vertical integrated electron content is concentrated in a narrow shell at the mean altitude of the ionosphere, the Faraday rotation angle ψ_F is given by:

$$\psi_F \approx \frac{1.35493 \cdot 10^{-5}}{\nu^2} \cdot \left(0.75 \cdot TEC\right) \cdot \left(-\mathbf{b} \cdot \mathbf{B}\right) \cdot \frac{\partial b}{\partial h} \qquad (1)$$

In this equation ν is the frequency of the radiation (in GHz), TEC is given in TECU = 10^{-16} m^2, **B** is the Earth magnetic field vector (in nanotesla) at the mean height of the ionosphere (420 km), **b** is the boresight unit vector from the instrument to the Earth and the last term is the partial deriva-

tive of slant-range to the vertical height, which converts TEC to a vertically integrated value to a slant-range integrated value. The values for the Earth magnetic field **B** are taken from the International Geomagnetic Reference Field IGRF 11 (http://www.ngdc.noaa.gov/IAGA/vmod/igrf.html).

3 Radar Backscatter from the Wind Roughened Ocean Surface

The microwave backscatter from rough ocean surface is mainly caused by Bragg scattering from small surface capillary waves that are in equilibrium with the surface wind stress. The GMF of the L-band radar backscatter σ_0 can be expanded into a Fourier series of even harmonic functions in the relative wind direction φ_r [*Wentz,* 1991; *Isoguchi and Shimada*, 2009; *Yueh et al.*, 2010]. We keep terms up to 2nd order:

$$\sigma_{0,p}\left(W,\varphi_r\right) = B_{0,p}\left(W\right) + B_{1,p}\left(W\right)\cdot\cos\left(\varphi_r\right) + B_{2,p}\left(W\right)\cdot\cos\left(2\cdot\varphi_r\right) \tag{2}$$

The harmonic coefficients $B_{k,p}$, k=0,1,2, depend on surface wind speed W, polarization p =VV, HH, VH, HV and EIA. Using our match-up data set (section 2) we regress the σ_0 measurements to the set of even harmonic basis functions (1; $\cos(\varphi_r)$; $\cos(2\cdot\varphi_r)$) in each of the 1 m/s wide wind speed bins. The results for $B_{k,p}$, k=0,1,2, p=VV,HH,VH,HV in each bin are then fitted by a 5th order polynomial in W, which vanishes at W = 0:

$$B_{k,p}\left(W\right) = \sum_{i=1}^{5} b_{ki,p}\cdot W^i \tag{3}$$

The values of the coefficients $b_{ki,p}$ for the 3 Aquarius horns and polarizations VV, HH and VH are listed in file *ts01.txt* of the auxiliary material. The cross-pol channels VH and HV are assumed to be identical in the Aquarius TOA σ_0. The wind speed dependence of the harmonic coefficient $B_{0,p}(W)$ is displayed in Figure 1. Figure 2 shows the wind direction dependence of $\sigma_{0,p}$ at 3 different wind speeds: 6.5, 10.5 and 14.5 m/s.

Several interesting results can be seen from these figures. For VV and HH all 3 harmonic coefficients loose sensitivity to wind speed at high winds (W > 20 m/s). This behavior was also observed with the radar backscatter GMF at higher frequencies: C-band [*Hersbach et al.*, 2007] and Ku-band [*Smith and Wentz*, 1999; *Ricciardulli and Wentz*, 2011]. The cross-pol channel VH

seems to keep sensitivity to wind speeds even above 25 m/s. In our GMF we linearly extrapolate $B_{0,p}$ if W>28 m/s and $B_{1,p}$ and $B_{2,p}$ if W>22 m/s. We also see from Figure 2 that the wind-directional signal is very small below 8 m/s. Actually the figure indicates that at lower wind speeds this small directional signal of VV and HH has an opposite sign than at higher wind speeds. This observation agrees with the results of the PALSAR (Phased-Array L-Band Synthetic Aperture Radar) campaign [*Isoguchi and Shimada*, 2009]. On the other hand, such a behavior of the directional signal is not evident in either the C-band nor the Ku-band GMF, which both show a significant directional backscatter signal down to at least 5 m/s and the signal has the same sign at all wind speeds. At this point it is not clear what causes this behavior of the L-band directional signal at low winds.

Another important feature, in which the radar backscatter at L-band differs noticeably from the higher frequencies (C-band, Ku-band) and which is not yet understood, shows up in Figure 3, which displays the total backscatter $\sigma_{0,p}$ for VV and HH as function of wind speed for upwind ($\varphi_r = 0°$), downwind ($\varphi_r = 180°$) and crosswind ($\varphi_r = 90°$) observations. Above 5 m/s the crosswind signal completely loses sensitivity to wind speed. The VV-pol σ_0 even becomes non-monotonic with increasing W.

The sensitivity loss to wind speed of the L-band σ_0 at high wind speeds and for crosswind observations will become important for measuring wind speeds from L-band radar observations, which we will discuss in detail in section 5.

4 Emission from the Wind Roughened Ocean Surface

4.1 Emission from the Specular Ocean Surface

At a given frequency, the surface emissivity E can be modeled with a specular part E_0 and a part caused by ocean roughness ΔE_{rough}:

$$E = E_0\left(T_S, S, \theta\right) + \Delta E_{rough} \tag{4}$$

The emissivity of the specular ocean surface E_0 is by far the largest part. It depends on sea surface temperature T_S, sea surface salinity S, EIA θ and polarization p=V,H. E_0 is determined by the complex dielectric constant (permittivity) of sea water ε through the Fresnel equations:

$$E_{0,p} = 1 - \left| r_p \right|^2, \quad p = V / H - \text{pol}$$

$$r_V = \frac{\varepsilon(T_S,S)\cdot\cos(\theta) - \sqrt{\varepsilon(T_S,S) - \sin^2(\theta)}}{\varepsilon(T_S,S)\cdot\cos(\theta) + \sqrt{\varepsilon(T_S,S) - \sin^2(\theta)}} \qquad r_H = \frac{\cos(\theta) - \sqrt{\varepsilon(T_S,S) - \sin^2(\theta)}}{\cos(\theta) + \sqrt{\varepsilon(T_S,S) - \sin^2(\theta)}} \tag{5}$$

Meissner and Wentz [2004] provided a fit for ε, which was based on modeling the frequency dependence through a double Debye relaxation law. An ensemble of weighted data from laboratory measurements and SSM/I observations was used in order to fit the Debye relaxation parameters by minimizing the total error between observations and model. A minor update of this fit for ε was done in [*Meissner and Wentz*, 2012] by incorporating results from WindSat measurements at C-band and X-band. This is the dielectric model that we have used for this study with two small amendments, which we would like to mention here: There is a typo in the sign of the parameter d_3 in Table 7 of [*Meissner and Wentz*, 2012]. The correct value is $d_3 = -0.35594 \cdot 10^{-6}$. In addition, the T_S dependence of the 2nd Debye relaxation frequency ν_2 in equation (17) of [*Meissner and Wentz*, 2004] had been changed from $b_{10} \cdot T_S$ to $b_{10} \cdot (T_S + 30°C)/2$. This change has already been used in [*Meissner and Wentz*, 2012] but it was not listed. It should be noted that no Aquarius measurements have been used in the development of the dielectric model.

In order to compute $E_{0,p}$ (T_S, S) in the derivation of the GMF for the wind induced ocean surface emissivity we use the ancillary HYCOM SSS field as described in section 2. The important assumption is that when taking long-term global averages there is no crosstalk error between the HYCOM SSS ancillary fields and wind speed W. Such a crosstalk error could introduce a spurious signal in the GMF. The validity of that assumption has been tested by comparing HYCOM SSS with in-situ buoy measurements from the ARGO network, indicating no noticeable systematic correlation between HYCOM – buoy SSS and wind speed [*Lagerloef and Kao*, 2013]. It has also been justified a posteriori by comparing Aquarius SSS, which is using our roughness correction algorithm, with SSS from ARGO drifters, showing again no noticeable correlation between Aquarius - ARGO SSS and wind speed [*Abe and Ebuchi*, 2013].

4.2 Wind Induced Emissivity for V-Pol and H-Pol

In general, the ocean surface emissivity is influenced by wind speed through three different mechanisms:

1. Large gravity waves, whose wavelengths are long compared with the radiation wavelength. These large-scale waves mix vertical and horizontal polarizations and change the local incidence angle of the electromagnetic radiation. This mechanism is described by the geometric optics approach.
2. Small gravity-capillary waves, which are riding on top of the large-scale waves, and whose RMS height is small compared with the radiation wavelength. These small-scale waves cause diffraction (Bragg scattering) of radiation that is backscattered from the ocean surface. From Kirchhoff's law it follows that they also affect the passive microwave emission of the sea surface.
3. Sea foam, which arises as a mixture of air and water at the wind roughened ocean surface, and which leads to a general increase in the surface emissivity. This effect becomes dominant at high wind speeds at C-band and higher frequencies [*Monahan and O'Muircheartaigh*, 1980].

The emissivity signal that is produced by these mechanisms is largely isotropic, which means it is independent on relative wind direction φ_r. However, processes 1 and 2 give rise to small anisotropic contributions, which cause a dependence on φ_r.

According to equation (4), the roughness signal ΔE_{rough} is computed by subtracting the specular surface emissivity E_0 from the measured value of the total emissivity E in the match-up data set.

As a first step in the GMF derivation we parameterize ΔE_{rough} as function of wind speed W, relative wind direction φ_r and SST T_S: $\Delta E_{rough}=\Delta E_{W0}(W, \varphi_r, T_S)$. For the full roughness correction in section 6 we will also add scatterometer observations and significant wave height data into the model function for ΔE_{rough}.

Meissner and Wentz [2012] found that for higher frequencies (C-band and above) ΔE_{rough} is approximately proportional to the specular surface emissivity E_0. This can be understood within the geometric optics approach by the fact that the wind roughened surface mixes the vertical and horizontal polarizations of the specular surface and the mixing increases with increasing emissivity of the specular surface. We follow the same approach at L-band and model the SST dependence of ΔE_{rough} as:

$$\Delta E_{W0,p} = \delta_p\left(W,\varphi_r\right)\cdot\frac{E_{0,p}\left(T_S\right)}{E_{0,p}\left(T_{ref}\right)} \qquad T_{ref} = 20^{\circ}C \tag{6}$$

Figure 4 shows that this behaviour is indeed approximately correct for SST values between 0°C and 25°C: The decrease of ΔE_{W0} (squares in the right panel) with increasing T_S is similar as the decrease of E_0 (left panel) in this temperature interval and the ratio $\Delta E_{W0}/E_0$ (triangles) stays approximately constant. One can see from the left panel in Figure 4 that over the whole dynamic range of ocean SST (0^oC to 30^oC) the value of E_0 of the Aquarius channels changes by about 10%. One should note that we have not considered any dependence on salinity in (6) despite the fact that the L-band emissivity is sensitive to salinity. Over the whole dynamic range of ocean salinity (30 psu to 40 psu), the value of E_0 of the Aquarius channels changes only by about 4%. Figure 4 also shows that at very high SST the ansatz in equation (6) becomes less accurate. One reason for this might be that the HYCOM reference SSS, which is used in the computation of E_0, does not fully capture the freshening due to rain in tropical regions [*Boutin et al.*, 2013] and therefore slightly overestimates the salinity. The consequence is an underestimate of the value for E_0 and thus a slight overestimate of the value for ΔE_{W0}, which is evident in Figure 4. Another reason could be that the ansatz (6) itself breaks down at high SST. As stated, it is based on the geometric optics approach and at L-band other mechanisms such as Bragg scattering become important. This issue needs to be kept in mind to account for possible errors in the retrieved Aquarius salinity at higher SST. Overall, as Figure 4 shows, introducing the SST dependence according to (6) is an improvement over assuming no SST dependence in ΔE_{W0}.

The model function for the form factor δ is again an even 2nd order harmonic expansion:

$$\delta_p\left(W,\varphi_r\right) = A_{0,p}\left(W\right) + A_{1,p}\left(W\right)\cdot\cos\left(\varphi_r\right) + A_{2,p}\left(W\right)\cdot\cos\left(2\cdot\varphi_r\right) \tag{7}$$

The harmonic coefficients $A_{k,p}$, k=0,1,2 depend on surface wind speed W, polarization p =V,H and EIA. We follow the same procedure as for the derivation of the L-band radar backscatter GMF. The values for $\delta_p = \Delta E_{W0,p} / E_{0,p}$ are regressed to the set of even harmonic basis functions $(1; \cos(\varphi_r); \cos(2\cdot\varphi_r))$ in each of the 1 m/s wide wind speed bins. The results for $A_{k,p}$, k=0,1,2 in each bin are then again fitted by a 5th order polynomial in W, which vanishes at W = 0:

$$A_{k,p}(W) = \sum_{i=1}^{5} a_{ki,p} \cdot W^i \tag{8}$$

File *ts02.txt* of the auxiliary material lists the values of the coefficients a_{ki} for the 3 Aquarius horns and the V-pol and H-pol polarizations. The wind speed dependence of the 3 harmonic coefficients $A_{k,p}$ (W), k=0,1,2, p=V,H are plotted in Figure 5 for V-pol and in Figure 6 for H-pol. For computing the error bars in A_0 we use the standard deviation of the measurements of ΔE_W in each wind speed bin. The error bars for the higher harmonics A_1 and A_2 are the residuals of the harmonic fit (7).

One important feature that is obvious from Figure 5 and Figure 6 is the linear rise at high wind speeds of the isotropic part $A_{0,p}$, which is by far the largest term in the wind induced emissivity ΔE_{W0}. In contrast to the radar backscatter GMF, which starts to saturate above 25 m/s, the wind induced emissivity keeps good sensitivity even at very high wind speeds. The good sensitivity of the emissivity at high wind speeds has also been observed at SMOS [*Reul et al.,* 2012]. It is due to the emission from foam covered ocean surface, which becomes the dominant mechanism in the surface emission at higher wind speeds. The same behaviors are observed in the GMF for both emissivity [*Meissner and Wentz*, 2012] and radar backscatter [*Hersbach et al.*, 2007; *Ricciardulli and Wentz*, 2011; *Meissner et al.,* 2011b] at higher frequencies. Another difference between emissivity and radar backscatter GMF is that there is no sensitivity loss of ΔE_{W0} to wind speed at crosswind observations. This can be seen from Figure 5 and Figure 6, as the magnitude of the isotropic part A_0 is much larger than the one of the higher harmonics A_1 and A_2, which depend on wind direction. Thus the impact of wind direction on the total value (7) is small. Both of these differences between passive and active L-band sensors will become important in section 5 for the measurement of L-band wind speeds.

The curves in Figure 5 and Figure 6 suggest to linearly extrapolate the wind speed dependence of $A_{0,p}$ (W) and to keep the values of $A_{1,p}$ (W) and $A_{2,p}$ (W) constant if W>25 m/s.

Figure 7 shows the directional signal of ΔE_{W0} at 3 different wind speeds: 6.5, 10.5 and 14.5 m/s. The signal is small below 8 m/s. At the high incidence angle (horn 3) the 1st harmonic A_1 dominates the V-pol signal whereas the 2nd harmonic A_2 dominates the H-pol signal, as it is the case at higher frequencies [*Meissner and Wentz,* 2002, 2012]. The small 2nd harmonic A_2 at low wind

speeds has the opposite sign than at high wind speeds. This behavior is similar to what we have already observed for the L-band radar backscatter GMF in section 3. This feature has so far only been observed at L-band and the physical mechanism of its s cause is not yet understood. Above 8 m/s the directional signal in all 3 horns becomes sizeable for both polarizations and it is important to remove it from the observation in order to meet the accuracy requirement of 0.2 psu in the SSS measurement.

Finally, we want to note that the Aquarius measurements allow the derivation of a GMF at the EIA of the 3 Aquarius horns. The interpolation procedure of *Meissner and Wentz* [2012] can be used to extend it to other EIA values.

4.3 Wind Direction Signal of the 3rd Stokes Parameter

In addition to V-pol and H-pol, the Aquarius radiometer measures the 3rd Stokes parameter U. The main purpose of doing this is to have the ability to accurately correct for the rotation ψ of the electromagnetic polarization basis between Earth observation point and antenna. This polarization rotation ψ has 2 components $\psi = \psi_{ion} + \psi_{geo}$:

1. The Faraday rotation ψ_{ion}, which actively rotates the electromagnetic polarization vector when traveling from the top of the atmosphere (TOA) to the top of the ionosphere (TOI).
2. The passive geometric polarization rotation ψ_{geo} between Earth and antenna polarization basis vectors [*Meissner and Wentz*, 2006; *Dinnat and LeVine*, 2007; *Piepmeier et al.*, 2008; *Meissner et al.*, 2011a].

The ionospheric part ψ_{ion} scales with the inverse square of the frequency. In case of Aquarius this means that its size amounts to about 80 - 90% of the total polarization rotation angle ψ assuming the spacecraft flies at or near it nominal attitude.

The polarization rotation mixes the 2nd Stokes $Q = T_{BV} - T_{BH}$ and the 3rd Stokes parameter U according to:

$$\begin{pmatrix} Q \\ U \end{pmatrix}_{TOI} = \begin{bmatrix} \cos(2\psi) & -\sin(2\psi) \\ +\sin(2\psi) & \cos(2\psi) \end{bmatrix} \cdot \begin{pmatrix} Q \\ U \end{pmatrix}_{TOA} \tag{9}$$

Equation (9) implies that:

$$Q_{TOI}^{\ 2} + U_{TOI}^{\ 2} = Q_{TOA}^{\ 2} + U_{TOA}^{\ 2} \tag{10}$$

The TOI TB values are obtained from the measured antenna temperatures after removing cross-polarization contamination in the antenna and correcting for intrusion of celestial radiation (cold space, galaxy, sun, moon) into the Aquarius field of view [*Wentz et al.*, 2012; 2014]. The TOA TB for Q and U are related to their surface values after correcting for atmospheric attenuation [*Wentz et al.*, 2012]. This means in particular that $U_{TOA} \approx \tau^2 U_{surf}$. τ is the value for the atmospheric transmittance [*Meissner and Wentz*, 2012], which is very close to 1.

The Aquarius salinity retrieval algorithm [*Wentz et al.*, 2012] assumes that there is no 3rd Stokes surface signal ($U_{surf} = U_{TOA} = 0$). Equation (10) allows then the retrieval of the TOA 2nd Stokes Q_{TOA} from the measurements Q_{TOI} and U_{TOI} and thus for an accurate correction of the polarization basis rotation. On the other hand, if a value for the rotation angle $\psi = \psi_{ion} + \psi_{geo}$ is available, which is independent of the Aquarius measurement, it can be used together with the measurements for Q_{TOI} and U_{TOI} to obtain a prediction for U_{TOA} and thus for the surface 3rd Stokes U_{surf}. The small geometric part ψ_{geo} of the rotation angle can be computed from the pointing geometry [*Meissner and Wentz*, 2006; *Meissner et al.*, 2011a]. The large ionospheric part ψ_{ion} (Faraday rotation) can be predicted from ancillary maps of the ionospheric TEC, as explained in section 2.5.

Figure 8 shows the directional signal U_{surf} for Aquarius horn 1 that is obtained this way at 4 different wind speeds: 7.5 m/s, 10.5 m/s, 13.5 m/s and 16.5 m/s. Below 7.5 m/s the surface 3rd Stokes is indeed very small, which justifies the assumption of the Aquarius salinity retrieval algorithm to neglect it. However, at higher wind speed, the3rd Stokes surface signal becomes sizeable. Though the data are noisy, which is mainly due to the uncertainties in the TEC maps and the knowledge of the scaling factor (section 2.5), the expected odd harmonic signal clearly shows up:

$$U_{surf} = A_{1,U}(W) \cdot \sin(\varphi_r) + A_{2,U}(W) \cdot \sin(2 \cdot \varphi_r) \tag{11}$$

The harmonic coefficients increase with wind speed and at 16.5 m/s the peak-to-peak amplitude of the 3rd Stokes signal reaches +/- 1.5 K for horn 1. We find that the size of this signal decreas-

es for the higher incidence angles. Compared to horn 1, the peak to peak amplitude is about 80% for horn 2 and 45% for horn 3.

5 Wind Speed Retrievals from Combined Passive and Active Observations

5.1 Maximum Likelihood Estimation (MLE)

We use the GMF for the radar backscatter cross section σ_0 and the wind induced surface emissivity ΔE_{W0} that we have derived in section 3 and section 4, respectively, to estimate Aquarius ocean surface wind speeds. The Aquarius wind speed retrieval algorithm is a MLE minimizing the weighted sum of square differences between the Aquarius observations and the GMF. For this study we consider two Aquarius wind speed products:

1. A wind speed based on scatterometer HH-pol observations, which we call HH wind.
2. A wind speed based on scatterometer HH-pol and radiometer H-pol observations, which we call HHH wind.

The MLE for the HH wind speed retrieval algorithm is:

$$\chi^2_{HH}(W) = \frac{\left[\sigma^{measured}_{0,HH} - \sigma^{GMF}_{0,HH}(W,\varphi_r)\right]^2}{\mathrm{var}\left(\sigma_{0,HH}\right)} + \frac{\left[W - W_{NCEP}\right]^2}{\mathrm{var}\left(W_{NCEP}\right)} \quad (12)$$

The MLE for the HHH wind speed retrieval algorithm is:

$$\chi^2_{HHH}(W) = \frac{\left[\sigma^{measured}_{0,HH} - \sigma^{GMF}_{0,HH}(W,\varphi_r)\right]^2}{\mathrm{var}\left(\sigma_{0,HH}\right)} + \frac{\left[T^{measured}_{B,surf,H} - T^{GMF}_{B,surf,H}(W,\varphi_r)\right]^2}{\mathrm{var}\left(T_{B,surf,H}\right)} + \frac{\left[W - W_{NCEP}\right]^2}{\mathrm{var}\left(W_{NCEP}\right)} \quad (13)$$

In both cases the wind direction is obtained from the ancillary NCEP GDAS field (section 2.4).

The combination of simultaneous active and passive observations for wind speed measurements has already been studied with the SEASAT scatterometer (SASS) – radiometer (SMMR) system [*Moore et al.*, 1982] and recently applied to Aquarius [*Yueh and Chaubell*, 2012; *Yueh et al.*, 2013]. At L-band frequencies the inclusion of radiometer observations into the wind speed retrieval improves the skill at high wind speeds and for cross-wind observations in which the scatterometer starts loosing sensitivity to wind speed, as we have discussed in section 3.

The HH-wind, though less accurate than the HHH wind at higher wind speeds, becomes useful if a wind speed is needed at the stages of the salinity retrieval algorithm in which calibrated radiometer TB are not yet available. This is the case in the calibration drift correction [*Piepmeier et al.*, 2013] or the removal of celestial radiation (galaxy, sun) that gets reflected from the ocean surface [*Wentz et al.*, 2012].

The poor sensitivity of the radar backscatter σ_{0HH} at crosswind observations (Figure 2), which has already been mentioned in section 3, makes it necessary to use an auxiliary field. Therefore, we are assimilating the NCEP wind speed W_{NCEP} as background field into the HH MLE (12) for the HH wind speed algorithm. As a consequence, the algorithm will converge to this background field at crosswind. The HHH wind algorithm does not need the auxiliary field, as the H-pol emissivity does not show the crosswind sensitivity loss. Nevertheless, we have decided to use W_{NCEP} as background field in the HHH MLE (13) as well.

In order to compute the radiometer H-pol GMF in the HHH wind speed retrieval algorithm, we need an ancillary first guess fields for SSS. One possibility is to take a climatology salinity field (e.g. from the World Ocean Atlas WOA) or a model (e.g. HYCOM). It is also possible to do the HHH wind speed retrieval iteratively. In a first step one retrieves HH wind speed, which uses scatterometer observations only and therefore does not need any ancillary input SSS. In the 2nd step one uses this HH wind speed to retrieve SSS. The final step is to take this SSS as ancillary input in the HHH wind algorithm.

5.2 Determination of Channel Weights

The various terms in the MLE of equations (12) and (13) are weighted by their inverse estimated variances, which are the squares of the estimated errors. Our estimated errors include instrument noise, knowledge errors in the instrument parameters (e.g. EIA), uncertainties in the GMF and errors in the ancillary fields that are used in the GMF (e.g. SST, SSS). In order to calculate these estimated errors we have computed the standard deviations of the difference between measured and GMF value for σ_0 and ΔE_{W0} in our match-up data set. In case of the background field W_{NCEP}, we take the standard deviation between W_{NCEP} and the imager wind speed. All of these estimated error values contain the error from the imager wind speed and the sampling mismatch between imager and Aquarius observation. This contribution should not be included in MLE

weights, as it is neither related to the Aquarius measurement nor the GMF and it therefore needs to be backed out in a root sum square sense from the standard deviation. We have allocated a total error of $\Delta W=0.6$ m/s for the uncertainty in the imager wind speed and the sampling mismatch error, which is based on validation studies [*Meissner et al.*, 2011b]. The GMF for σ_0 and ΔE_{W0} can be used to translate this value into an equivalent error for σ_0 and ΔE_{W0}. This error is then removed from the standard deviation to give the final values for the channel weights. In the wind speed retrieval algorithm we need to know a first-guess value for the wind speed in order to look up the value of the estimated error that is tabulated in file *ts03.txt* of the auxiliary material, because the tabulated error values depend on wind speed. We are using W_{NCEP} to do that.

We have found that when using these channel weights in the MLE, the inclusion of any of the additional scatterometer channels (VV, VH, HV) or the V-pol radiometer channel does not lead to further improvement of the retrieved Aquarius wind speed. The VV-pol scatterometer channel contains information on the surface roughness that is orthogonal to the information given by surface wind speed, as we will discuss in sections 6.1 and 6.2. Moreover, as it can be seen from Figure 3, σ_{0VV} becomes not only insensitive but even non-monotonous as function of wind speed for cross-wind observations, which can introduce multiple local minima in the cost function of the MLE. Section 6 will show that the VV-pol is still useful for the surface roughness correction of the emissivity, but we do not include it in the wind speed retrievals. The signal to noise ratio of the radar cross-pol channels VH and HV is too small to make these channels useful to be included into the MLE. The V-pol radiometer channel is less sensitive to wind speed but more sensitive to SSS than the radiometer H-pol channel. This channel is used in the actual SSS retrieval algorithm [*Wentz et al.*, 2012].

5.3 Performance Estimate of Aquarius Wind Speed Retrievals

In order to assess the accuracy of the Aquarius HH and HHH wind speed products we have compared them with the WindSat wind speeds of our match-up data set (section 2.2). Figure 9 shows the values for bias and standard deviations stratified as function of WindSat wind speed. For comparison, we have also included the statistic result for NCEP wind speed versus imager wind speed in Figure 9. It can be seen that over the whole wind speed range both HH and HHH wind speeds perform significantly better than NCEP, which is used as a background field in the MLE (section 5.1).

Figure 10 shows the joint probability density function between Aquarius HHH and WindSat wind speeds and Figure 11 between Aquarius and buoy wind speeds from the match-up set that has been described in section 2.3. The black dashed lines in both figures indicate the bias between Aquarius wind speed and the validation wind. Table 1 lists the standard deviations between several Aquarius wind speed products and WindSat.

Figure 9, Figure 10, and Figure 11 show that no significant systematic wind speed biases exist between Aquarius HHH wind speeds and any of the validation sets below 25 m/s. Unfortunately very few rain-free Aquarius or validation data exist above 25 m/s. The next section will give a performance estimate of high Aquarius wind speeds based on a study of selected cases.

Figure 9 also shows that for higher wind speeds the HHH winds perform better than the HH winds. In particular, above 20 m/s the HH wind performance starts to degrade. This is expected, because, as discussed in sections 3 and 4, the radar backscatter GMF starts loosing sensitivity at higher wind speeds whereas the wind induced emissivity does not. Below 8 m/s the performance of scatterometer only (HH) and combined radiometer-scatterometer (HHH) wind speeds are basically identical.

Creating a triple collocation match-up set between Aquarius, WindSat and buoys allows the computation of the standard deviation of the mutual difference of each pair of the three wind speed data sets at the same observation time and location. This triple collocation match-up set comprises more than 4,000 data. The results are listed in the left columns of Table 2. Because the three measurements are independent, the errors of the single measurement σ_i can be computed from the standard deviations of the three mutual differences σ_{ij} :

$$\sigma_i^2 = \frac{1}{2}\left(\sigma_{ij}^2 + \sigma_{ik}^2 - \sigma_{jk}^2\right) \quad i, j, k = 1, 2, 3 \tag{13}$$

The results of the triple collocation analysis of Aquarius HHH, WindSat and buoy wind speeds are listed in the right columns of Table 2. It should be kept in mind that the Aquarius observations have the lowest resolution (100 – 150 km) compared with WindSat (35 km) and the buoys (point observation). The error figure for the buoys in Table 2 is largely dominated by sampling mismatch between the different resolutions. Nevertheless, these results demonstrate that the

quality of the Aquarius wind speed at its 100 km resolution matches the quality of the wind speed products from the two imager instruments (WindSat, SSMIS) and that from the QuikSCAT [*Ricciardulli and Wentz*, 2011; *Meissner et al.*,, 2011b] and ASCAT [*Verspeek et al.*, 2010] scatterometers.

The probability density functions for the wind speed distributions of the Aquarius – WindSat match-ups are shown in Figure 12 and for the Aquarius – buoy match-ups in Figure 13. There is very good agreement between Aquarius HHH and the WindSat and buoy pdf. As expected, the half-width of the Aquarius HHH wind distribution is slightly smaller than the one of WindSat and the buoys because the Aquarius winds have a lower resolution. The NCEP GDAS distribution, which is also shown in Figure 12, is shifted slightly towards lower wind speeds. This feature is prevalent when comparing NCEP GDAS wind speeds with satellite derived wind speeds and has already been observed in other studies [*Meissner et al.*, 2001]

5.4 Aquarius Wind Speeds in Storms

The capability of L-band radiometers to measure wind speed in hurricanes has been demonstrated by *Reul et al.* [2012] for SMOS. We conclude our validation of the Aquarius HH and HHH wind speeds with a brief look at their performance in storms with strong winds and intense rain. Figure 14 shows the time series of the along-track cross section of one of the Aquarius horns through the center of three storms: one tropical cyclone (hurricane Katia, left panel) and two extratropical cyclones (center and right panels). In the first case we use HRD wind fields (section 2.4) and in the latter two cases the RSS WindSat all-weather wind speed [*Meissner and Wentz*, 2009] for comparison. In all three cases we have turned off the rain-flagging that has been applied as Q/C in the construction of the match-up set (section 2.2), and therefore the cases shown in Figure 14 do contain rain. Collocated imager rain rates from WindSat [*Hilburn and Wentz*, 2008] are available for the last two cases and plotted as red lines. The HHH wind speeds match very well the reference, HRD or WindSat all-weather winds, even in winds as high as 40 m/s and in intense rain. The HH wind speed becomes inaccurate above 25 m/s, which is again likely due to the sensitivity loss of the scatterometer GMF at high winds. The results indicate that combined L-band scatterometer and radiometer wind speed might be usable in strong storms and even if rain is present. We should caution, however, as a systematic study of the rain effect at L-band is still outstanding. While the atmospheric attenuation at L-band frequencies is very small

even in rain [*Wentz*, 2005], it is not clear if and how rain splashing at the ocean surface can have an impact on the surface roughness and on the quality of the retrieved wind speeds [*Weissman et al.*, 2012; *Boutin et al.*, 2013].

6 Surface Roughness Correction for the Aquarius Ocean Salinity Retrieval Algorithm

6.1 Full Model Function for the Radiometer Surface Roughness Correction

The full model function for the roughness correction of the Aquarius surface brightness temperature also includes scatterometer VV-pol and WH (wave height) observations. As we will see in section 6.4, this leads to a small but noticeable improvement in the accuracy of the roughness correction and thus in the accuracy of the SSS. We write the model function as a sum of three terms, whose size and importance decrease with ascending order:

$$\Delta E_{rough} = \Delta E_{W0}\left(W, \varphi_r, T_S\right) + \Delta E_{W1}\left(W, \sigma'_{0,VV}\right) + \Delta E_{W2}\left(W, WH\right) \tag{14}$$

For the wind speed we use the HHH wind in all three terms. The largest (0^{th} order) term in this sum is $\Delta E_{W0}(W, \varphi_r, T_S)$, which is the wind induced emissivity GMF that we have derived and discussed in section 4.

The next-to-leading order term $\Delta E_{W1}(W, \sigma'_{0,VV})$ is a 2-dimensional lookup table that depends on HHH wind speed and the measurement of the VV-pol radar cross section after removing the wind direction signal according to equation (2).

$$\sigma'_{0,VV} \equiv \sigma^{meas}_{0,VV} - \left[B_{1,VV}\left(W_{NCEP}\right) \cdot \cos\left(\varphi_r\right) + B_{2,VV}\left(W_{NCEP}\right) \cdot \cos\left(2 \cdot \varphi_r\right) \right] \tag{15}$$

The scatterometer VV-pol has not been used in the retrieval of the Aquarius wind speed and can therefore contain additional valuable information for the surface roughness correction. In order to derive the lookup table ΔE_{W1}, we compute the residuals between the observation for the wind induced surface emissivity and the GMF $\Delta E_{W0}(W, \varphi_r, T_S)$ and average it into equal 2-dimensional $[W, \sigma'_{0,VV}]$ intervals. The result is displayed in Figure 15 for horn 3. For visual reasons we have linearly scaled the units of the cross section into equivalent wind speeds. This scaling is based on the GMF values for $B_{0,VV}(W)$ in section 3. The left panel in Figure 15 con-

tains the population density of each [W, $\sigma'_{0,VV}$] interval. The center panel shows ΔE_{W1} for the V-pol and the right panel for the H-pol. The V-pol ΔE_{W1} is small over most of the [W, $\sigma'_{0,VV}$]-region. However, the H-pol ΔE_{W1} is sizeable both in the case of high winds relative to small $\sigma'_{0,VV}$ as well as small winds relative to large $\sigma'_{0,VV}$. Its absolute value exceeds 0.4 K in those regions of the [W, $\sigma'_{0,VV}$]-diagram. That shows that the VV-pol radar measurement contains indeed additional valuable information on the surface roughness that is not contained in the Aquarius HHH wind speed.

Finally, the 2nd order term ΔE_{W2} (W, WH) in equation (14) is a 2-dimensional lookup table depending on wind speed W and wave height WH. The wave height values come from the NOAA/NCEP Wave Watch III model (section 2.4). In order to derive ΔE_{W2} (W, WH) we repeat the procedure above but this time computing the residuals between the observation for the wind induced surface emissivity and the sum ($\Delta E_{W0} + \Delta E_{W1}$) and bin it into equally spaced [W, WH] intervals. The results for the population density and the values for ΔE_{W2} are shown in Figure 16 for horn 3. We see that most of the surface roughness information is already contained in wind speed and the scatterometer VV-pol measurement and thus in the terms ΔE_{W0} and ΔE_{W1}. Consequently, the dependence of the residuals ΔE_{W2} on WH is weak.

File *ts04.txt* in the auxiliary material provides the full look-up tables for ΔE_{W1} (W, $\sigma'_{0,VV}$) and file *ts05.txt* provides the full look-up table for ΔE_{W2} (W, WH). 2-dimensional [W, $\sigma'_{0,VV}$] or [W, WH] intervals with population less than 100 are regarded as underpopulated and the values of ΔE_{W1} or ΔE_{W2} are not used in the roughness correction and they are also not shown in the diagrams of Figure 15 or Figure 16. In those cases we decided to just take $\Delta E_{rough}=\Delta E_{W0.}$

We need to note that our choice (14) for the form of the roughness correction GMF is by no means unique. For example, one could consider a parameterization for the 1st order term that depends on [$\sigma'_{0,VV}$, $\sigma'_{0,HH}$] rather than on [W, $\sigma'_{0,VV}$].

6.2 Dependence on Input Wind Speed

It is also important to point out that the roughness correction GMF does depend on which input wind speed is used. Our GMF (14) and the values for the look-up tables for ΔE_{W1} and ΔE_{W2} are based on HHH wind speeds. For the derivation of ΔE_{W0} we had used imager wind speeds from our match-up data set, which, as seen in Figure 9, matches the HHH wind speeds very well. For

demonstration, let us now present a case for the roughness correction in which no L-band scatterometer measurements but only ancillary NCEP wind vector and WH fields are available. The residuals between observed wind induced emissivity and 0^{th} order GMF ΔE_{W0} can be written as a 2-dimensional look-up table $\Delta E'$ (W_{NCEP}, WH), which is displayed in Figure 17. When comparing it with Figure 15 and Figure 16 it is evident that, if combined with NCEP wind speeds, the WH contains important information on the surface roughness in a similar way as the scatterometer observations do. If W_{NCEP} is used in the roughness correction and if there is no scatterometer measurement available, it is useful to include WH information into the GMF. On the other hand, as we have seen in section 6.1, if WH data are included into the GMF (14) in addition to $\sigma_{0,HH}$ and $\sigma_{0,VV}$, the resulting dependence on WH is very weak. Accordingly, the improvement in the accuracy is only marginal. We hope that our results might help to understand this issue sometime in the future within the framework of the theory of scattering and emission of electromagnetic radiation from rough ocean surfaces.

It should also become clear from this discussion that it is important to input the Aquarius HHH wind speed product into equation (14) and into the look-up tables for ΔE_{W1} (W, $\sigma'_{0,VV}$) and ΔE_{W2} (W, WH). Using W_{NCEP} rather than W_{HHH} could result in inaccuracies. Conversely, the look-up table $\Delta E'$ from Figure 17 takes the NCEP wind speeds as input and not the HHH wind speeds.

6.3 Components and Flow of Surface Roughness Correction Algorithm

We are now in a position to put together all the parts of the surface roughness correction for the Aquarius salinity retrieval algorithm. Figure 18 shows a flow diagram with the major components and how they interact. It also exhibits what observations and ancillary data are used during each step.

6.4 Accuracy of Roughness Correction Algorithm

The accuracy of the surface roughness correction algorithm can be assessed by comparing measured with computed surface brightness temperatures. In the computation we use the ancillary HYCOM SSS field. The result is presented in Table 3, which lists the RMS difference between measured and computed surface brightness temperatures for the 6 Aquarius channels. In order to demonstrate the importance of the surface roughness input parameter that is available to perform the correction, we have compared 5 cases:

1. Ancillary NCEP wind speed and direction only. The surface roughness GMF consists only of the 0th order term ΔE_{W0} (W_{NCEP}, φ_r, T_S).
2. WH data in addition to that, which is the case discussed in section 6.2. The GMF contains the additional term $\Delta E'$ (W_{NCEP}, WH).
3. HHH wind speeds, which requires HH-pol scatterometer measurements. The surface roughness GMF consists of the 0th order term ΔE_{W0} (W_{HHH}, φ_r, T_S) from equation (14).
4. Scatterometer VV-pol observation in addition to that. The surface roughness GMF is the sum $\Delta E_{W0} + \Delta E_{W1}$ from equation (14).
5. WH data in addition to that. In this case the surface roughness GMF is the full equation (14).

The by far largest improvement occurs between the 2nd and the 3rd step with the inclusion of the scatterometer HH-pol observation, which leads to a drop in the RMS error by about 22 – 29% for the V-pol channels and about 37 – 45% for the H-pol channels. This demonstrates the importance of the ability to use the scatterometer observations in the roughness correction. It is far superior over having only ancillary numerical weather prediction wind speed fields and WH model data available. In that respect, the Aquarius sensor has a distinct advantage over SMOS [*Font et al.*, 2004], which has only an L-band radiometer but no radar on board.

Finally, we should mention that the global accuracy estimate for the RMS between measured and computed surface TB of case 5 in Table 3 translates into a global error for the retrieved Aquarius SSS of approximately 0.50 – 0.53 psu, based on the translation 1 K (ΔT_B) = 2 psu (ΔSSS), if only V-pol channels are used in the retrievals,. This is to be compared to error figures of about 0.71 psu if no scatterometer is used (case 2 in Table 3).

The error figures of case 5 in Table 3 are larger than the requirement of 0.2 psu, but it should be kept in mind that this accuracy value applies to a single 1.44 s observation cycle. Further noise reduction is obtained after averaging the single 1.44 s measurements of the 3 horns into monthly 150 km maps.

7 Comparison with Other Studies

In this section, we compare our L-band GMF and L-band wind speed retrievals with the findings of other previous studies.

Most importantly, we find very good agreement, within the margins of error, between our isotropic wind induced emissivity A_0 (W) and the corresponding result of the SMOS analysis [*Guimbard et al.*, 2012; *Yin et al.,* 2013] for winds below 20 m/s. The SMOS study has limited its wind speed range to below 20 m/s. The curves given in [*Guimbard et al.;* 2012; *Yin et al.*, 2013] were interpolated to the incidence angles of the Aquarius horns in order to compare results. This agreement demonstrates a high level of consistency between the SMOS and Aquarius analyses of wind induced emissivity, which holds despite the fact that the size of Aquarius footprints (100 - 150 km) are more than twice as large as SMOS footprints (40 km). Moreover, comparison of Aquarius wind speeds with buoys, which provide a point measurement of wind speed, have revealed no significant biases (section 5.3). This indicates that the GMF of the wind induced emissivity at L-band has little or no dependence on footprint size and resolution of the sensor.

In another study, the predictions of the 2-scale model with the DV2 spectrum [*Dinnat et al.,* 2003, 2012] show relatively good agreement with the Aquarius derived GMF over the wind speed range 2- 15 m/s. The RMS between the 2-scale model and the Aquarius data is 0.08 – 0.12 K for the V-pol channels and 0.18 K – 0.25 K for the H-pol channels. In order to compute these numbers an average bias over the whole wind speed range has been removed in each horn [*Dinnat et al.*, 2012]. This bias can reflect an absolute calibration offset in the instrument, which is impossible to determine from the instrument parameters. As explained in section 2.1, the Aquarius TB are matched to the TB computed from the geophysical model over the global ocean.

The pre-launch WISE [*Camps et al.*, 2004; *Etcheto et al.*, 2004] and PALS [*Yueh et al.*, 2010] campaigns have provided model fits for the isotropic part of the wind induced emissivity model. They have assumed a linear increase of ΔE_W with wind speed. The reason for this assumption was simply a lack of data at higher wind speeds in both campaigns, which did not allow for a more accurate determination of the GMF. At wind speeds below 6 m/s the PALS emissivity agrees well with our GMF for both V-pol and H-pol and so does the WISE emissivity for H-pol. The WISE prediction for the V-pol emissivity is much too small at the middle and outer horns, being almost zero at horn 3. All other studies and measurements show a sizeable V-pol emissivity even at 45^o incidence. Because of their assumed linear increase with wind speed, neither the

PALS nor the WISE GMF can describe the wind induced emissivity well enough at wind speeds above 6 m/s to be used in actual salinity retrievals of SMOS or Aquarius.

Earlier versions of our wind emissivity GMF [*Meissner et al.,* 2012a, 2012b] were based on only a few months of data compared with the one full year that was used in this study. The reduced data volume results in higher noise especially at higher wind speeds. The previous analysis was not able to give reliable predictions above 18 m/s. The most important difference between our previous work and that reported here concerns the surface roughness correction. The earlier study used NCEP wind speeds whereas the present study uses the Aquarius HHH wind speeds. The significant positive impact of this change to the accuracy of the surface roughness correction is demonstrated in section 6.4.

Due to the strong similarity in the approaches for deriving the L-band wind emissivity and radar GMF we also expect general agreement between the GMF of the CAP algorithm [*Yueh et al.*, 2013] and our algorithm, which is used in the ADPS Version 3.0 data release. The most noticeable difference between these two GMFs is the 2nd harmonic coefficient A_2 of the V-pol wind emissivity signal at high incidence angles. Whereas the results for horn 1 agree within the margins of error, our A_2 coefficient for horn 3 is only half the size of the CAP value. Our results for the wind direction signal in the 3rd Stokes parameter U (section 4.3) is about 15 - 20% smaller than CAP. This lies within the margins of error.

There are, however, more noticeable discrepancies between CAP and our algorithm when it comes to retrieving wind speed and using the winds in the surface roughness correction of the salinity retrieval. The most important differences are the combinations of scatterometer and radiometer channels that both algorithms use in their wind speed retrievals and how these channels get weighted in the MLE. CAP includes the scatterometer VV-pol and the radiometer V-pol into their MLE. We do not. We include the scatterometer VV-pol in the roughness correction in addition to the HH wind speed in the form of a correction table, ΔE_{W1}, as discussed in section 6.1. The reason is the poor correlation of σ_{0VV} with wind speed, in particular at cross-wind observations. In addition, the values of our estimated errors for σ_0 and ΔE_{W0} in the MLE are different than those used in the CAP algorithm, which includes only the instrument noise figures. These are the K_p-values for the radar measurements and the noise equivalent delta temperature (NEDT) values for the radiometer measurements after applying appropriate noise reduction to account for

the sampling onto the 1.44 s observation cycle. The CAP noise values are about 2 – 4 times smaller than our estimated error values. Finally, the CAP retrieval process is a 1-step process that retrieves wind speed and ocean surface salinity simultaneously by performing a MLE in 2-dimensional space that is spanned by both parameters. Our algorithm first retrieves wind speed and then removes the surface roughness effect from the measured TB using this wind speed. The roughness corrected TB is then used in the salinity retrieval.

Examples of how the differences of the GMF and algorithms impact the wind speed performance are shown in Table 1 and Figure 12. In both cases, exactly the same observations were used for the results of our algorithm as for the CAP Version 2.5.1 data. The most noticeable differences between CAP V2.5.1 and our algorithm are:

1. The standard deviations of the Aquarius - WindSat wind speed differences: 0.70 m/s (HHH winds), 0.80 m/s (HH winds), 0.93 m/s (CAP V2.5.1). These differences reflect a higher noise in the CAP retrievals.
2. The unphysical shape of the wind speed distribution, which deviates from the expected Rayleigh shape. This issue has already been noted in the CAP wind speed validation study [*Fore et al.*, 2014].

8 Summary and Conclusions

In order to measure sea surface salinity with the required accuracy it is necessary to remove the ocean surface roughness signal from the observed Aquarius brightness temperatures. This requires an accurate knowledge of the signal itself as well as the ocean surface wind speed.

We have derived a GMF for this signal at L-band frequencies. The derivation is based on a match-up data set consisting of one full year of Aquarius radiometer TB and radar backscatter σ_0 measurements with satellite microwave imager (WindSat, F17 SSMIS) wind speeds in rain-free scenes. It also includes important ancillary information from collocated HYCOM salinity, NOAA SST, NCEP GDAS wind speed and direction fields and the NOAA Wave Watch III significant wave height model.

The central step in the roughness correction is the combination of Aquarius HH-pol scatterometer and H-pol radiometer measurements to derive a wind speed, called HHH wind. The accuracy

of the roughness correction algorithm can be further improved by incorporating additional information from the scatterometer VV-pol and wave height data. We have demonstrated that a roughness correction that is able to use active in addition to passive L-band measurement reduces the RMS error of the ocean salinity measurement by about 40%. This is an important step towards reaching the strict Aquarius mission requirement of 0.2 psu salinity accuracy and gives the Aquarius instrument a clear advantage over SMOS, which has no scatterometer.

Our study has also indicated that the L-band 3rd Stokes parameter has a sizeable wind direction signal above 10 m/s.

As part of assessing the accuracy of the roughness correction, we have performed a validation of the Aquarius HHH wind speed against WindSat and buoy wind speeds. We have seen that its precision is at least as good as that of many other active and passive microwave satellite wind speeds (WindSat, SSMIS, QuikSCAT, ASCAT). Preliminary results even indicate promising performance in storms with high winds and intense rain, though a systematic study of rain splashing effects on the ocean surface and its effect on wind speed measurements is still outstanding.

The data volume is limited in case of Aquarius due to its very narrow Earth swath. In addition, the resolution (85 – 125 km) is not particularly good. The Aquarius HHH wind speed is therefore not as useful as a geophysical product as other satellite wind speeds. However, we expect that a similar wind speed accuracy can be achieved in case of the SMAP (Soil Moisture Active Passive) mission [*Entekhabi et al*., 2010], whose launch is scheduled for fall 2014. SMAP has a 1000 km wide swath and will provide combined active/passive observations at 40 km resolution, which will make the SMAP wind speed a useful product for meteorological and oceanographical applications. The better resolution of SMAP will result in a slightly noisier wind speed than for Aquarius but, considering the excellent precision we have obtained for the Aquarius wind speeds, that is not expected to be a major issue.

Acknowledgements

This work has been supported by NASA contract NNG04HZ29C. We would like to thank the members of the Aquarius cal/val and science teams, in particular Gary Lagerloef, David LeVine, Simon Yueh, Yi Chao, Tong Lee, Shannon Brown, Emmanuel Dinnat, Alex Fore, Hsun-Ying Kao and Sid Misra for numerous useful discussions.

References

Abe, H., and N. Ebuchi (2013), Evaluation of sea surface salinity observed by Aquarius and SMOS, paper presented at the SMOS-Aquarius Workshop, IFREMER, Brest, France, (http://www.smosaquarius2013.org/).

Biswas, S., L. Jones, D. Rocca, and J.-C. Gallio (2012), Aquarius/SAC-D Microwave Radiometer (MWR): Instrument description & brightness temperature calibration, paper presented at the IEEE International Geoscience and Remote Sensing Symposium (IGARSS), Munich, doi: 10.1109/IGARSS.2012.6350705.

Boutin, J., N. Martin, G. Reverdin, X. Yin, and F. Gaillard (2013), Sea surface freshening inferred from SMOS and ARGO salinity: impact of rain, *Ocean Sci.,* 9, 183-192, doi: 10.5194/os-9-183-2013.

Camps, A., J. Font, M. Vall-llossera, C. Gabarro, I. Corbella, N. Duffo, F. Torres, S. Blanch, A. Aguasca, R. Villarino, L. Enrique, J. J. Miranda, J. J. Arenas, A. Julia, J. Etcheto, V. Caselles, A. Weill, J. Boutin, S. Contardo, R. Niclos, R. Rivas, S. C. Reising, P. Wursteisen, M. Berger, and M. Martin-Neira (2004), The WISE 2000 and 2001 field experiments in support of the SMOS mission: Sea surface L-band brightness temperature observations and their application to multi-angular salinity retrieval, *IEEE Transactions on Geoscience and Remote Sensing, 42*(4), 804-823, doi: 10.1109/TGRS.2003.819444.

Dinnat, E., J. Boutin , G. Caudal, and J. Etcheto (2003), Issues concerning the sea emissivity modeling at L-band for retrieving surface salinity, *Radio Sci., 38* (4), 8060, doi: 10.1029/2002RS002637.

Dinnat, E., and D. LeVine, Effects of the antenna aperture on remote sensing of sea surface salinity at L-band (2007), *IEEE Transactions on Geoscience and Remote Sensing, 45*(7), 2051 - 2060, doi: 10.1109/TGRS.2007.890807.

Dinnat, E, D. LeVine, S. Abraham, P. De Matthaeis, and C. Utku (2012), Comparison of Aquarius measurements and radiative transfer models at L-band, *Proceedings of the 12th Specialist Meeting on Microwave Radiometry and Remote Sensing of the Environment (MicroRad)*, doi: 10.1109/MicroRad.2012.6185231.

Entekhabi, D., E. Njoku, P. O'Neill, K. Kellogg, W. Crow, W. Edelstein, J. K. Entin, S. Goodman, T. Jackson, J. Johnson, J. Kimball, J. Piepmeier, R. Koster, N. Martin, K. McDonald, M. Moghaddam, S. Moran, R. Reichle, J. Shi, M. Spencer, S. Thurman, L. Tsang, and J. Van Zyl (2010), The Soil Moisture Active Passive (SMAP) mission, *Proc. IEEE*, *98*(5), 704-716, doi: 10.1109/JPROC.2010.2043918.

Etcheto, J., E. Dinnat, J. Boutin, A. Camps, J. Miller, S. Contardo, J. Wesson, J. Font, and D. Long (2004), Wind speed effect on L-band brightness temperature inferred from EuroSTARRS and WISE 2001 field experiments, *IEEE Transactions on Geoscience and Remote Sensing, 42*(10), 2206 – 2213, doi: 10.1109/TGRS.2004.834644.

Font, J., G. Lagerloef, D. Le Vine, A. Camps, and O. Zanife (2004), The determination of surface salinity with the European SMOS space mission, *IEEE Transactions on Geoscience and Remote Sensing*, *42*(10), 2196-2205, doi: 10.1109/TGRS.2004.834649.

Fore, A., S. Yueh, W. Tang, A. Hayashi, and G. Lagerloef (2014), Aquarius wind speed products: algorithms and validation, *IEEE Transactions on Geoscience and Remote Sensing*, *52*(5), 2920 – 2926, doi: 10.1109/TGRS.2013.2267616.

Guimbard, S., J. Gourrion, M. Portabella, A. Turiel, C. Gabarro, and J. Font (2012), SMOS semi-empirical ocean forward model adjustment, *IEEE Transactions on Geoscience and Remote Sensing*, *50*(5), 1676-1687, doi: 10.1109/TGRS.2012.2188410.

Hilburn, K., and F. Wentz (2008), Intercalibrated passive microwave rain products from the unified microwave ocean retrieval algorithm (UMORA), *J. Appl. Meteorol. Climatol., 47*(3), 778-794, doi: 10.1175/2007JAMC1635.1.

Hersbach, H., A. Stoffelen, and S. de Haan (2007), An improved C-band scatterometer ocean geophysical model function: CMOD5, *J. Geophys. Res., 112,* C03006, doi: 10.1029/2006JC003743.

Hollinger, J. (1971), Passive microwave measurements of sea surface roughness, *IEEE Trans. Geosci. Electron., GE-9* (3), 165-169, doi: 10.1109/TGE.1971.271489.

Isoguchi, O., and M. Shimada (2009), An L-band ocean geophysical model function derived from PALSAR, *IEEE Transactions on Geoscience and Remote Sensing*, *47*(7), 1925-1936, doi:10.1109/TGRS.2008.2010864.

Klobuchar, J. (1987), Ionospheric time delay algorithm for single frequency GPS users, *IEEE Transactions on Aerospace and Electronics Systems, AES-23* (3), 325 – 331, doi: 10.1109/TAES.1987.310829.

Lagerloef, G., F. Colomb, D. Le Vine, F. Wentz, S. Yueh, C. Ruf, J. Lilly, J. Gunn, Y. Chao, A. deCharon, G. Feldman, and C. Swift (2008), The Aquarius/Sac-D mission: Designed to meet the salinity remote-sensing challenge, *Oceanography*, *21*(1), 68-81, doi: 10.5670/oceanog.2008.68.

Lagerloef, G., and H.-Y. Kao (2013), Aquarius Data Release V2.0: Validation Analysis, paper presented at the SMOS-Aquarius Workshop, IFREMER, Brest, France, (http://www.smosaquarius2013.org/).

LeVine, D., and S. Abraham (2002), The effect of the ionosphere on remote sensing of sea surface salinity from space: absorption and emission at L Band, *IEEE Transactions on Geoscience and Remote Sensing*, *40*(4), 771–782, doi: 10.1109/TGRS.2002.1006342.

Le Vine, D., E. Dinnat, S. Abraham, P. De Matthaeis, and F. Wentz (2011), The Aquarius simulator and cold-sky calibration, *IEEE Transactions on Geoscience and Remote Sensing*, 49(9), 3198 - 3210, doi: 10.1109/TGRS.2011.2161481.

Mannucci, A., B. Wilson, D.Yuan, C. Ho, U. Lindqwister, and T. Runge (1998), A global mapping technique for GPS-derived ionospheric total electron content measurements, *Radio Sci., 33* (3), 565 – 582, doi: 10.1029/97RS02707.

Meissner, T., D. Smith, and F. Wentz (2001), A 10-year intercomparison between collocated SSM/I oceanic surface wind speed retrievals and global analyses, *J. Geophys. Res., 112,* C11731, doi: 10.1029/1999JC000098.

Meissner, T., and F. Wentz (2002), An updated analysis of the ocean surface wind direction signal in passive microwave brightness temperatures, *IEEE Transactions on Geoscience and Remote Sensing*, *40*(6), 1230-1240, doi: 10.1109/TGRS.2002.800231.

Meissner, T., and F. Wentz (2004), The complex dielectric constant of pure and sea water from microwave satellite observations, *IEEE Transactions on Geoscience and Remote Sensing*, *42*(9), 1836-1849, doi: 10.1109/TGRS.2004.831888.

Meissner, T., and F. Wentz (2006), Polarization rotation and the third Stokes parameter: The effects of spacecraft attitude and Faraday rotation, *IEEE Transactions on Geoscience and Remote Sensing, 44*(3), 506-515, doi: 10.1109/TGRS.2005.858413.

Meissner, T., and F. Wentz (2009), Wind vector retrievals under rain with passive satellite microwave radiometers, *IEEE Transactions on Geoscience and Remote Sensing, 47*(9), 3065-3083, doi: 10.1109/TGRS.2009.2027012.

Meissner, T., F. Wentz, and D. Draper (2011a), GMI Calibration Algorithm and Analysis Theoretical Basis Document, Version F, Remote Sensing Systems, Santa Rosa, CA, RSS report 111311, http://www.remss.com/papers/gmi_ATBD.pdf.

Meissner, T., L. Ricciardulli, and F. Wentz (2011b), All-weather wind vector measurements from intercalibrated active and passive microwave satellite sensors, paper presented at the *IEEE International Geoscience and Remote Sensing Symposium (IGARSS)*, Vancouver, B.C., Canada, doi: 10.1109/IGARSS.2011.6049354.

Meissner, T., and F. Wentz (2012), The emissivity of the ocean surface between 6 and 90 GHz over a large range of wind speeds and earth incidence angles, *IEEE Transactions on Geoscience and Remote Sensing, 50*(8), 3004-3026, doi: 10.1109/TGRS.2011.2179662.

Meissner, T., F. Wentz, G. Lagerloef, and D. LeVine (2012a), The Aquarius salinity retrieval algorithm, paper presented at the *12th Specialist Meeting on Microwave Radiometry and Remote Sensing of the Environment*, Rome, Italy, 2012, doi: 10.1109/MicroRad.2012.6185227.

Meissner, T., F. Wentz, K. Hilburn, G. Lagerloef, and D. LeVine (2012b), The Aquarius salinity retrieval algorithm, paper presented at the *IEEE International Geoscience and Remote Sensing Symposium (IGARSS)*, Munich, Germany, doi: 10.1109/IGARSS.2012.6351557.

Meissner, T. (2014), Performance Degradation and Q/C Flagging of Aquarius L2 Salinity Retrievals, RSS Tech. Report 01202014, Remote Sensing Systems, Santa Rosa, California, (ftp://podaac-ftp.jpl.nasa.gov/allData/aquarius/docs/v3/).

Misra, S., and C. Ruf (2008), Detection of radio-frequency interference for the Aquarius radiometer, *IEEE Transactions on Geoscience and Remote Sensing,46*(10), 3123-3128, doi: 10.1109/TGRS.2008.920371.

Monahan, E., and I. O'Muircheartaigh (1980), Optimal power-law description of oceanic white-cap coverage dependence on wind speed, *J. Phys. Oceanography.*, 10, 2094-2099, doi: http://dx.doi.org/10.1175/1520-0485(1980)010<2094:OPLDOO>2.0.CO;2.

Moore, R., I. Birrer, E. Bracalente, G. Dome, and F. Wentz (1982), Evaluation of atmospheric attenuation from SMMR brightness temperature for the SEASAT satellite scatterometer, *J. Geophys. Res., 87*(C5), 3337-3354, doi: 10.1029/JC087iC05p03337.

Piepmeier, J., D. Long, and E. Njoku (2008), Stokes antenna temperatures, *IEEE Transactions on Geoscience and Remote Sensing, 46*(2), 516-527, doi: 10.1109/TGRS.2007.909597.

Piepmeier. J., S. Brown, J. Gales, L. Hong, G. Lagerloef, D. Le Vine, P. de Matthaeis, T. Meissner, R. Bindlish, and T. Jackson (2013), Aquarius radiometer post-launch calibration for product version 2, Aquarius Project Document: AQ-014-PS-0015, (http://podaac.jpl.nasa.gov/SeaSurfaceSalinity/Aquarius).

Powell, M., S. Houston, L. Amat, and N. Morisseau-Leroy (1998), The HRD real-time hurricane wind analysis system, *J. Wind Eng. Ind. Aerodyn,. 77/78*, 53-64, doi: 10.1016/S0167-6105(98)00131-7.

Reul, N., J. Tenerelli, B. Chapron, D. Vandemark, Y. Quilfen, and Y. Kerr (2012), SMOS satellite L-band radiometer: A new capability for ocean surface remote sensing in hurricanes, *J. Geophys. Res., 117*, C02006, doi: 10.1029/2011JC007474.

Reynolds, R., and T. Smith (1994), Improved global sea surface temperature analyses using optimum interpolation, *J. Climate 7*(6), 929–948, doi: 10.1175/1520-0442(1994)007<0929:IGSSTA>2.0.CO;2.

Ricciardulli, L., and F. Wentz (2011), Reprocessed QuikSCAT (V04) wind vectors with Ku-2011 Geophysical Model Function, RSS Technical Report 043011, Remote Sensing Systems, Santa Rosa, California, (http://www.remss.com/papers/rsstech/2011_043011_ricciardulli_qscat_ku2011.pdf).

Rybicki, G., and A. Lightman (1979), *Radiative Processes in Astrophysics*, Wiley, New York.

Verspeek, J., A. Stoffelen, M. Portabella, H. Bonekamp, C. Anderson, and J. F. Saldana (2010), Validation and calibration of ASCAT using CMOD5.n, *IEEE Transactions on Geoscience and Remote Sensing, 48*(1), 386 - 395, doi: 10.1109/TGRS.2009.2027896.

Weissman, D., B. Stiles, S. Hristova-Veleva, D. Long, D. Smith, K. Hilburn, and W. Jones (2012), Challenges to satellite sensors of ocean winds: Addressing precipitation effects, *J. Atmos. Oceanic Technol.*, *29*(3), 356–374, doi: 10.1175/JTECH-D-11-00054.1.

Wentz, F. (1991), A simplified wind vector algorithm for satellite scatterometers, *J. Atmos. Oceanic Technol. 8*(5)*,* 697 – 704, doi: http://dx.doi.org/10.1175/1520-0426(1991)008<0697:ASWVAF>2.0.CO;2.

Wentz, F., and D. Smith (1999), A model function for the ocean-normalized radar cross section at 14 GHz derived from NSCAT observations, *J. Geophys. Res., 105*(C5), 11499-11514, doi: 10.1029/98JC02148.

Wentz, F. (2005), The effects of cloud and rain on the Aquarius salinity retrieval, Algorithm Theoretical Basis Document, RSS Technical Report 3031805, Remote Sensing Systems, Santa Rosa, California, (http://www.remss.com/papers/aquarius/rain_effect_on_salinity.pdf).

Wentz, F. et al. (2012), Aquarius salinity retrieval algorithm, Algorithm Theoretical Basis Document, Version 2, Addendum I (2012), Addendum II (2013), Addendum III (2014), RSS Technical Report 082912, Remote Sensing Systems, Santa Rosa, California, (http://podaac.jpl.nasa.gov/SeaSurfaceSalinity/Aquarius).

Yin, X., J. Boutin, N. Martin, and P. Spurgeon, Optimization of L-band sea surface emissivity models deduced from SMOS data (2012), *IEEE Transactions on Geoscience and Remote Sensing, 50*(5), 1414 - 1426, doi: 10.1109/TGRS.2012.2184547.

Yueh, S. (2000), Estimates of Faraday rotation with passive microwave polarimetry for microwave remote sensing of Earth surfaces, *IEEE Transactions on Geoscience and Remote Sensing, 38*(5), 2434-2438, doi:10.1109/36.868900.

Yueh, S., S. Dinardo, A. Fore, and F. Li (2010), Passive and active L-band microwave observations and modeling of ocean surface winds, *IEEE Transactions on Geoscience and Remote Sensing, 48*(8), 3087-3100, doi:10.1109/36.752213.

Yueh, S., and J. Chaubell (2012), Sea surface salinity and wind retrieval using combined passive and active L-band microwave observations, *IEEE Transactions on Geoscience and Remote Sensing*, *50*(4), 1022-1032, doi:10.1109/TGRS.2011.2165075.

Yueh, S., A. Fore, A. Freedman, J. Chaubell, W. Tang, and G. Neumann (2012): Aquarius Scatterometer Algorithm Theoretical Basis Document, Version 1, Jet Propulsion Laboratory, March 15, 2012, (http://podaac.jpl.nasa.gov/SeaSurfaceSalinity/Aquarius).

Yueh, S., W. Tang, A. Fore, G, Neumann, A. Hayashi, A. Freedman, J. Chaubell, and G. Lagerloef (2013), L-band passive and active microwave geophysical model functions of ocean surface winds and applications to Aquarius retrieval, *IEEE Transactions on Geoscience and Remote Sensing*, *51*(9), 4619 -4662, doi:10.1109/TGRS.2013.2266915.

Tables

Table 1. Standard deviation (in m/s) of differences between various Aquarius L-band wind speed products (HHH, HH, CAP Version 2.5.1) and WindSat wind speeds.

Wind Speed Products	σ
Aquarius HHH - WindSat	0.70
Aquarius HH – WindSat	0.80
Aquarius CAP – WindSat	0.93

Table 2. Triple collocation: Aquarius HHH, WindSat, buoy wind speeds. The left side shows the standard deviation of the mutual differences. The right side shows the errors of the individual products estimated from the triple collocation method. All units are m/s.

Wind Speed Product Differences	σ	Individual Wind Speed Product	σ
Aquarius HHH - WindSat	0.61	Aquarius HHH	0.42
Aquarius HHH – Buoy	1.06	WindSat	0.44
Buoy - WindSat	1.07	Buoy	0.97

Table 3. Performance of surface roughness correction: RMS difference between measured and computed surface brightness temperatures for the 6 Aquarius channels (in Kelvin).

Input Parameters	1V	1H	2V	2H	3V	3H
NCEP wind speed only	0.362	0.374	0.363	0.396	0.359	0.431
NCEP wind speed + WH	0.356	0.365	0.358	0.385	0.354	0.414
HHH wind speed only	0.253	0.230	0.264	0.220	0.277	0.228
HHH wind speed + σ_{0VV}	0.249	0.211	0.261	0.204	0.272	0.207
HHH wind speed + σ_{0VV} + WH	0.244	0.207	0.256	0.200	0.268	0.205

Figures

Figure 1. The 0^{th} harmonic B_0 of the scatterometer GMF as function of wind speed for the channels VV (left), HH (middle), and VH (right). The Aquarius data are indicated by black diamonds for horn 1, blue triangles for horn 2 and red squares for horn 3. The full lines are the 5^{th} order polynomial fits. For readability, the error bars are shown only at every 3^{rd} data point.

Figure 2. The wind direction dependence of the scatterometer cross section σ_0 of Aquarius horn 3 channels VV (left), HH (middle), and VH (right) at 3 different wind speeds: 6.5 m/s (black diamonds), 10.5 m/s (blue triangles), 14.5 m/s (red squares).

Figure 3. Scatterometer GMF of Aquarius horn 3 channels VV (left) and HH (right): up-wind (black), cross-wind (blue), down-wind (red).

Figure 4. Left panel: The value of the form factor δ (specular emissivity relative to its value at $T_{ref} = 20^oC$) of Aquarius horn 3 as function of SST. Right panel: The wind induced emissivity averaged over a representative sample of wind speeds as function of SST. The full lines/squares are the Aquarius data. The dashed lines/triangles are the Aquarius data after dividing by the form factor δ. The blue graphs are for V-pol. The red graphs are for H-pol after shifting by -1.0 K for readability. The values have been multiplied by a common surface temperature of 290 K.

Figure 5. The harmonic coefficients A_k, k=0,1,2, of the wind induced emissivity GMF as function of wind speed for V-pol. The values have been multiplied by a common surface temperature of 290 K. The Aquarius data are indicated by black diamonds for horn 1, blue triangles for horn 2 and red squares for horn 3. The full lines are the 5^{th} order polynomial fits. For readability, the error bars are shown only at every 3^{rd} data point.

Figure 6. The harmonic coefficients A_k, k=0,1,2, of the wind induced emissivity GMF as function of wind speed for H-pol. The values have been multiplied by a common surface temperature of 290 K. The Aquarius data are indicated by black diamonds for horn 1, blue triangles for horn 2 and red squares for horn 3. The full lines are the 5^{th} order polynomial fits. For readability, the error bars are shown only at every 3^{rd} data point.

Figure 7. The wind direction dependence of the wind induced emissivity ΔE_W of Aquarius horn 3 V-pol (left) and H-pol (right) at 3 different wind speeds: 6.5 m/s (black diamonds), 10.5 m/s (blue triangles), 14.5 m/s (red squares). The values have been multiplied by a common surface temperature of 290 K and the isotropic part A_0 has been subtracted.

Figure 8. The wind direction dependence of the 3^{rd} Stokes parameters U at the ocean surface U_{surf} of Aquarius horn 1 at 4 different wind speeds: 7.5 m/s (black diamonds), 10.5 m/s (blue triangles), 13.5 m/s (green squares), 16.5 m/s (red circles). The symbols indicate the Aquarius data and the full lines the 2^{nd} order harmonic fit of equation (11). The values have been multiplied by a common surface temperature of 290 K.

Figure 9. Performance statistics of rain-free Aquarius wind speeds summed over all 3 horns and stratified with respect to WindSat wind speed. Dashed lines/triangles display the biases and full lines/squares display the standard deviation. The black curves are NCEP GDAS – WindSat wind speeds, the blue curves are Aquarius HH –WindSat wind speeds and the red curves are Aquarius

HHH – WindSat wind speeds. The x-axis wind speed values are the arithmetic average between WindSat wind speed and Aquarius / NCEP GDAS wind speeds.

Figure 10. Normalized joint probability distribution function for rain-free Aquarius HHH wind speeds versus collocated WindSat wind speeds. The contour lines are spaced approximately dual logarithmically in order to emphasize the distribution tails. The dashed black line represents the Aquarius-WindSat wind speed bias.

Figure 11. Normalized joint probability distribution function for rain-free Aquarius HHH wind speeds versus collocated buoy wind speeds. The contour lines are spaced approximately dual logarithmically in order to emphasize the distribution tails. The dashed black line represents the Aquarius-buoy wind speed bias.

Figure 12. Probability distribution function (in s/m) of rain-free Aquarius HHH wind speeds (red line) collocated with WindSat (purple), CAP Version 2.5.1 (light blue) and NCEP GDAS (green). The size of the wind speed bins is 0.1 m/s.

Figure 13. Probability distribution function (in s/m) of rain-free Aquarius HHH winds (red line) collocated with buoys (black). The size of the wind speed bins is 0.1 m/s.

Figure 14. Along-track cross section of rain-free Aquarius HHH (blue squares) and HH (green triangles) wind speeds (in m/s) for three storms: Left panel: Aquarius horn 2 on 09/06/2011 (Hurricane Katia). The black line is the HRD model wind speed field after shifting it along the storm track to the time of the ascending Aquarius overpass and resampling it to the Aquarius resolution. Middle panel: Aquarius horn 1 in extra-tropical cyclone centered near [50N, 50W] on 11/30/2012. Right panel: Aquarius horn 3 in rain intense extra-tropical cyclone centered near [40N, 180W] on 04/12/2013. In the last two cases the black line in the WindSat all-weather wind speed and the red line is the WindSat surface rain rate (mm/h).

Figure 15. The correction $\Delta E_1 (W_{HHH}, \sigma'_{0VV})$ to the wind induced emissivity for Aquarius horn 3. The left panel shows the population density in each $[W_{HHH}, \sigma'_{0VV}]$ bin, the middle panel shows ΔE_1 for the V-pol emissivity and the right panel shows ΔE_1 for the H-pol emissivity. The emissivity values have been multiplied by a common surface temperature of 290 K. The σ'_{0VV} denotes the VV scatterometer cross section after removing the wind direction signal. The values of σ'_{0VV} have been scaled to equivalent wind speeds: An interval of 1 m/s of the y-axis corresponds to a value of $\sigma'_{0VV} = 0.002$ (in real units).

Figure 16. The correction $\Delta E_2 (W_{HHH}, WH)$ to the wind induced emissivity for Aquarius horn 3. The left panel shows the population density in each $[W_{HHH}, WH]$ bin, the middle panel shows ΔE_2 for the V-pol emissivity and the right panel shows ΔE_2 for the H-pol emissivity. The emissivity values have been multiplied by a common surface temperature of 290 K.

Figure 17. The correction $\Delta E' (W_{NCEP}, WH)$ to the wind induced emissivity for Aquarius horn 3. The left panel shows the population density in each $[W_{NCEP}, WH]$ bin, the middle panel shows $\Delta E'$ for the V-pol emissivity and the right panel shows $\Delta E'$ for the H-pol emissivity. The emissivity values have been multiplied by a common surface temperature of 290 K.

Figure 18. Flow diagram of the Aquarius surface roughness correction algorithm.

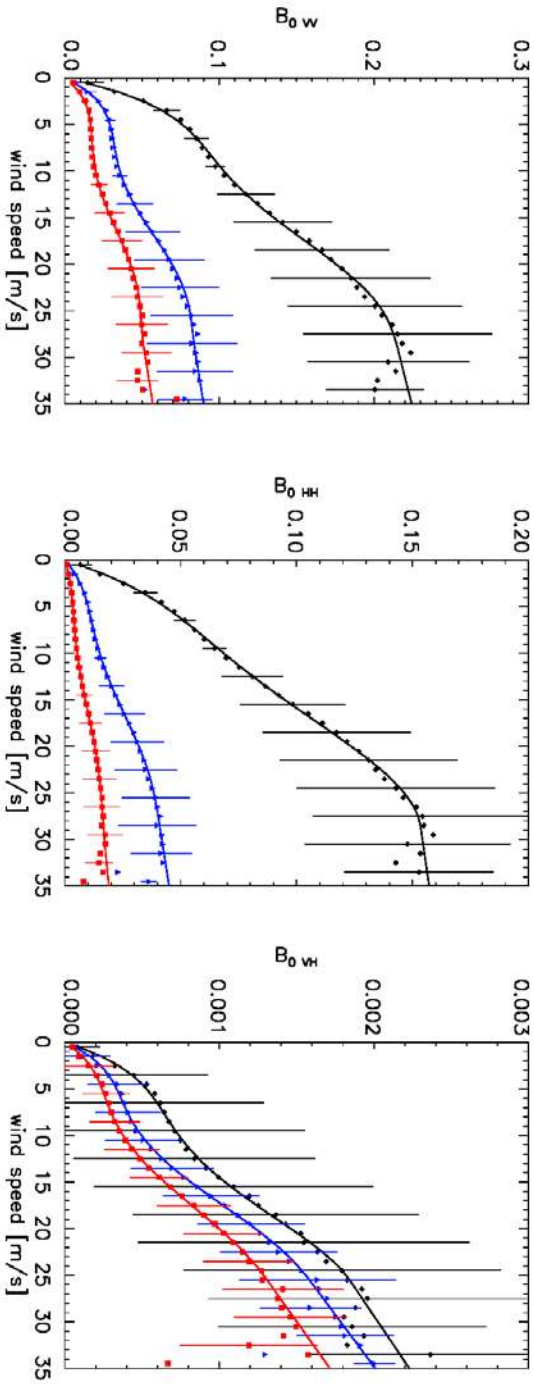
$B_{0\,w}$
0.0
0.1
0.2
0.3
0 5 10 15 20 25 30 35
wind speed [m/s]
$B_{0\,HF}$
0.00
0.05
0.10
0.15
0.20
0 5 10 15 20 25 30 35
wind speed [m/s]
$B_{0\,VF}$
0.000
0.001
0.002
0.003
0 5 10 15 20 25 30 35
wind speed [m/s]

Figure 1

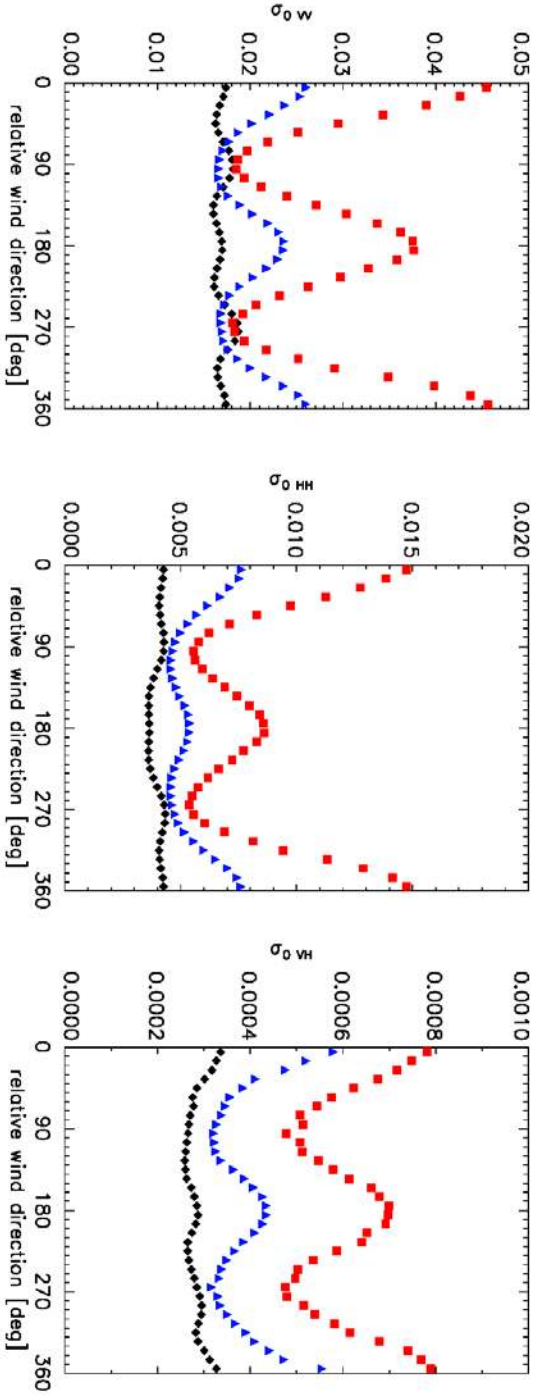
σ0 w
0.00
0.01
0.02
0.03
0.04
0.05
0
90
180
270
360
relative wind direction [deg]
σ0 HH
0.000
0.005
0.010
0.015
0.020
0
90
180
270
360
relative wind direction [deg]
σ0 VH
0.0000
0.0002
0.0004
0.0006
0.0008
0.0010
0
90
180
270
360
relative wind direction [deg]

Figure 2

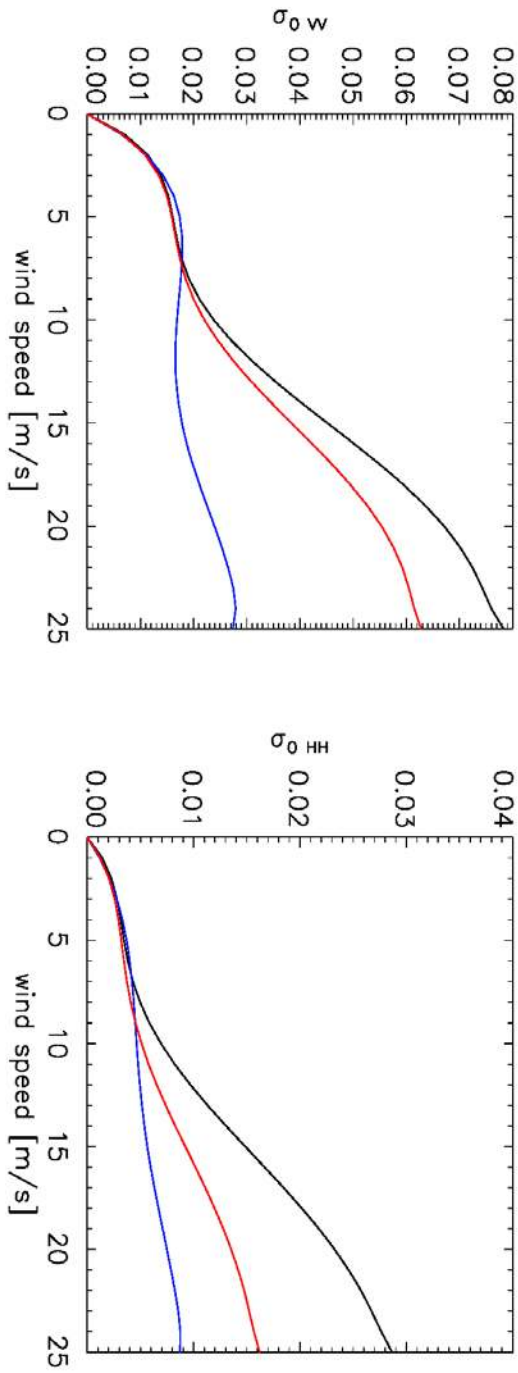
σ0 w
0.00
0.01
0.02
0.03
0.04
0.05
0.06
0.07
0.08
0
5
10
15
20
25
wind speed [m/s]
σ0 HH
0.00
0.01
0.02
0.03
0.04
0
5
10
15
20
25
wind speed [m/s]

Figure 3

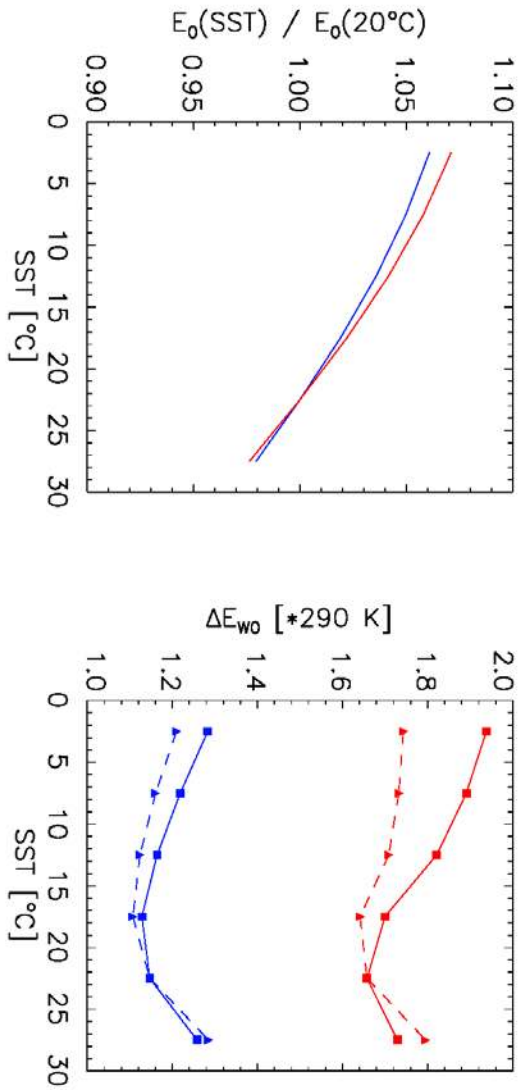
E0(SST) / E0(20°C)
0.90
0.95
1.00
1.05
1.10
0
5
10
15
20
25
30
SST [°C]
ΔEwo [*290 K]
1.0
1.2
1.4
1.6
1.8
2.0
0
5
10
15
20
25
30
SST [°C]

Figure 4

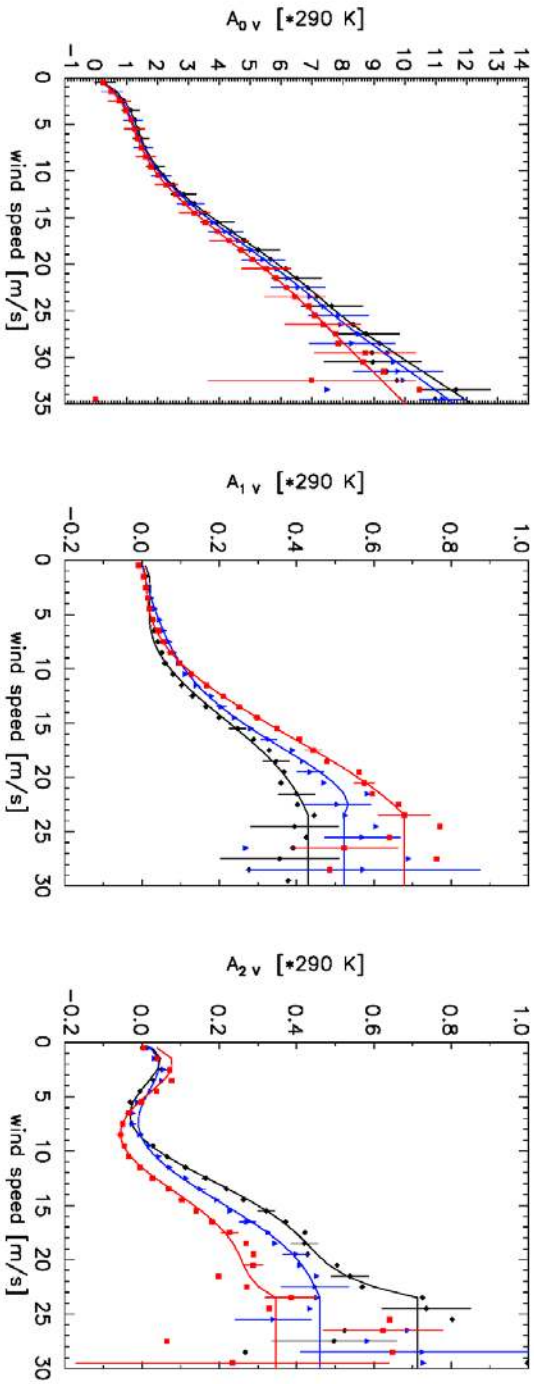
A0 v [*290 K]
wind speed [m/s]
A1 v [*290 K]
wind speed [m/s]
A2 v [*290 K]
wind speed [m/s]

Figure 5

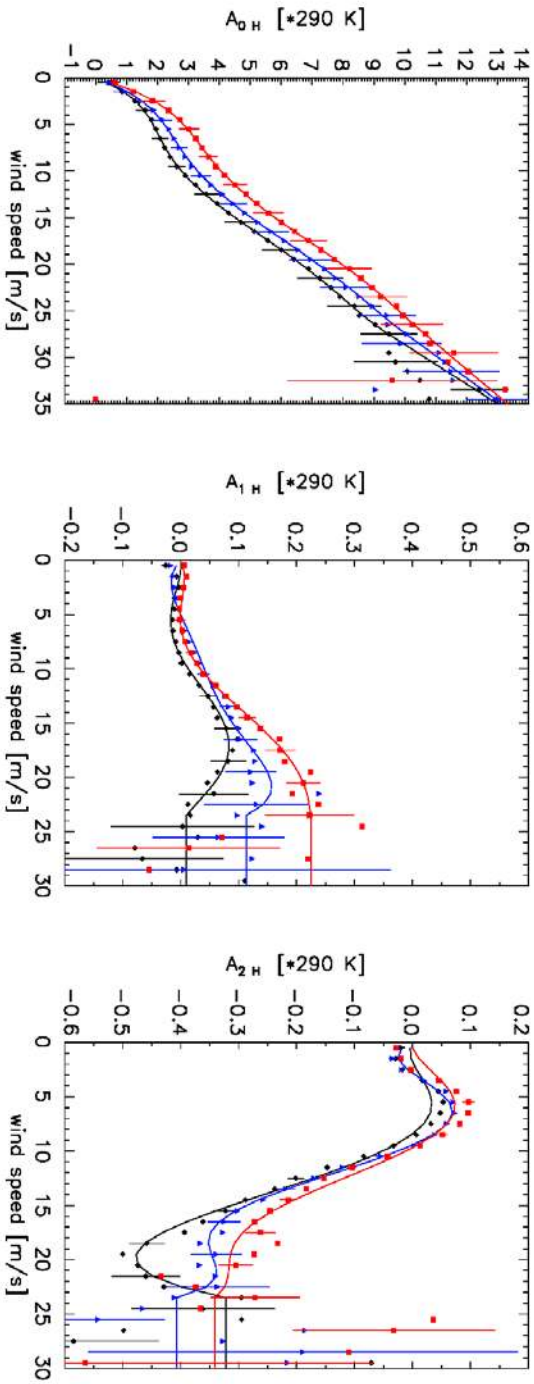
A0 H [*290 K]
wind speed [m/s]
A1 H [*290 K]
wind speed [m/s]
A2 H [*290 K]
wind speed [m/s]

Figure 6

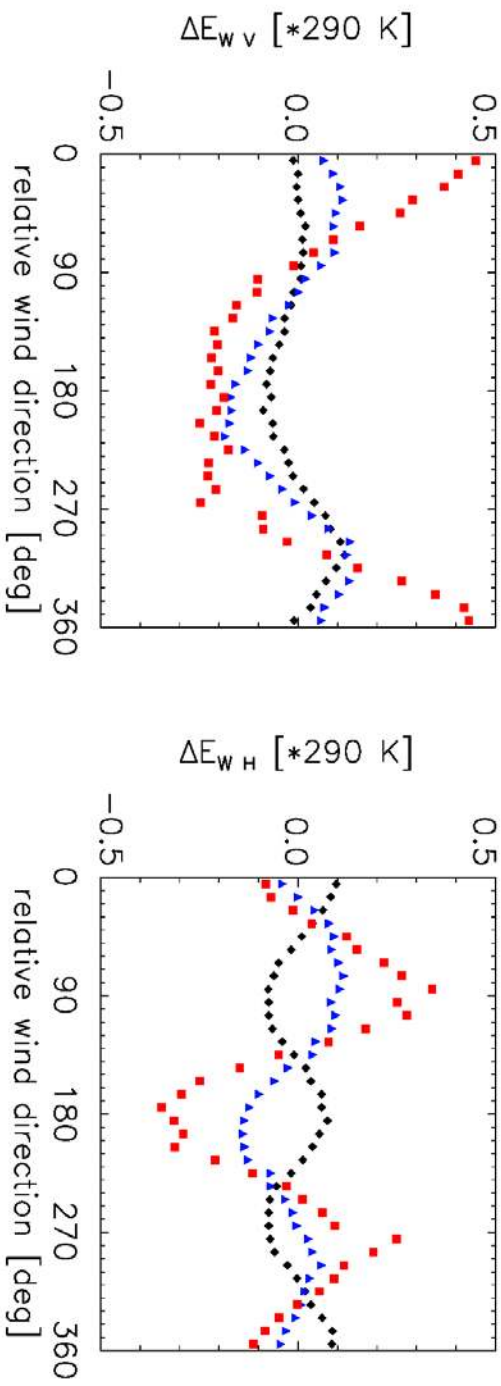
$\Delta E_{w\,v}$ [*290 K]
−0.5
0.0
0.5
0
90
180
270
360
relative wind direction [deg]
$\Delta E_{w\,h}$ [*290 K]
−0.5
0.0
0.5
0
90
180
270
360
relative wind direction [deg]

Figure 7

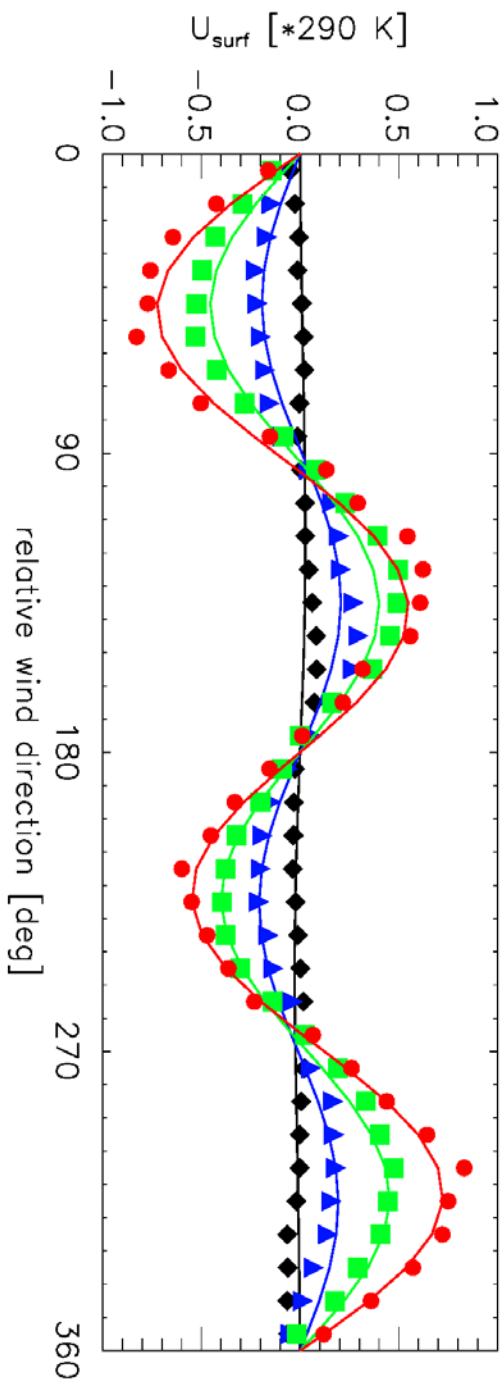
U_surf [*290 K]
−1.0
−0.5
0.0
0.5
1.0
0
90
180
270
360
relative wind direction [deg]

Figure 8

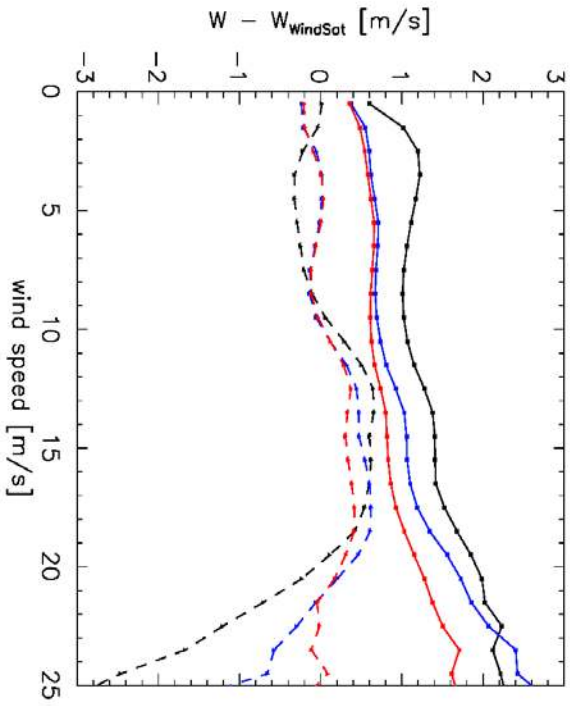

Figure 9

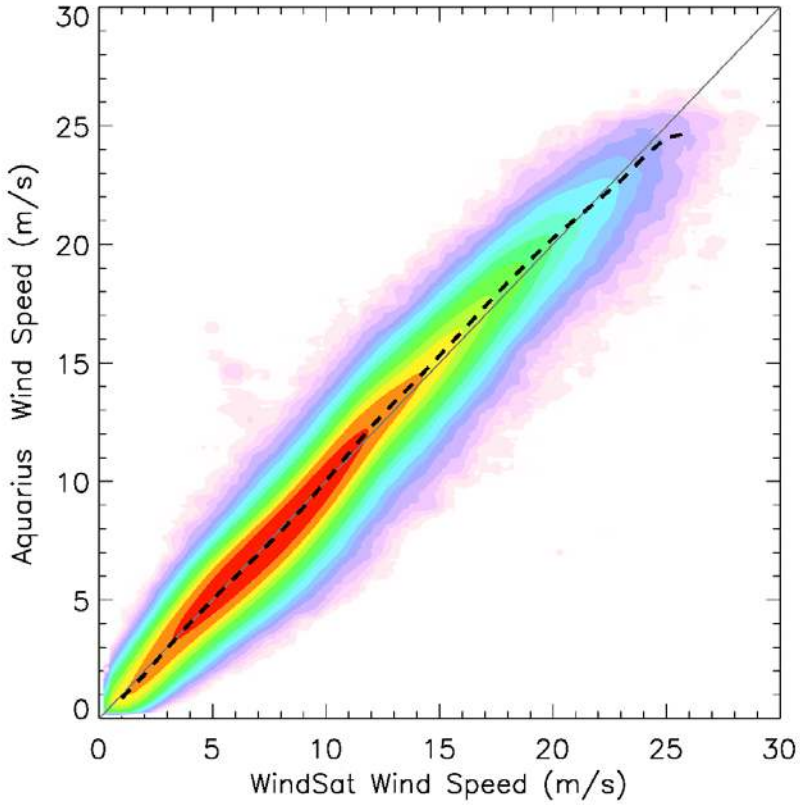

Figure 10

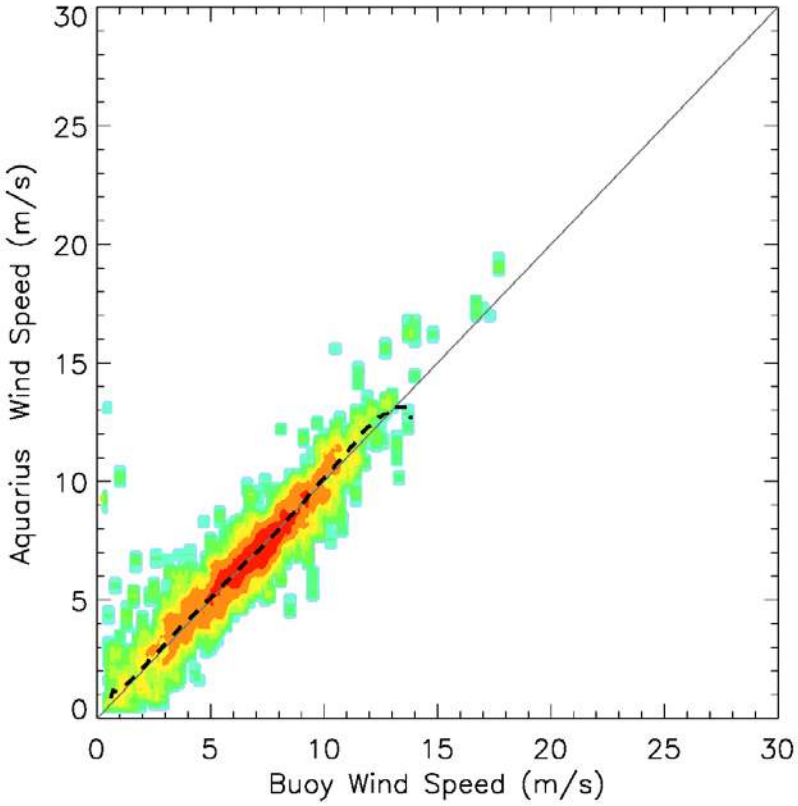

Figure 11

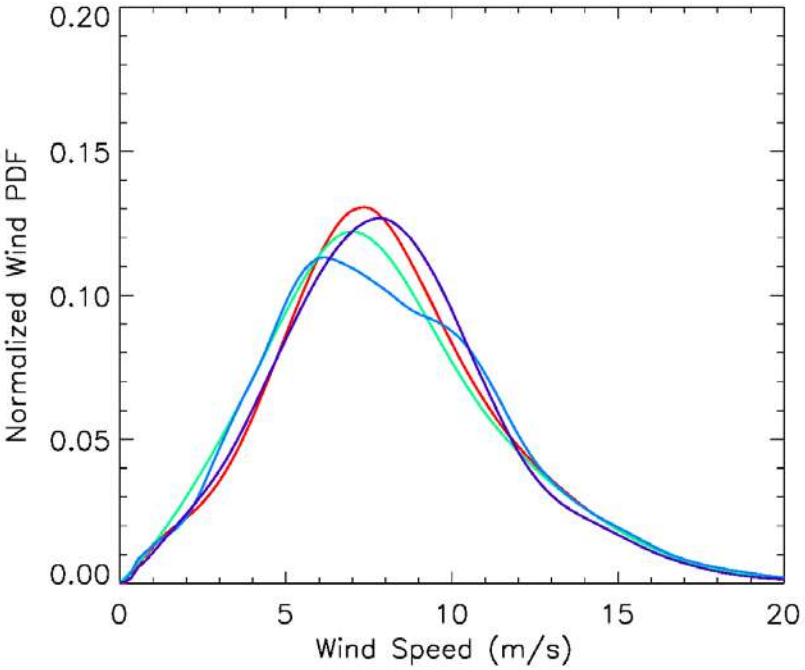
0.20
0.15
0.10
0.05
0.00
Normalized Wind PDF
0
5
10
15
20
Wind Speed (m/s)

Figure 12

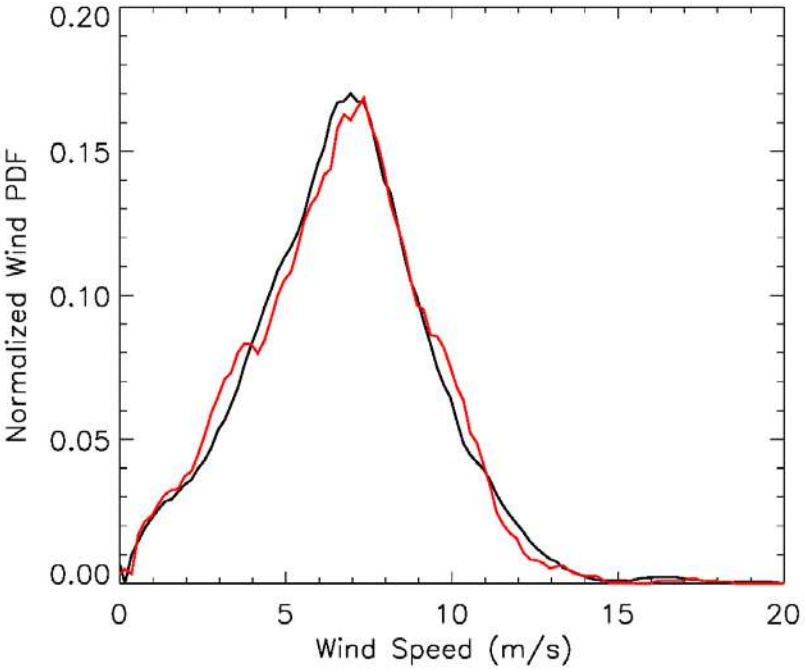
0.20
0.15
0.10
0.05
0.00
Normalized Wind PDF
0
5
10
15
20
Wind Speed (m/s)

Figure 13

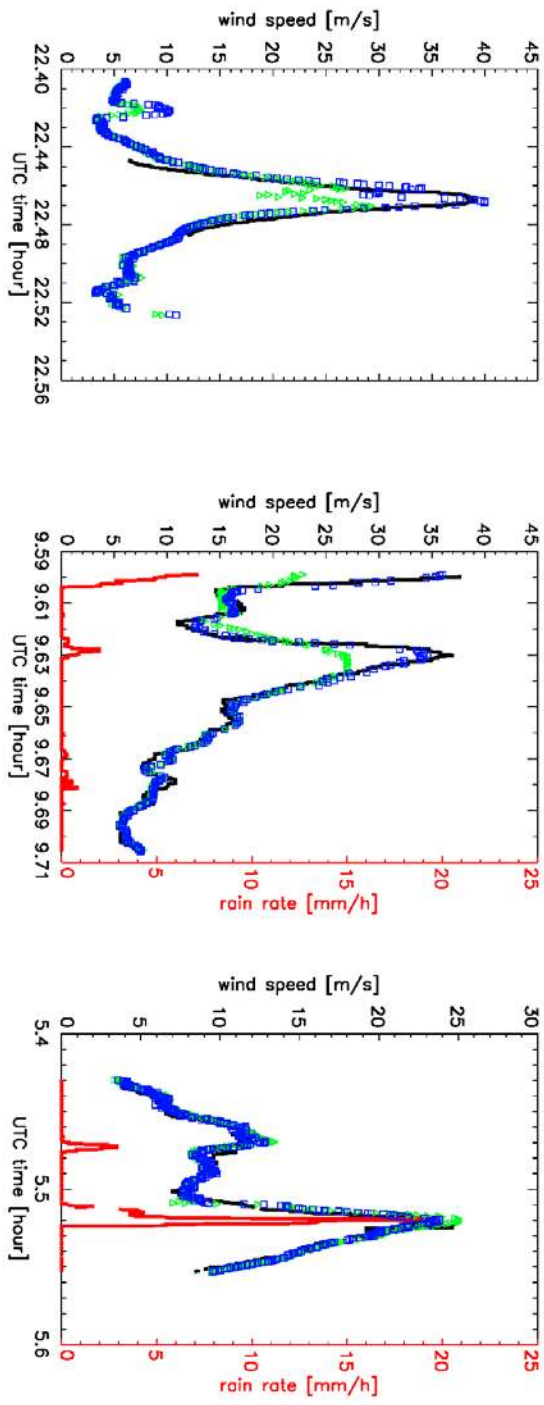

Figure 14

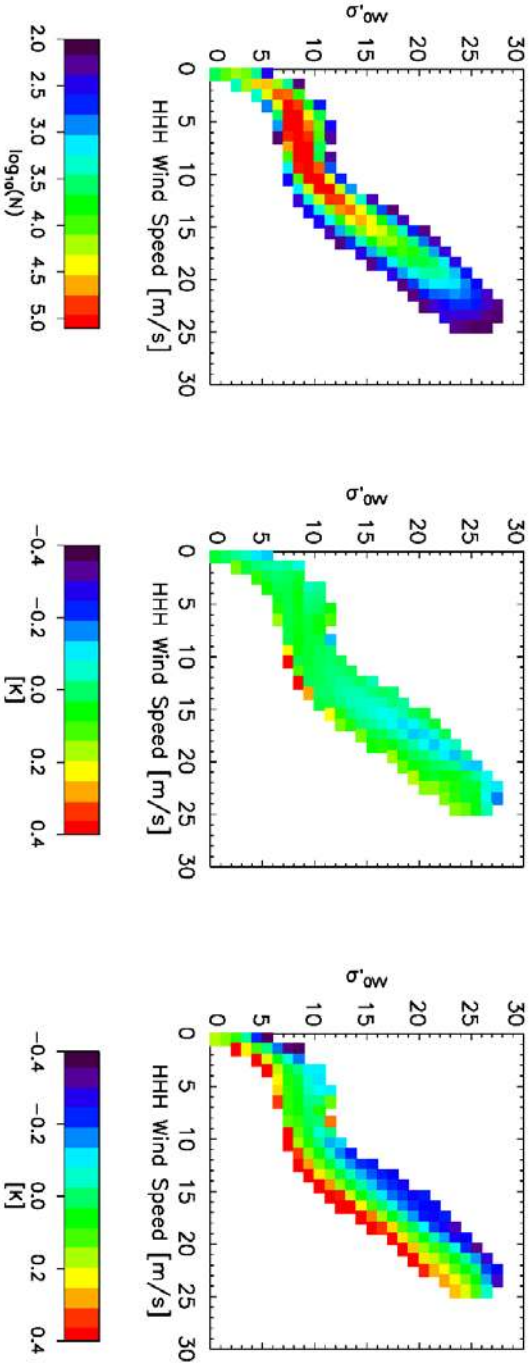

Figure 15

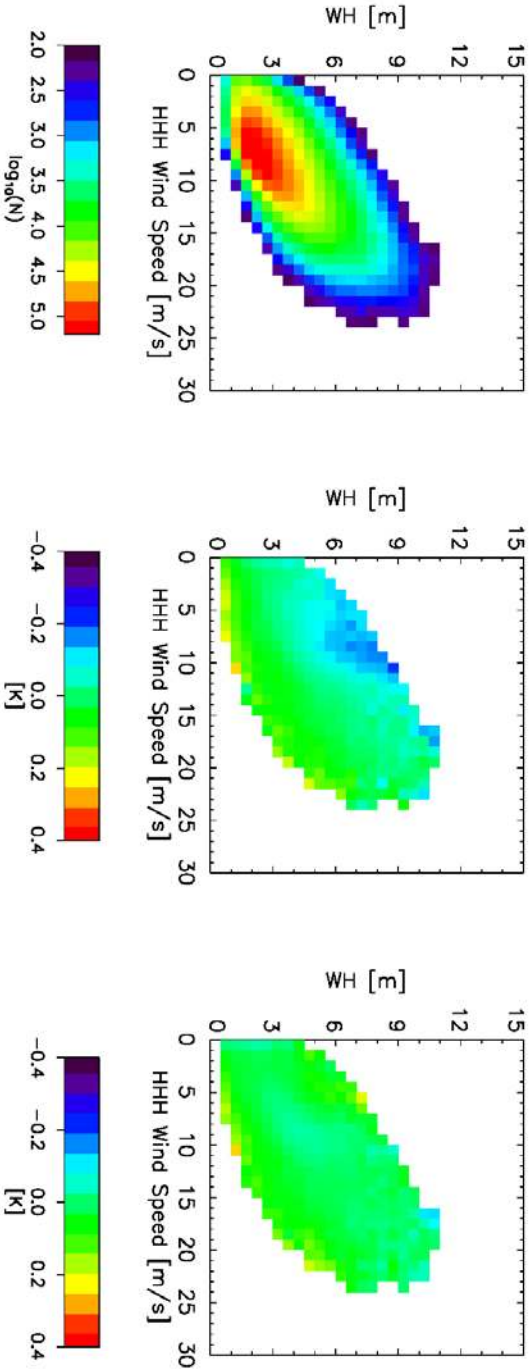
WH [m]
HHH Wind Speed [m/s]
log10(N)
WH [m]
HHH Wind Speed [m/s]
[K]
WH [m]
HHH Wind Speed [m/s]
[K]

Figure 16

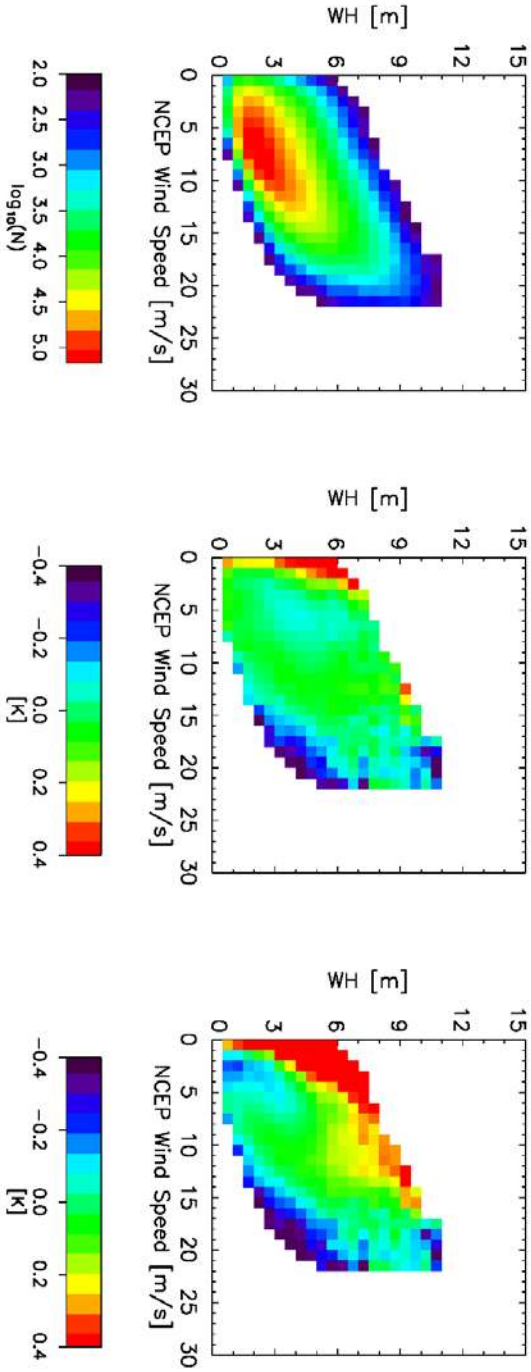
WH [m]
NCEP Wind Speed [m/s]
log10(N)
WH [m]
NCEP Wind Speed [m/s]
[K]
WH [m]
NCEP Wind Speed [m/s]
[K]

Figure 17

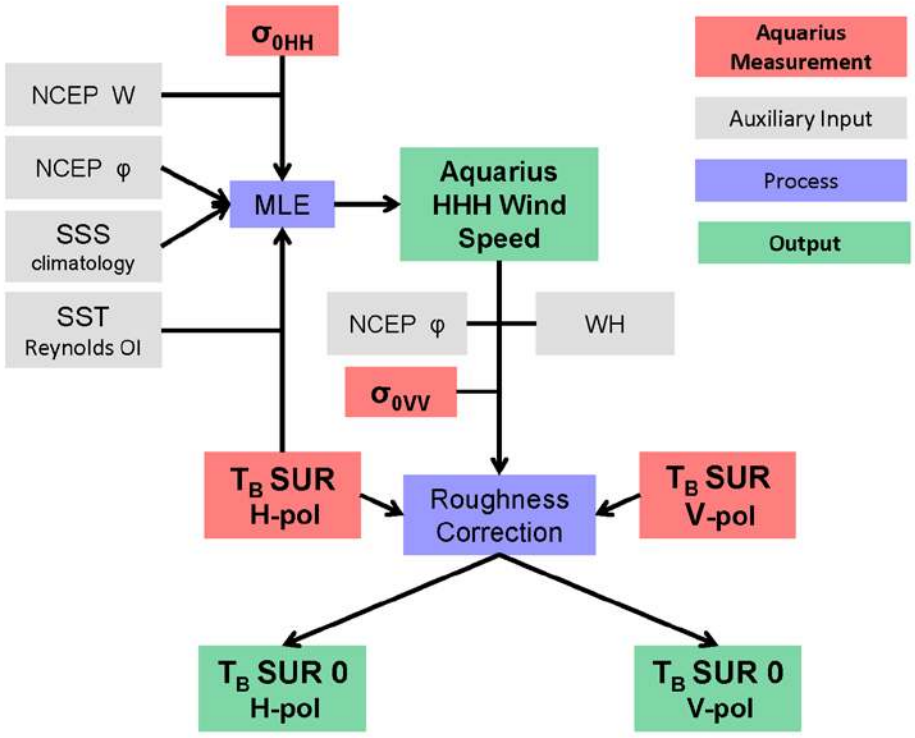
σ0HH
NCEP W
NCEP φ
SSS
climatology
SST
Reynolds OI
MLE
Aquarius
HHH Wind
Speed
NCEP φ
WH
σ0VV
TB SUR
H-pol
Roughness
Correction
TB SUR
V-pol
TB SUR 0
H-pol
TB SUR 0
V-pol
Aquarius
Measurement
Auxiliary Input
Process
Output

Figure 18

Auxiliary Material for

A geophysical model for the emission and scattering of L-band microwave radiation from rough ocean surfaces.

Thomas Meissner and Frank J. Wentz

(Remote Sensing Systems, 444 Tenth Street, Suite 200, Santa Rosa, CA 95401, USA)

Journal of Geophysical Research, Oceans, 2014

Introduction

This auxiliary material includes tables containing coefficients for the various geophysical model functions that are used in this publication.

1. ts01.txt: The coefficients b_{ki} of the 5th order polynomial fit to the harmonic coefficients of the scatterometer GMF. k=0,1,2 indicates the order of the harmonic and i=1,2,3,4,5 the order of the power in the polynomial. The values are provided for all 3 radiometers and polarizations VV, HH, and VH. The value for i=1,2,3,4,5 is the 1st column and the value for b_{ki} is the 2nd column.

2. ts02.txt: The coefficients a_{ki} of the 5th order polynomial fit to the harmonic coefficients of the wind induced emissivity GMF. k=0,1,2 indicates the order of the harmonic and i=1,2,3,4,5 the order of the power in the polynomial. The values are provided for all 3 radiometers and V-pol and H-pol. The value for i=1,2,3,4,5 is the 1st column and the value for a_{ki} is the 2nd column.

3. ts03.txt: Expected errors for the channels (scatterometer HH and radiometer H-pol) that are used in the MLE as a function of surface wind speed. The 1st column is the wind speed. The next 3 columns are the expected standard deviations of σ_{0HH} [in real units], T_{BH} [in K] and the NCEP background wind speed W_{NCEP} [in m/s] for radiometer 1, 2 and 3, respectively.

4. ts04.txt: The correction ΔE_1 (W_{HHH}, σ'_{0VV}) to the wind induced emissivity. The values are provided for all 3 radiometers and polarizations V-pol and H-pol. The 1st column is the HHH wind speed W_{HHH} [in m/s], the 2nd column is the scatterometer VV-pol cross section σ'_{0VV} after removing the wind direction signal [in real units], the 3rd column is the number of observation in each interval, and the last column the value of ΔE_1 [multiplied by 290 K]. Intervals with less than 100 observations are not listed.

5. ts05.txt: The correction ΔE_2 (W_{HHH}, WH) to the wind induced emissivity. The values are provided for all 3 radiometers and polarizations V-pol and H-pol. The 1st column is the HHH wind speed W_{HHH} [in m/s], the 2nd column is the significant wave height WH [in m], the 3rd column is the number of observation in each interval, and the last column the value of ΔE_2 [multiplied by 290 K]. Intervals with less than 100 observations are not listed.

ts01.txt

```
radiometer 1
VV
b 0i
  1    2.7669953402e-002
  2   -3.5648121980e-003
  3    2.5085738933e-004
  4   -7.6604470290e-006
  5    8.3403936421e-008

radiometer 1
VV
b 1i
  1    3.1471932686e-004
  2   -1.0708873066e-004
  3    9.8366727292e-006
  4   -1.5828345752e-007
  5   -2.3597221602e-009

radiometer 1
VV
b 2i
  1    1.9129701422e-003
  2   -1.4546678790e-003
  3    2.1484907649e-004
  4   -9.9712358461e-006
  5    1.5136841055e-007

radiometer 1
HH
b 0i
  1    1.2755914080e-002
  2   -1.1566306028e-003
  3    7.5880134855e-005
  4   -2.1193397012e-006
  5    1.9732074898e-008

radiometer 1
HH
b 1i
  1    3.6370936768e-004
  2   -1.1753728728e-004
  3    1.3593095709e-005
  4   -3.4977915542e-007
  5    8.1882224455e-010

radiometer 1
HH
b 2i
  1    1.5807451212e-003
  2   -9.5377945712e-004
  3    1.3424379381e-004
```

```
  4   -6.0496459000e-006
  5    8.9841023600e-008

radiometer 1
VH
b 0i
  1    1.9041911638e-004
  2   -2.4137499915e-005
  3    1.6633064884e-006
  4   -4.5692164746e-008
  5    4.1017449367e-010

radiometer 1
VH
b 1i
  1   -2.5270345066e-005
  2    1.9095363812e-005
  3   -2.7666404448e-006
  4    1.3956850131e-007
  5   -2.3159389660e-009

radiometer 1
VH
b 2i
  1   -3.0904528219e-005
  2    6.9945782218e-006
  3   -4.5969356549e-007
  4    1.4793445441e-008
  5   -2.0473917589e-010

radiometer 2
VV
b 0i
  1    1.2863352200e-002
  2   -2.0993592491e-003
  3    1.6518875147e-004
  4   -5.4682006056e-006
  5    6.4132838313e-008

radiometer 2
VV
b 1i
  1    5.2348832960e-004
  2   -2.0409803674e-004
  3    2.6073582526e-005
  4   -1.1566411871e-006
  5    1.7537140274e-008

radiometer 2
VV
b 2i
  1    5.5889743658e-004
  2   -5.0187584565e-004
  3    7.9280278992e-005
```

```
  4   -3.6902553692e-006
  5    5.4847783328e-008

radiometer 2
HH
b 0i
  1    3.7572819799e-003
  2   -5.3258749393e-004
  3    4.3724484672e-005
  4   -1.4681802479e-006
  5    1.7169850326e-008

radiometer 2
HH
b 1i
  1    3.3829156489e-004
  2   -1.3147938974e-004
  3    1.8137648631e-005
  4   -7.9436180922e-007
  5    1.1628671488e-008

radiometer 2
HH
b 2i
  1    3.7371603939e-004
  2   -2.4023678467e-004
  3    3.4716850703e-005
  4   -1.5485629837e-006
  5    2.2414676330e-008

radiometer 2
VH
b 0i
  1    1.3790708068e-004
  2   -2.2047630792e-005
  3    1.8770726934e-006
  4   -6.2770930814e-008
  5    7.2517799883e-010

radiometer 2
VH
b 1i
  1    4.7769227366e-007
  2    2.5545436707e-006
  3   -4.5579483792e-007
  4    2.5765445741e-008
  5   -4.5614845733e-010

radiometer 2
VH
b 2i
  1   -1.2471120703e-005
  2    2.0557144375e-006
  3    1.5545411606e-008
```

```
  4   -5.1412937047e-009
  5    1.0030170313e-010

radiometer 3
VV
b 0i
  1    7.9812841854e-003
  2   -1.4250014823e-003
  3    1.1846924116e-004
  4   -4.0865529161e-006
  5    4.9691503580e-008

radiometer 3
VV
b 1i
  1    2.8558723483e-004
  2   -1.1332749701e-004
  3    1.4903721848e-005
  4   -6.4922700321e-007
  5    9.4205608577e-009

radiometer 3
VV
b 2i
  1    4.4372478525e-004
  2   -3.1164511936e-004
  3    4.9980678917e-005
  4   -2.3909290707e-006
  5    3.6603560390e-008

radiometer 3
HH
b 0i
  1    1.4664950940e-003
  2   -2.4374331007e-004
  3    2.1823161004e-005
  4   -7.7367920090e-007
  5    9.4709584062e-009

radiometer 3
HH
b 1i
  1    1.2856275234e-004
  2   -5.0136994111e-005
  3    7.3669264038e-006
  4   -3.1710126109e-007
  5    4.4180628101e-009

radiometer 3
HH
b 2i
  1    1.5707164701e-004
  2   -9.3649029302e-005
  3    1.3860196514e-005
```

```
  4   -6.3232563194e-007
  5    9.3928175374e-009

radiometer 3
VH
b 0i
  1    9.7111150301e-005
  2   -1.5524769836e-005
  3    1.3641790391e-006
  4   -4.5902503063e-008
  5    5.3015300281e-010

radiometer 3
VH
b 1i
  1    2.3716636960e-006
  2    4.8176236632e-007
  3   -9.6942418523e-008
  4    6.1691070717e-009
  5   -1.1276100998e-010

radiometer 3
VH
b 2i
  1   -2.2014555824e-006
  2   -3.4305836137e-007
  3    2.4793080821e-007
  4   -1.6036928492e-008
  5    2.8900573608e-010
```

ts02.txt

```
radiometer 1
V
a 0i
  1    5.7894060320e-001
  2   -1.0473595790e-001
  3    9.9200140518e-003
  4   -3.6291757411e-004
  5    4.6589912401e-006

radiometer 1
V
a 1i
  1    2.1216534279e-002
  2   -7.1813519762e-003
  3    9.1738225933e-004
  4   -3.9535822500e-005
  5    5.6502242949e-007

radiometer 1
V
a 2i
  1    6.6222103677e-002
  2   -2.8388133825e-002
  3    3.7501350060e-003
  4   -1.8446699362e-004
  5    3.1286830745e-006

radiometer 1
H
a 0i
  1    7.7153019419e-001
  2   -1.2715188465e-001
  3    1.1329089683e-002
  4   -4.0789149957e-004
  5    5.2183370672e-006

radiometer 1
H
a 1i
  1    3.3306056615e-003
  2   -3.7204789320e-003
  3    6.2494297864e-004
  4   -3.2678064089e-005
  5    5.3603866560e-007

radiometer 1
H
a 2i
  1   -1.2192070798e-002
  2    8.8557322073e-003
  3   -1.2734161054e-003
```

```
  4    5.1704466145e-005
  5   -5.8171521631e-007

radiometer 2
V
a 0i
  1    5.0281588143e-001
  2   -8.4035755450e-002
  3    7.8518455026e-003
  4   -2.8030380618e-004
  5    3.5109805876e-006

radiometer 2
V
a 1i
  1    1.5596703582e-003
  2    2.3582984624e-003
  3   -3.4662668911e-004
  4    2.6606348124e-005
  5   -6.1842609629e-007

radiometer 2
V
a 2i
  1    5.1196349082e-002
  2   -1.8202980254e-002
  3    2.0749477038e-003
  4   -8.6995183107e-005
  5    1.2436524520e-006

radiometer 2
H
a 0i
  1    8.4965177001e-001
  2   -1.2443856200e-001
  3    1.0359930394e-002
  4   -3.5549109274e-004
  5    4.3636667626e-006

radiometer 2
H
a 1i
  1   -1.8863269506e-002
  2    6.5676785996e-003
  3   -7.3111819961e-004
  4    3.7255111733e-005
  5   -6.8989289663e-007

radiometer 2
H
a 2i
  1   -4.8938315835e-002
  2    2.6541378947e-002
  3   -3.7836135549e-003
```

```
  4    1.9204055354e-004
  5   -3.2620602022e-006

radiometer 3
V
a 0i
  1    4.7027203005e-001
  2   -7.6334662983e-002
  3    6.9857495929e-003
  4   -2.4303426684e-004
  5    2.9390853226e-006

radiometer 3
V
a 1i
  1    9.1197181127e-003
  2   -3.0431623312e-003
  3    5.0839571367e-004
  4   -2.0375986729e-005
  5    2.4580823525e-007

radiometer 3
V
a 2i
  1    9.3408423686e-002
  2   -3.3492931571e-002
  3    3.8025601997e-003
  4   -1.6925890570e-004
  5    2.6396519557e-006

radiometer 3
H
a 0i
  1    1.0601673642e+000
  2   -1.4677107298e-001
  3    1.1480019211e-002
  4   -3.8084012081e-004
  5    4.5485097434e-006

radiometer 3
H
a 1i
  1    9.6160121528e-003
  2   -4.3505334225e-003
  3    6.0718079191e-004
  4   -2.7536464802e-005
  5    4.0733177632e-007

radiometer 3
H
a 2i
  1   -5.1974877527e-003
  2    1.0855313411e-002
  3   -1.8411735248e-003
```

```
4    9.5714130699e-005
5   -1.6059448322e-006
```

ts03.txt

Wind speed	Radiometer 1			Radiometer 2			Radiometer 3		
	sigma0 HH	TB H	W NCEP	sigma0 HH	TB H	W NCEP	sigma0 HH	TB H	W NCEP
0	0.002162	0.204694	1.118146	0.000478	0.196523	1.118146	0.000222	0.218601	1.118146
1	0.002811	0.216598	1.035427	0.000657	0.227773	1.035427	0.000253	0.244698	1.035427
2	0.003554	0.237533	0.941831	0.000837	0.260301	0.941831	0.000324	0.281098	0.941831
3	0.003397	0.244513	0.942946	0.000803	0.255531	0.942946	0.000319	0.281507	0.942946
4	0.003128	0.241825	0.961688	0.000755	0.244097	0.961688	0.000273	0.265312	0.961688
5	0.003005	0.237435	0.967645	0.000692	0.233588	0.967645	0.000257	0.253008	0.967645
6	0.002742	0.232175	0.965748	0.000605	0.223152	0.965748	0.000247	0.241897	0.965748
7	0.002561	0.232554	0.966377	0.000561	0.21475	0.966377	0.000251	0.232883	0.966377
8	0.002669	0.238376	0.982044	0.000589	0.214677	0.982044	0.000252	0.230973	0.982044
9	0.003058	0.243367	1.036862	0.000661	0.223211	1.036862	0.000284	0.241124	1.036862
10	0.003575	0.246757	1.121006	0.000768	0.235413	1.121006	0.000364	0.259865	1.121006
11	0.004267	0.264352	1.2319	0.000999	0.257846	1.2319	0.000474	0.286123	1.2319
12	0.005234	0.292643	1.344265	0.001326	0.291839	1.344265	0.000663	0.316673	1.344265
13	0.006088	0.316431	1.407236	0.001615	0.321048	1.407236	0.000803	0.339212	1.407236
14	0.006793	0.336506	1.427256	0.001938	0.336179	1.427256	0.000874	0.353528	1.427256
15	0.007678	0.361546	1.449059	0.002158	0.352008	1.449059	0.001027	0.377721	1.449059
16	0.008665	0.38954	1.527995	0.002431	0.393054	1.527995	0.001215	0.419884	1.527995
17	0.009586	0.416811	1.583605	0.002833	0.444346	1.583605	0.001321	0.467506	1.583605
18	0.010366	0.455024	1.64357	0.003222	0.483129	1.64357	0.001476	0.495254	1.64357
19	0.011534	0.489119	1.840392	0.003846	0.5	1.840392	0.001586	0.5	1.840392
20	0.012506	0.5	2.07388	0.003906	0.5	2.07388	0.001705	0.5	2.07388
21	0.013046	0.5	2.328262	0.003823	0.5	2.328262	0.001769	0.5	2.328262
22	0.013826	0.5	2.637159	0.004314	0.5	2.637159	0.0016	0.5	2.637159
23	0.014606	0.5	2.946057	0.004805	0.5	2.946057	0.001431	0.5	2.946057
24	0.015386	0.5	3.254955	0.005297	0.5	3.254955	0.001262	0.5	3.254955
25	0.016166	0.5	3.563852	0.005788	0.5	3.563852	0.001094	0.5	3.563852

ts04.txt

```
radiometer 1
V
    0.5   0.0040      10229     0.0040
    0.5   0.0120      15912    -0.0049
    0.5   0.0200      13403    -0.0292
    0.5   0.0280       3965    -0.0574
    0.5   0.0360        292    -0.0567

    1.5   0.0120       1045     0.1917
    1.5   0.0200       8447     0.0422
    1.5   0.0280      23236    -0.0055
    1.5   0.0360      30708    -0.0282
    1.5   0.0440      18143    -0.0519
    1.5   0.0520       3553    -0.0638
    1.5   0.0600        163    -0.0712

    2.5   0.0280        162     0.8728
    2.5   0.0360       3571     0.1038
    2.5   0.0440      25586    -0.0011
    2.5   0.0520      52715    -0.0298
    2.5   0.0600      38559    -0.0265
    2.5   0.0680       3244    -0.0332

    3.5   0.0440        114     0.6997
    3.5   0.0520       5147     0.0434
    3.5   0.0600      66566     0.0051
    3.5   0.0680     117641     0.0068
    3.5   0.0760      13183    -0.0132
    3.5   0.0840        363     0.0133

    4.5   0.0600       2566     0.0942
    4.5   0.0680     117475     0.0218
    4.5   0.0760     181912     0.0067
    4.5   0.0840      23573    -0.0138
    4.5   0.0920       1426     0.0165

    5.5   0.0680       9084     0.0769
    5.5   0.0760     255013     0.0147
    5.5   0.0840     163786    -0.0094
    5.5   0.0920      26611    -0.0151
    5.5   0.1000       1128     0.0319

    6.5   0.0680        284     0.4528
    6.5   0.0760      47586     0.0516
    6.5   0.0840     401153     0.0090
    6.5   0.0920     107114    -0.0218
    6.5   0.1000       8804    -0.0148
    6.5   0.1080        186    -0.0664

    7.5   0.0760       2694     0.1210
    7.5   0.0840     195813     0.0366
```

7.5	0.0920	368850	0.0059
7.5	0.1000	28063	-0.0492
7.5	0.1080	960	-0.1195
7.5	0.1160	117	-0.2181
8.5	0.0760	143	0.3551
8.5	0.0840	22244	0.0956
8.5	0.0920	370929	0.0276
8.5	0.1000	137197	-0.0021
8.5	0.1080	3190	-0.1954
8.5	0.1160	456	-0.1821
9.5	0.0840	2365	0.1300
9.5	0.0920	93385	0.0497
9.5	0.1000	297331	0.0140
9.5	0.1080	31280	-0.0213
9.5	0.1160	1331	-0.2402
9.5	0.1240	277	-0.2669
10.5	0.0840	196	0.2080
10.5	0.0920	12724	0.0602
10.5	0.1000	143421	0.0144
10.5	0.1080	148377	0.0005
10.5	0.1160	9419	-0.0241
10.5	0.1240	626	-0.1950
10.5	0.1320	172	-0.2918
11.5	0.0920	1318	0.0827
11.5	0.1000	28781	0.0056
11.5	0.1080	124940	-0.0128
11.5	0.1160	75412	-0.0026
11.5	0.1240	4930	-0.0056
11.5	0.1320	471	-0.1132
11.5	0.1400	131	-0.1285
12.5	0.0920	213	0.1929
12.5	0.1000	3758	-0.0047
12.5	0.1080	35094	-0.0378
12.5	0.1160	88575	-0.0327
12.5	0.1240	45176	-0.0183
12.5	0.1320	4269	0.0054
12.5	0.1400	484	0.0240
12.5	0.1480	140	0.1246
13.5	0.1000	509	0.0009
13.5	0.1080	4869	-0.0565
13.5	0.1160	30330	-0.0682
13.5	0.1240	59861	-0.0609
13.5	0.1320	31760	-0.0447
13.5	0.1400	4774	-0.0139
13.5	0.1480	604	0.0817
13.5	0.1560	175	0.1220
14.5	0.1000	131	-0.0217

14.5	0.1080	651	−0.0583
14.5	0.1160	4446	−0.0932
14.5	0.1240	20554	−0.1014
14.5	0.1320	38038	−0.0852
14.5	0.1400	24197	−0.0616
14.5	0.1480	5144	−0.0345
14.5	0.1560	766	0.0268
14.5	0.1640	215	0.0989
15.5	0.1080	194	0.1461
15.5	0.1160	550	−0.0181
15.5	0.1240	2942	−0.1073
15.5	0.1320	13537	−0.1077
15.5	0.1400	24828	−0.1047
15.5	0.1480	17890	−0.0941
15.5	0.1560	5035	−0.0606
15.5	0.1640	947	0.0091
15.5	0.1720	268	0.0863
15.5	0.1800	117	0.1320
16.5	0.1160	154	0.0301
16.5	0.1240	520	−0.0560
16.5	0.1320	2365	−0.1073
16.5	0.1400	8451	−0.1184
16.5	0.1480	15088	−0.1139
16.5	0.1560	12509	−0.1043
16.5	0.1640	4611	−0.0822
16.5	0.1720	1018	−0.0293
16.5	0.1800	272	0.0479
17.5	0.1240	126	−0.0248
17.5	0.1320	382	−0.0384
17.5	0.1400	1359	−0.0659
17.5	0.1480	4988	−0.0952
17.5	0.1560	8956	−0.1028
17.5	0.1640	7895	−0.1081
17.5	0.1720	3576	−0.0904
17.5	0.1800	979	−0.0240
17.5	0.1880	276	0.0649
17.5	0.1960	128	0.0966
18.5	0.1320	115	0.0642
18.5	0.1400	239	−0.0742
18.5	0.1480	970	−0.0388
18.5	0.1560	2837	−0.0409
18.5	0.1640	5114	−0.0814
18.5	0.1720	5083	−0.0891
18.5	0.1800	2822	−0.0953
18.5	0.1880	927	−0.0424
18.5	0.1960	288	−0.0019
18.5	0.2040	116	0.1495
19.5	0.1480	190	0.0910
19.5	0.1560	607	−0.0046

19.5	0.1640	1772	-0.0233
19.5	0.1720	2704	-0.0299
19.5	0.1800	2936	-0.0606
19.5	0.1880	2050	-0.0844
19.5	0.1960	886	-0.0483
19.5	0.2040	251	0.0143
20.5	0.1560	139	0.0551
20.5	0.1640	400	0.0616
20.5	0.1720	946	0.0717
20.5	0.1800	1416	0.0130
20.5	0.1880	1558	-0.0229
20.5	0.1960	1376	-0.0608
20.5	0.2040	658	-0.0552
21.5	0.1640	104	0.1418
21.5	0.1720	311	0.0881
21.5	0.1800	619	0.0739
21.5	0.1880	920	0.0751
21.5	0.1960	940	0.0376
21.5	0.2040	657	0.0172
22.5	0.1720	114	0.1164
22.5	0.1800	226	0.1316
22.5	0.1880	317	0.1181
22.5	0.1960	453	0.0921
22.5	0.2040	477	0.0927
23.5	0.1880	174	0.1593
23.5	0.1960	207	0.1245
23.5	0.2040	287	0.1823
24.5	0.1960	133	0.1494
24.5	0.2040	176	0.1943
25.5	0.1960	112	0.2196
25.5	0.2040	112	0.2847

radiometer 1
H

0.5	0.0040	10229	0.1111
0.5	0.0120	15912	0.0701
0.5	0.0200	13403	-0.0279
0.5	0.0280	3965	-0.2038
0.5	0.0360	292	-0.4010
1.5	0.0120	1045	0.4792
1.5	0.0200	8447	0.2326
1.5	0.0280	23236	0.0823
1.5	0.0360	30708	-0.0156
1.5	0.0440	18143	-0.1487
1.5	0.0520	3553	-0.3431
1.5	0.0600	163	-0.5406

2.5	0.0280	162	1.0679
2.5	0.0360	3571	0.3179
2.5	0.0440	25586	0.0895
2.5	0.0520	52715	-0.0316
2.5	0.0600	38559	-0.1350
2.5	0.0680	3244	-0.2560
3.5	0.0440	114	1.0214
3.5	0.0520	5147	0.1810
3.5	0.0600	66566	0.0312
3.5	0.0680	117641	-0.0319
3.5	0.0760	13183	-0.0895
3.5	0.0840	363	-0.1502
4.5	0.0600	2566	0.2171
4.5	0.0680	117475	0.0619
4.5	0.0760	181912	-0.0044
4.5	0.0840	23573	-0.0816
4.5	0.0920	1426	-0.0944
5.5	0.0680	9084	0.1822
5.5	0.0760	255013	0.0495
5.5	0.0840	163786	-0.0401
5.5	0.0920	26611	-0.1085
5.5	0.1000	1128	-0.1017
6.5	0.0680	284	0.7073
6.5	0.0760	47586	0.1135
6.5	0.0840	401153	0.0134
6.5	0.0920	107114	-0.0877
6.5	0.1000	8804	-0.1140
6.5	0.1080	186	-0.1105
7.5	0.0760	2694	0.1950
7.5	0.0840	195813	0.0645
7.5	0.0920	368850	-0.0199
7.5	0.1000	28063	-0.1247
7.5	0.1080	960	-0.1461
7.5	0.1160	117	-0.1363
8.5	0.0760	143	0.4716
8.5	0.0840	22244	0.1540
8.5	0.0920	370929	0.0327
8.5	0.1000	137197	-0.0614
8.5	0.1080	3190	-0.2427
8.5	0.1160	456	-0.1669
9.5	0.0840	2365	0.2028
9.5	0.0920	93385	0.1054
9.5	0.1000	297331	0.0007
9.5	0.1080	31280	-0.1349
9.5	0.1160	1331	-0.2978
9.5	0.1240	277	-0.3318

10.5	0.0840	196	0.3752
10.5	0.0920	12724	0.1592
10.5	0.1000	143421	0.0649
10.5	0.1080	148377	-0.0437
10.5	0.1160	9419	-0.1831
10.5	0.1240	626	-0.2895
10.5	0.1320	172	-0.3823
11.5	0.0920	1318	0.2875
11.5	0.1000	28781	0.1161
11.5	0.1080	124940	0.0276
11.5	0.1160	75412	-0.0829
11.5	0.1240	4930	-0.2067
11.5	0.1320	471	-0.2945
11.5	0.1400	131	-0.3131
12.5	0.0920	213	0.7051
12.5	0.1000	3758	0.2165
12.5	0.1080	35094	0.0760
12.5	0.1160	88575	-0.0058
12.5	0.1240	45176	-0.1136
12.5	0.1320	4269	-0.2198
12.5	0.1400	484	-0.2546
12.5	0.1480	140	-0.2441
13.5	0.1000	509	0.5187
13.5	0.1080	4869	0.1780
13.5	0.1160	30330	0.0528
13.5	0.1240	59861	-0.0349
13.5	0.1320	31760	-0.1424
13.5	0.1400	4774	-0.2352
13.5	0.1480	604	-0.2673
13.5	0.1560	175	-0.2654
14.5	0.1000	131	0.9524
14.5	0.1080	651	0.3649
14.5	0.1160	4446	0.1461
14.5	0.1240	20554	0.0284
14.5	0.1320	38038	-0.0559
14.5	0.1400	24197	-0.1610
14.5	0.1480	5144	-0.2479
14.5	0.1560	766	-0.2922
14.5	0.1640	215	-0.3405
15.5	0.1080	194	0.7996
15.5	0.1160	550	0.4248
15.5	0.1240	2942	0.1314
15.5	0.1320	13537	0.0236
15.5	0.1400	24828	-0.0689
15.5	0.1480	17890	-0.1733
15.5	0.1560	5035	-0.2564
15.5	0.1640	947	-0.2959
15.5	0.1720	268	-0.3187

15.5	0.1800	117	−0.3155
16.5	0.1160	154	0.8530
16.5	0.1240	520	0.3965
16.5	0.1320	2365	0.1563
16.5	0.1400	8451	0.0261
16.5	0.1480	15088	−0.0632
16.5	0.1560	12509	−0.1681
16.5	0.1640	4611	−0.2538
16.5	0.1720	1018	−0.2975
16.5	0.1800	272	−0.3197
17.5	0.1240	126	0.6882
17.5	0.1320	382	0.3837
17.5	0.1400	1359	0.2032
17.5	0.1480	4988	0.0598
17.5	0.1560	8956	−0.0550
17.5	0.1640	7895	−0.1661
17.5	0.1720	3576	−0.2483
17.5	0.1800	979	−0.3052
17.5	0.1880	276	−0.3167
17.5	0.1960	128	−0.3449
18.5	0.1320	115	0.6936
18.5	0.1400	239	0.3662
18.5	0.1480	970	0.2053
18.5	0.1560	2837	0.0866
18.5	0.1640	5114	−0.0374
18.5	0.1720	5083	−0.1528
18.5	0.1800	2822	−0.2408
18.5	0.1880	927	−0.3062
18.5	0.1960	288	−0.3596
18.5	0.2040	116	−0.2853
19.5	0.1480	190	0.4465
19.5	0.1560	607	0.2389
19.5	0.1640	1772	0.1324
19.5	0.1720	2704	0.0180
19.5	0.1800	2936	−0.1173
19.5	0.1880	2050	−0.2323
19.5	0.1960	886	−0.3061
19.5	0.2040	251	−0.3482
20.5	0.1560	139	0.4720
20.5	0.1640	400	0.3250
20.5	0.1720	946	0.1999
20.5	0.1800	1416	0.0518
20.5	0.1880	1558	−0.0893
20.5	0.1960	1376	−0.2048
20.5	0.2040	658	−0.2982
21.5	0.1640	104	0.4780
21.5	0.1720	311	0.2993
21.5	0.1800	619	0.1892

21.5	0.1880	920	0.0825
21.5	0.1960	940	-0.0306
21.5	0.2040	657	-0.1415
22.5	0.1720	114	0.3796
22.5	0.1800	226	0.2459
22.5	0.1880	317	0.1783
22.5	0.1960	453	0.0833
22.5	0.2040	477	-0.0006
23.5	0.1880	174	0.2517
23.5	0.1960	207	0.1884
23.5	0.2040	287	0.1270
24.5	0.1960	133	0.2270
24.5	0.2040	176	0.1879
25.5	0.1960	112	0.2787
25.5	0.2040	112	0.3255

radiometer 2
V

0.5	0.0015	5083	0.0035
0.5	0.0045	10076	-0.0099
0.5	0.0075	13070	-0.0232
0.5	0.0105	9939	-0.0564
0.5	0.0135	2831	-0.0928
0.5	0.0165	277	-0.0989
1.5	0.0075	1114	0.1214
1.5	0.0105	8314	0.0202
1.5	0.0135	20723	-0.0183
1.5	0.0165	26790	-0.0398
1.5	0.0195	17053	-0.0521
1.5	0.0225	4759	-0.0528
1.5	0.0255	473	-0.0260
2.5	0.0135	198	0.3024
2.5	0.0165	4356	0.0565
2.5	0.0195	25186	-0.0137
2.5	0.0225	49631	-0.0247
2.5	0.0255	36388	-0.0056
2.5	0.0285	4502	0.0117
2.5	0.0315	109	-0.0602
3.5	0.0195	580	0.1899
3.5	0.0225	14804	0.0182
3.5	0.0255	90785	0.0031
3.5	0.0285	77501	0.0241
3.5	0.0315	7043	-0.0251
3.5	0.0345	373	-0.0361
4.5	0.0225	831	0.1755

4.5	0.0255	51477	0.0175
4.5	0.0285	193427	0.0255
4.5	0.0315	44997	-0.0003
4.5	0.0345	9978	-0.0197
4.5	0.0375	1067	0.0249
5.5	0.0255	17610	0.0509
5.5	0.0285	253933	0.0153
5.5	0.0315	121550	0.0104
5.5	0.0345	29496	-0.0172
5.5	0.0375	6096	0.0125
5.5	0.0405	287	0.0238
6.5	0.0255	3407	0.0826
6.5	0.0285	201581	0.0179
6.5	0.0315	269114	0.0023
6.5	0.0345	43735	-0.0202
6.5	0.0375	9717	-0.0058
6.5	0.0405	247	0.0474
7.5	0.0255	332	0.3060
7.5	0.0285	84315	0.0179
7.5	0.0315	399066	0.0059
7.5	0.0345	63761	-0.0155
7.5	0.0375	7315	0.0005
7.5	0.0405	228	-0.0619
8.5	0.0285	16237	0.0405
8.5	0.0315	303747	0.0164
8.5	0.0345	172718	-0.0038
8.5	0.0375	5340	-0.0215
8.5	0.0405	252	-0.1632
9.5	0.0285	1374	0.0701
9.5	0.0315	96913	0.0139
9.5	0.0345	262263	0.0056
9.5	0.0375	37503	-0.0003
9.5	0.0405	547	-0.0979
10.5	0.0285	184	0.1746
10.5	0.0315	11902	0.0230
10.5	0.0345	131693	-0.0010
10.5	0.0375	136883	-0.0026
10.5	0.0405	13539	0.0099
10.5	0.0435	273	-0.0732
11.5	0.0315	1283	0.1083
11.5	0.0345	21961	-0.0058
11.5	0.0375	105805	-0.0161
11.5	0.0405	80552	-0.0124
11.5	0.0435	10234	0.0077
11.5	0.0465	419	0.0205
12.5	0.0315	246	0.0770

12.5	0.0345	2168	0.0190
12.5	0.0375	20764	-0.0246
12.5	0.0405	71753	-0.0315
12.5	0.0435	56197	-0.0256
12.5	0.0465	11769	-0.0043
12.5	0.0495	957	0.0400
12.5	0.0525	112	-0.0267
13.5	0.0345	367	0.0721
13.5	0.0375	2182	-0.0091
13.5	0.0405	14279	-0.0402
13.5	0.0435	44631	-0.0459
13.5	0.0465	43776	-0.0416
13.5	0.0495	14577	-0.0220
13.5	0.0525	2046	0.0174
13.5	0.0555	245	0.0478
14.5	0.0345	116	0.1895
14.5	0.0375	369	0.1049
14.5	0.0405	1961	-0.0198
14.5	0.0435	8934	-0.0506
14.5	0.0465	25458	-0.0577
14.5	0.0495	31216	-0.0664
14.5	0.0525	15406	-0.0513
14.5	0.0555	3922	-0.0141
14.5	0.0585	547	0.0118
14.5	0.0615	127	0.0141
15.5	0.0405	356	0.1788
15.5	0.0435	1236	-0.0506
15.5	0.0465	4839	-0.0472
15.5	0.0495	13449	-0.0770
15.5	0.0525	21014	-0.0880
15.5	0.0555	14173	-0.0817
15.5	0.0585	5086	-0.0524
15.5	0.0615	1164	-0.0137
15.5	0.0645	268	0.0007
16.5	0.0435	230	0.0125
16.5	0.0465	687	-0.0374
16.5	0.0495	2314	-0.0487
16.5	0.0525	6939	-0.0836
16.5	0.0555	12433	-0.0879
16.5	0.0585	10938	-0.0950
16.5	0.0615	5648	-0.0957
16.5	0.0645	1851	-0.0521
16.5	0.0675	445	0.0027
16.5	0.0705	139	-0.0186
17.5	0.0465	136	0.1819
17.5	0.0495	348	0.0403
17.5	0.0525	1240	-0.0288
17.5	0.0555	3412	-0.0470
17.5	0.0585	6627	-0.0711

17.5	0.0615	7374	−0.0834
17.5	0.0645	5009	−0.1066
17.5	0.0675	2460	−0.0846
17.5	0.0705	725	−0.0259
17.5	0.0735	169	0.0269
18.5	0.0525	264	0.0491
18.5	0.0555	742	−0.0034
18.5	0.0585	1742	−0.0290
18.5	0.0615	3475	−0.0458
18.5	0.0645	4155	−0.0612
18.5	0.0675	3393	−0.0836
18.5	0.0705	2223	−0.0932
18.5	0.0735	826	−0.0952
18.5	0.0765	258	−0.0423
19.5	0.0555	183	0.1712
19.5	0.0585	370	0.0541
19.5	0.0615	889	0.0248
19.5	0.0645	1880	−0.0108
19.5	0.0675	2346	−0.0238
19.5	0.0705	1818	−0.0240
19.5	0.0735	1559	−0.0528
19.5	0.0765	896	−0.0897
20.5	0.0585	111	0.0856
20.5	0.0615	257	0.1352
20.5	0.0645	495	0.0452
20.5	0.0675	1074	0.0181
20.5	0.0705	1287	0.0146
20.5	0.0735	1154	0.0600
20.5	0.0765	778	0.0088
21.5	0.0645	210	0.1477
21.5	0.0675	301	0.0754
21.5	0.0705	547	0.0389
21.5	0.0735	731	0.0385
21.5	0.0765	457	0.0567
22.5	0.0675	109	0.1743
22.5	0.0705	199	0.0995
22.5	0.0735	372	0.0352
22.5	0.0765	357	0.0956
23.5	0.0705	109	0.0602
23.5	0.0735	178	0.0320
23.5	0.0765	247	0.1306
24.5	0.0765	173	0.0686

radiometer 2
H

0.5	0.0015	5083	0.1038
0.5	0.0045	10076	0.0920
0.5	0.0075	13070	0.0616
0.5	0.0105	9939	−0.0563
0.5	0.0135	2831	−0.2580
0.5	0.0165	277	−0.4856
1.5	0.0075	1114	0.4415
1.5	0.0105	8314	0.2246
1.5	0.0135	20723	0.0872
1.5	0.0165	26790	−0.0069
1.5	0.0195	17053	−0.1428
1.5	0.0225	4759	−0.3089
1.5	0.0255	473	−0.4691
2.5	0.0135	198	0.6012
2.5	0.0165	4356	0.2755
2.5	0.0195	25186	0.0939
2.5	0.0225	49631	−0.0264
2.5	0.0255	36388	−0.1302
2.5	0.0285	4502	−0.2280
2.5	0.0315	109	−0.4485
3.5	0.0195	580	0.3883
3.5	0.0225	14804	0.1399
3.5	0.0255	90785	0.0182
3.5	0.0285	77501	−0.0441
3.5	0.0315	7043	−0.1072
3.5	0.0345	373	−0.1750
4.5	0.0225	831	0.3191
4.5	0.0255	51477	0.0967
4.5	0.0285	193427	0.0243
4.5	0.0315	44997	−0.0470
4.5	0.0345	9978	−0.1122
4.5	0.0375	1067	−0.1012
5.5	0.0255	17610	0.1529
5.5	0.0285	253933	0.0503
5.5	0.0315	121550	−0.0131
5.5	0.0345	29496	−0.0907
5.5	0.0375	6096	−0.1005
5.5	0.0405	287	−0.1029
6.5	0.0255	3407	0.1892
6.5	0.0285	201581	0.0660
6.5	0.0315	269114	−0.0040
6.5	0.0345	43735	−0.0847
6.5	0.0375	9717	−0.0863
6.5	0.0405	247	−0.0516
7.5	0.0255	332	0.2990
7.5	0.0285	84315	0.0778
7.5	0.0315	399066	0.0078

7.5	0.0345	63761	−0.0679
7.5	0.0375	7315	−0.0477
7.5	0.0405	228	0.1515
8.5	0.0285	16237	0.1104
8.5	0.0315	303747	0.0420
8.5	0.0345	172718	−0.0449
8.5	0.0375	5340	−0.0235
8.5	0.0405	252	0.0852
9.5	0.0285	1374	0.1322
9.5	0.0315	96913	0.0859
9.5	0.0345	262263	−0.0012
9.5	0.0375	37503	−0.1057
9.5	0.0405	547	−0.0551
10.5	0.0285	184	0.2742
10.5	0.0315	11902	0.1412
10.5	0.0345	131693	0.0541
10.5	0.0375	136883	−0.0456
10.5	0.0405	13539	−0.1634
10.5	0.0435	273	−0.1284
11.5	0.0315	1283	0.3211
11.5	0.0345	21961	0.1211
11.5	0.0375	105805	0.0295
11.5	0.0405	80552	−0.0713
11.5	0.0435	10234	−0.1855
11.5	0.0465	419	−0.1975
12.5	0.0315	246	0.4798
12.5	0.0345	2168	0.2805
12.5	0.0375	20764	0.1056
12.5	0.0405	71753	0.0149
12.5	0.0435	56197	−0.0815
12.5	0.0465	11769	−0.1855
12.5	0.0495	957	−0.2420
12.5	0.0525	112	−0.3055
13.5	0.0345	367	0.4629
13.5	0.0375	2182	0.2561
13.5	0.0405	14279	0.1094
13.5	0.0435	44631	0.0148
13.5	0.0465	43776	−0.0727
13.5	0.0495	14577	−0.1762
13.5	0.0525	2046	−0.2487
13.5	0.0555	245	−0.3011
14.5	0.0345	116	0.6925
14.5	0.0375	369	0.4685
14.5	0.0405	1961	0.2542
14.5	0.0435	8934	0.1268
14.5	0.0465	25458	0.0236
14.5	0.0495	31216	−0.0679

14.5	0.0525	15406	−0.1599
14.5	0.0555	3922	−0.2311
14.5	0.0585	547	−0.3101
14.5	0.0615	127	−0.3824
15.5	0.0405	356	0.5661
15.5	0.0435	1236	0.2889
15.5	0.0465	4839	0.1599
15.5	0.0495	13449	0.0313
15.5	0.0525	21014	−0.0535
15.5	0.0555	14173	−0.1426
15.5	0.0585	5086	−0.2130
15.5	0.0615	1164	−0.2712
15.5	0.0645	268	−0.3682
16.5	0.0435	230	0.4976
16.5	0.0465	687	0.3313
16.5	0.0495	2314	0.2015
16.5	0.0525	6939	0.0553
16.5	0.0555	12433	−0.0249
16.5	0.0585	10938	−0.1125
16.5	0.0615	5648	−0.2056
16.5	0.0645	1851	−0.2622
16.5	0.0675	445	−0.3001
16.5	0.0705	139	−0.3783
17.5	0.0465	136	0.6271
17.5	0.0495	348	0.4216
17.5	0.0525	1240	0.2549
17.5	0.0555	3412	0.1167
17.5	0.0585	6627	0.0186
17.5	0.0615	7374	−0.0635
17.5	0.0645	5009	−0.1823
17.5	0.0675	2460	−0.2559
17.5	0.0705	725	−0.2990
17.5	0.0735	169	−0.3477
18.5	0.0525	264	0.4403
18.5	0.0555	742	0.2803
18.5	0.0585	1742	0.1623
18.5	0.0615	3475	0.0738
18.5	0.0645	4155	−0.0155
18.5	0.0675	3393	−0.1337
18.5	0.0705	2223	−0.2458
18.5	0.0735	826	−0.3310
18.5	0.0765	258	−0.4020
19.5	0.0555	183	0.5163
19.5	0.0585	370	0.3775
19.5	0.0615	889	0.2305
19.5	0.0645	1880	0.1246
19.5	0.0675	2346	0.0391
19.5	0.0705	1818	−0.0473
19.5	0.0735	1559	−0.1700

19.5	0.0765	896	−0.2864
20.5	0.0585	111	0.5161
20.5	0.0615	257	0.4557
20.5	0.0645	495	0.2633
20.5	0.0675	1074	0.1552
20.5	0.0705	1287	0.0941
20.5	0.0735	1154	0.0228
20.5	0.0765	778	−0.0996
21.5	0.0645	210	0.3862
21.5	0.0675	301	0.2897
21.5	0.0705	547	0.1819
21.5	0.0735	731	0.0985
21.5	0.0765	457	0.0295
22.5	0.0675	109	0.4487
22.5	0.0705	199	0.2919
22.5	0.0735	372	0.1718
22.5	0.0765	357	0.1140
23.5	0.0705	109	0.3468
23.5	0.0735	178	0.2189
23.5	0.0765	247	0.1859
24.5	0.0765	173	0.2330

radiometer 3

V

0.5	0.0010	3328	0.0131
0.5	0.0030	8170	−0.0187
0.5	0.0050	12127	−0.0460
0.5	0.0070	9140	−0.0730
0.5	0.0090	2344	−0.1253
0.5	0.0110	259	−0.1434
1.5	0.0050	1914	0.1045
1.5	0.0070	11707	0.0054
1.5	0.0090	26489	−0.0321
1.5	0.0110	27658	−0.0516
1.5	0.0130	12384	−0.0601
1.5	0.0150	2350	−0.0481
1.5	0.0170	123	−0.0924
2.5	0.0090	1658	0.0632
2.5	0.0110	17779	−0.0051
2.5	0.0130	50967	−0.0264
2.5	0.0150	47312	−0.0107
2.5	0.0170	6841	0.0071
3.5	0.0110	663	0.0460
3.5	0.0130	17523	−0.0111

3.5	0.0150	101090	-0.0011
3.5	0.0170	62478	0.0238
3.5	0.0190	4773	-0.0720
3.5	0.0210	352	-0.0528
4.5	0.0130	3072	0.0191
4.5	0.0150	97671	-0.0025
4.5	0.0170	149542	0.0346
4.5	0.0190	22927	-0.0395
4.5	0.0210	3587	-0.0297
5.5	0.0130	731	0.0563
5.5	0.0150	93006	-0.0018
5.5	0.0170	245258	0.0262
5.5	0.0190	42958	-0.0209
5.5	0.0210	8999	-0.0143
5.5	0.0230	274	0.0363
6.5	0.0130	111	0.1287
6.5	0.0150	73121	0.0001
6.5	0.0170	353051	0.0230
6.5	0.0190	65360	0.0060
6.5	0.0210	7324	0.0282
6.5	0.0230	151	0.0848
7.5	0.0150	34434	0.0015
7.5	0.0170	385056	0.0290
7.5	0.0190	106464	0.0098
7.5	0.0210	3240	0.0358
8.5	0.0150	7328	-0.0034
8.5	0.0170	259486	0.0369
8.5	0.0190	213236	0.0074
8.5	0.0210	3626	0.0048
8.5	0.0230	143	-0.1512
9.5	0.0150	1186	0.1985
9.5	0.0170	76483	0.0349
9.5	0.0190	266525	0.0129
9.5	0.0210	51703	-0.0103
9.5	0.0230	490	-0.0205
10.5	0.0150	299	0.5836
10.5	0.0170	8246	-0.0010
10.5	0.0190	115910	0.0135
10.5	0.0210	153205	-0.0124
10.5	0.0230	19046	-0.0227
10.5	0.0250	389	-0.0108
11.5	0.0170	1198	0.0888
11.5	0.0190	15743	0.0069
11.5	0.0210	93636	-0.0084
11.5	0.0230	88103	-0.0326
11.5	0.0250	15224	-0.0214

11.5	0.0270	716	-0.0107
12.5	0.0170	222	0.3869
12.5	0.0190	1716	-0.0058
12.5	0.0210	15010	-0.0097
12.5	0.0230	62836	-0.0284
12.5	0.0250	62238	-0.0489
12.5	0.0270	17609	-0.0389
12.5	0.0290	1728	-0.0147
12.5	0.0310	182	-0.0679
13.5	0.0190	289	0.2484
13.5	0.0210	1479	-0.0182
13.5	0.0230	10109	-0.0187
13.5	0.0250	37510	-0.0573
13.5	0.0270	46270	-0.0646
13.5	0.0290	19431	-0.0594
13.5	0.0310	3360	-0.0353
13.5	0.0330	484	-0.0156
13.5	0.0350	117	-0.0230
14.5	0.0210	271	0.0023
14.5	0.0230	1306	-0.0078
14.5	0.0250	5952	-0.0344
14.5	0.0270	20207	-0.0679
14.5	0.0290	31256	-0.0775
14.5	0.0310	19861	-0.0864
14.5	0.0330	5560	-0.0709
14.5	0.0350	895	-0.0337
14.5	0.0370	187	-0.0496
15.5	0.0230	180	0.1968
15.5	0.0250	821	0.0620
15.5	0.0270	3249	-0.0258
15.5	0.0290	10376	-0.0640
15.5	0.0310	19910	-0.0837
15.5	0.0330	16743	-0.1052
15.5	0.0350	7338	-0.0982
15.5	0.0370	1761	-0.0603
15.5	0.0390	359	-0.0110
15.5	0.0410	128	0.0134
16.5	0.0250	122	0.1145
16.5	0.0270	413	0.0608
16.5	0.0290	1719	-0.0269
16.5	0.0310	5404	-0.0488
16.5	0.0330	10755	-0.0765
16.5	0.0350	11672	-0.1055
16.5	0.0370	7184	-0.1375
16.5	0.0390	2513	-0.1153
16.5	0.0410	587	-0.0512
16.5	0.0430	173	0.0145
17.5	0.0290	232	0.1088

17.5	0.0310	842	0.0058
17.5	0.0330	2579	−0.0095
17.5	0.0350	5466	−0.0461
17.5	0.0370	7026	−0.0929
17.5	0.0390	5933	−0.1443
17.5	0.0410	3045	−0.1371
17.5	0.0430	793	−0.0936
17.5	0.0450	226	−0.0100
18.5	0.0310	142	0.0506
18.5	0.0330	382	0.0611
18.5	0.0350	1207	0.0286
18.5	0.0370	2746	−0.0165
18.5	0.0390	3727	−0.0542
18.5	0.0410	3871	−0.1101
18.5	0.0430	2986	−0.1442
18.5	0.0450	1195	−0.1124
18.5	0.0470	242	−0.0711
19.5	0.0350	245	0.1385
19.5	0.0370	759	0.0391
19.5	0.0390	1413	−0.0099
19.5	0.0410	2098	−0.0227
19.5	0.0430	2190	−0.0645
19.5	0.0450	1969	−0.1245
19.5	0.0470	1000	−0.1504
19.5	0.0490	345	−0.0482
20.5	0.0370	131	0.1017
20.5	0.0390	433	0.0518
20.5	0.0410	997	0.0187
20.5	0.0430	1224	−0.0081
20.5	0.0450	1200	−0.0247
20.5	0.0470	1147	−0.0437
20.5	0.0490	683	−0.1393
20.5	0.0510	306	−0.1428
21.5	0.0390	123	0.1466
21.5	0.0410	350	0.0393
21.5	0.0430	533	0.0127
21.5	0.0450	568	0.0352
21.5	0.0470	720	0.0304
21.5	0.0490	588	0.0035
21.5	0.0510	404	−0.0543
22.5	0.0410	122	0.1213
22.5	0.0430	211	0.1192
22.5	0.0450	291	0.0856
22.5	0.0470	401	0.0613
22.5	0.0490	407	0.0111
22.5	0.0510	356	0.0131
23.5	0.0450	235	0.1125
23.5	0.0470	217	0.0637

23.5	0.0490	224	0.0193
23.5	0.0510	209	0.0312
24.5	0.0470	144	0.1251
24.5	0.0490	120	0.1012
24.5	0.0510	102	0.0322

radiometer 3

H

0.5	0.0010	3328	0.1493
0.5	0.0030	8170	0.1198
0.5	0.0050	12127	0.0646
0.5	0.0070	9140	−0.0512
0.5	0.0090	2344	−0.2457
0.5	0.0110	259	−0.4514
1.5	0.0050	1914	0.3825
1.5	0.0070	11707	0.2050
1.5	0.0090	26489	0.0776
1.5	0.0110	27658	−0.0419
1.5	0.0130	12384	−0.2026
1.5	0.0150	2350	−0.3758
1.5	0.0170	123	−0.5108
2.5	0.0090	1658	0.3718
2.5	0.0110	17779	0.1752
2.5	0.0130	50967	0.0218
2.5	0.0150	47312	−0.0984
2.5	0.0170	6841	−0.1957
3.5	0.0110	663	0.3751
3.5	0.0130	17523	0.1539
3.5	0.0150	101090	0.0194
3.5	0.0170	62478	−0.0448
3.5	0.0190	4773	−0.1228
3.5	0.0210	352	−0.1229
4.5	0.0130	3072	0.1994
4.5	0.0150	97671	0.0593
4.5	0.0170	149542	0.0081
4.5	0.0190	22927	−0.0923
4.5	0.0210	3587	−0.1256
5.5	0.0130	731	0.2210
5.5	0.0150	93006	0.0643
5.5	0.0170	245258	0.0238
5.5	0.0190	42958	−0.0712
5.5	0.0210	8999	−0.1105
5.5	0.0230	274	−0.1239
6.5	0.0130	111	0.3151
6.5	0.0150	73121	0.0626

6.5	0.0170	353051	0.0324
6.5	0.0190	65360	−0.0421
6.5	0.0210	7324	−0.0314
6.5	0.0230	151	0.1037
7.5	0.0150	34434	0.0679
7.5	0.0170	385056	0.0475
7.5	0.0190	106464	−0.0195
7.5	0.0210	3240	0.0558
8.5	0.0150	7328	0.0979
8.5	0.0170	259486	0.0664
8.5	0.0190	213236	−0.0114
8.5	0.0210	3626	−0.0272
8.5	0.0230	143	0.2795
9.5	0.0150	1186	0.4268
9.5	0.0170	76483	0.1008
9.5	0.0190	266525	0.0125
9.5	0.0210	51703	−0.0907
9.5	0.0230	490	−0.0331
10.5	0.0150	299	0.9358
10.5	0.0170	8246	0.1429
10.5	0.0190	115910	0.0583
10.5	0.0210	153205	−0.0380
10.5	0.0230	19046	−0.1633
10.5	0.0250	389	−0.1417
11.5	0.0170	1198	0.3150
11.5	0.0190	15743	0.1237
11.5	0.0210	93636	0.0319
11.5	0.0230	88103	−0.0699
11.5	0.0250	15224	−0.1864
11.5	0.0270	716	−0.2595
12.5	0.0170	222	0.8657
12.5	0.0190	1716	0.2552
12.5	0.0210	15010	0.1140
12.5	0.0230	62836	0.0184
12.5	0.0250	62238	−0.0776
12.5	0.0270	17609	−0.1777
12.5	0.0290	1728	−0.2463
12.5	0.0310	182	−0.2602
13.5	0.0190	289	0.5804
13.5	0.0210	1479	0.2112
13.5	0.0230	10109	0.1215
13.5	0.0250	37510	0.0108
13.5	0.0270	46270	−0.0688
13.5	0.0290	19431	−0.1588
13.5	0.0310	3360	−0.2214
13.5	0.0330	484	−0.2550
13.5	0.0350	117	−0.2743

14.5	0.0210	271	0.4002
14.5	0.0230	1306	0.2627
14.5	0.0250	5952	0.1276
14.5	0.0270	20207	0.0233
14.5	0.0290	31256	-0.0550
14.5	0.0310	19861	-0.1436
14.5	0.0330	5560	-0.2125
14.5	0.0350	895	-0.2504
14.5	0.0370	187	-0.2844
15.5	0.0230	180	0.5497
15.5	0.0250	821	0.3370
15.5	0.0270	3249	0.1646
15.5	0.0290	10376	0.0471
15.5	0.0310	19910	-0.0391
15.5	0.0330	16743	-0.1272
15.5	0.0350	7338	-0.2029
15.5	0.0370	1761	-0.2385
15.5	0.0390	359	-0.2799
15.5	0.0410	128	-0.2572
16.5	0.0250	122	0.5610
16.5	0.0270	413	0.3531
16.5	0.0290	1719	0.2000
16.5	0.0310	5404	0.0771
16.5	0.0330	10755	-0.0145
16.5	0.0350	11672	-0.0993
16.5	0.0370	7184	-0.1939
16.5	0.0390	2513	-0.2465
16.5	0.0410	587	-0.2663
16.5	0.0430	173	-0.2666
17.5	0.0290	232	0.4362
17.5	0.0310	842	0.2779
17.5	0.0330	2579	0.1367
17.5	0.0350	5466	0.0329
17.5	0.0370	7026	-0.0568
17.5	0.0390	5933	-0.1779
17.5	0.0410	3045	-0.2577
17.5	0.0430	793	-0.2789
17.5	0.0450	226	-0.2520
18.5	0.0310	142	0.4693
18.5	0.0330	382	0.3215
18.5	0.0350	1207	0.2206
18.5	0.0370	2746	0.0859
18.5	0.0390	3727	-0.0058
18.5	0.0410	3871	-0.1172
18.5	0.0430	2986	-0.2303
18.5	0.0450	1195	-0.2821
18.5	0.0470	242	-0.3346
19.5	0.0350	245	0.4029

19.5	0.0370	759	0.2125
19.5	0.0390	1413	0.1061
19.5	0.0410	2098	0.0316
19.5	0.0430	2190	−0.0595
19.5	0.0450	1969	−0.1708
19.5	0.0470	1000	−0.2876
19.5	0.0490	345	−0.2740
20.5	0.0370	131	0.4099
20.5	0.0390	433	0.2322
20.5	0.0410	997	0.1333
20.5	0.0430	1224	0.0741
20.5	0.0450	1200	0.0086
20.5	0.0470	1147	−0.0908
20.5	0.0490	683	−0.2468
20.5	0.0510	306	−0.3624
21.5	0.0390	123	0.3811
21.5	0.0410	350	0.2093
21.5	0.0430	533	0.1600
21.5	0.0450	568	0.0999
21.5	0.0470	720	0.0334
21.5	0.0490	588	−0.0571
21.5	0.0510	404	−0.1773
22.5	0.0410	122	0.3329
22.5	0.0430	211	0.2408
22.5	0.0450	291	0.1960
22.5	0.0470	401	0.1008
22.5	0.0490	407	0.0314
22.5	0.0510	356	−0.0329
23.5	0.0450	235	0.2506
23.5	0.0470	217	0.1916
23.5	0.0490	224	0.1181
23.5	0.0510	209	0.0384
24.5	0.0470	144	0.2315
24.5	0.0490	120	0.1838
24.5	0.0510	102	0.0816

ts05.txt

```
radiometer 1
V
    0.5    0.75       2529     0.0789
    0.5    1.25      10834     0.0071
    0.5    1.75      12567    -0.0236
    0.5    2.25       9772    -0.0400
    0.5    2.75       4772    -0.0304
    0.5    3.25       1810    -0.0214
    0.5    3.75        883    -0.0566
    0.5    4.25        256    -0.0710

    1.5    0.75       3412     0.0894
    1.5    1.25      16261     0.0360
    1.5    1.75      22390    -0.0076
    1.5    2.25      19527    -0.0334
    1.5    2.75      11778    -0.0489
    1.5    3.25       6184    -0.0496
    1.5    3.75       3273    -0.0633
    1.5    4.25       1294    -0.0609
    1.5    4.75        519    -0.0747
    1.5    5.25        190    -0.1138

    2.5    0.75       3911     0.1299
    2.5    1.25      20456     0.0639
    2.5    1.75      31343     0.0126
    2.5    2.25      27836    -0.0210
    2.5    2.75      18282    -0.0432
    2.5    3.25      10356    -0.0608
    2.5    3.75       6322    -0.0649
    2.5    4.25       2747    -0.0769
    2.5    4.75       1240    -0.0808
    2.5    5.25        452    -0.1385
    2.5    5.75        188    -0.1019

    3.5    0.75       5681     0.1458
    3.5    1.25      30803     0.0787
    3.5    1.75      53004     0.0229
    3.5    2.25      44750    -0.0056
    3.5    2.75      29622    -0.0435
    3.5    3.25      18461    -0.0634
    3.5    3.75      10378    -0.0806
    3.5    4.25       5103    -0.0886
    3.5    4.75       2280    -0.0928
    3.5    5.25       1067    -0.1204
    3.5    5.75        523    -0.1260
    3.5    6.25        197    -0.0967

    4.5    0.75       6239     0.1572
    4.5    1.25      43420     0.0601
    4.5    1.75      84833     0.0332
    4.5    2.25      76648    -0.0027
```

4.5	2.75	48599	−0.0345
4.5	3.25	30027	−0.0601
4.5	3.75	18107	−0.0806
4.5	4.25	9185	−0.0810
4.5	4.75	4565	−0.0979
4.5	5.25	2168	−0.1044
4.5	5.75	923	−0.1167
4.5	6.25	355	−0.0918
4.5	6.75	133	−0.1381
5.5	0.75	4215	0.1687
5.5	1.25	47048	0.0600
5.5	1.75	119159	0.0267
5.5	2.25	114212	−0.0019
5.5	2.75	71991	−0.0233
5.5	3.25	42607	−0.0486
5.5	3.75	25695	−0.0708
5.5	4.25	14482	−0.0740
5.5	4.75	7591	−0.0846
5.5	5.25	3712	−0.0928
5.5	5.75	1693	−0.0887
5.5	6.25	679	−0.0879
5.5	6.75	239	−0.0889
6.5	0.75	2001	0.2387
6.5	1.25	36781	0.0752
6.5	1.75	138178	0.0261
6.5	2.25	155823	0.0049
6.5	2.75	94926	−0.0117
6.5	3.25	56813	−0.0393
6.5	3.75	33859	−0.0629
6.5	4.25	21290	−0.0688
6.5	4.75	11691	−0.0766
6.5	5.25	5985	−0.1029
6.5	5.75	2791	−0.0991
6.5	6.25	1125	−0.0995
6.5	6.75	448	−0.0946
6.5	7.25	169	−0.1095
7.5	0.75	512	0.3144
7.5	1.25	17080	0.0983
7.5	1.75	111985	0.0469
7.5	2.25	174456	0.0103
7.5	2.75	117893	−0.0031
7.5	3.25	69087	−0.0293
7.5	3.75	43173	−0.0478
7.5	4.25	27009	−0.0693
7.5	4.75	15850	−0.0861
7.5	5.25	8967	−0.1064
7.5	5.75	4164	−0.1097
7.5	6.25	2177	−0.1229
7.5	6.75	813	−0.1004
7.5	7.25	325	−0.0874
7.5	7.75	106	−0.0935

8.5	1.25	3996	0.1437
8.5	1.75	54522	0.0649
8.5	2.25	142276	0.0303
8.5	2.75	126364	0.0163
8.5	3.25	78560	-0.0164
8.5	3.75	49257	-0.0381
8.5	4.25	32936	-0.0639
8.5	4.75	20071	-0.0846
8.5	5.25	11534	-0.1101
8.5	5.75	6221	-0.1218
8.5	6.25	3110	-0.1342
8.5	6.75	1711	-0.1252
8.5	7.25	712	-0.1371
8.5	7.75	273	-0.1211
9.5	1.25	829	0.2565
9.5	1.75	14782	0.1013
9.5	2.25	75411	0.0456
9.5	2.75	107359	0.0232
9.5	3.25	80597	0.0063
9.5	3.75	53153	-0.0166
9.5	4.25	36516	-0.0417
9.5	4.75	23868	-0.0627
9.5	5.25	13563	-0.0851
9.5	5.75	8417	-0.1112
9.5	6.25	4637	-0.1287
9.5	6.75	2683	-0.1487
9.5	7.25	1332	-0.1298
9.5	7.75	488	-0.1087
9.5	8.25	141	-0.1728
10.5	1.25	198	0.1818
10.5	1.75	3696	0.0939
10.5	2.25	25512	0.0658
10.5	2.75	60464	0.0310
10.5	3.25	69574	0.0189
10.5	3.75	52350	0.0033
10.5	4.25	37850	-0.0156
10.5	4.75	25538	-0.0371
10.5	5.25	15950	-0.0577
10.5	5.75	9731	-0.0784
10.5	6.25	5741	-0.1041
10.5	6.75	3321	-0.1174
10.5	7.25	1939	-0.1296
10.5	7.75	782	-0.1704
10.5	8.25	459	-0.2112
10.5	8.75	164	-0.1372
11.5	1.75	1160	0.0863
11.5	2.25	8143	0.0710
11.5	2.75	25654	0.0470
11.5	3.25	44691	0.0310
11.5	3.75	46598	0.0164

11.5	4.25	38245	-0.0043
11.5	4.75	26505	-0.0194
11.5	5.25	17316	-0.0404
11.5	5.75	11403	-0.0573
11.5	6.25	6940	-0.0863
11.5	6.75	3568	-0.1056
11.5	7.25	2571	-0.1047
11.5	7.75	1112	-0.1328
11.5	8.25	619	-0.1786
11.5	8.75	215	-0.1767
11.5	9.25	125	-0.1503
12.5	1.75	407	0.0912
12.5	2.25	3356	0.0773
12.5	2.75	11148	0.0501
12.5	3.25	23425	0.0321
12.5	3.75	32286	0.0216
12.5	4.25	31431	0.0018
12.5	4.75	25816	-0.0069
12.5	5.25	17938	-0.0193
12.5	5.75	12384	-0.0429
12.5	6.25	7934	-0.0528
12.5	6.75	4689	-0.0600
12.5	7.25	2986	-0.0863
12.5	7.75	1583	-0.0912
12.5	8.25	776	-0.0871
12.5	8.75	386	-0.1296
12.5	9.25	141	-0.1665
13.5	1.75	138	0.1562
13.5	2.25	1216	0.0571
13.5	2.75	4709	0.0604
13.5	3.25	11669	0.0372
13.5	3.75	18523	0.0284
13.5	4.25	22569	0.0193
13.5	4.75	22338	-0.0095
13.5	5.25	17350	-0.0144
13.5	5.75	12165	-0.0307
13.5	6.25	8428	-0.0432
13.5	6.75	5315	-0.0448
13.5	7.25	3532	-0.0543
13.5	7.75	2424	-0.0745
13.5	8.25	1084	-0.0964
13.5	8.75	576	-0.0976
13.5	9.25	228	-0.1468
13.5	9.75	109	-0.1935
14.5	2.25	494	0.1149
14.5	2.75	2053	0.0574
14.5	3.25	5602	0.0497
14.5	3.75	9821	0.0306
14.5	4.25	13711	0.0284
14.5	4.75	14856	0.0065
14.5	5.25	13262	-0.0119

14.5	5.75	10965	-0.0225
14.5	6.25	7947	-0.0207
14.5	6.75	5770	-0.0582
14.5	7.25	3645	-0.0539
14.5	7.75	2772	-0.0612
14.5	8.25	1487	-0.1125
14.5	8.75	818	-0.0851
14.5	9.25	409	-0.0720
14.5	9.75	139	-0.1649
15.5	2.25	206	0.0673
15.5	2.75	733	0.0945
15.5	3.25	2287	0.0560
15.5	3.75	4835	0.0444
15.5	4.25	7521	0.0332
15.5	4.75	9323	0.0157
15.5	5.25	9659	-0.0114
15.5	5.75	8681	-0.0177
15.5	6.25	7140	-0.0140
15.5	6.75	5602	-0.0418
15.5	7.25	3889	-0.0471
15.5	7.75	2609	-0.0541
15.5	8.25	1694	-0.0605
15.5	8.75	922	-0.0631
15.5	9.25	586	-0.0569
15.5	9.75	146	-0.0571
15.5	10.25	104	-0.0540
16.5	2.75	281	0.0911
16.5	3.25	906	0.0608
16.5	3.75	2239	0.0458
16.5	4.25	3749	0.0608
16.5	4.75	5225	0.0310
16.5	5.25	6016	-0.0133
16.5	5.75	6186	-0.0026
16.5	6.25	5735	-0.0158
16.5	6.75	4746	-0.0260
16.5	7.25	3542	-0.0550
16.5	7.75	2302	-0.0429
16.5	8.25	1611	-0.0646
16.5	8.75	1183	-0.0771
16.5	9.25	633	-0.0397
16.5	9.75	239	-0.0151
16.5	10.25	143	-0.0324
17.5	2.75	127	0.0821
17.5	3.25	451	0.0892
17.5	3.75	886	0.0768
17.5	4.25	1593	0.0675
17.5	4.75	2330	0.0320
17.5	5.25	3281	0.0026
17.5	5.75	3884	-0.0003
17.5	6.25	3723	-0.0091
17.5	6.75	3644	-0.0187

17.5	7.25	2596	-0.0081
17.5	7.75	1974	-0.0459
17.5	8.25	1537	-0.0630
17.5	8.75	1077	-0.0534
17.5	9.25	672	-0.0651
17.5	9.75	379	0.0154
17.5	10.25	203	-0.0520
18.5	3.25	129	0.1227
18.5	3.75	383	0.1484
18.5	4.25	647	0.0578
18.5	4.75	1036	0.0428
18.5	5.25	1936	0.0245
18.5	5.75	2074	-0.0079
18.5	6.25	2358	0.0166
18.5	6.75	2452	0.0189
18.5	7.25	2000	-0.0171
18.5	7.75	1524	-0.0316
18.5	8.25	1227	-0.0555
18.5	8.75	978	-0.0713
18.5	9.25	694	-0.0489
18.5	9.75	405	-0.0495
18.5	10.25	343	-0.1228
18.5	10.75	123	-0.1124
19.5	3.75	177	0.1378
19.5	4.25	316	0.0782
19.5	4.75	492	0.1234
19.5	5.25	886	0.0534
19.5	5.75	1100	0.0107
19.5	6.25	1335	0.0276
19.5	6.75	1308	-0.0133
19.5	7.25	1247	-0.0412
19.5	7.75	1077	-0.0332
19.5	8.25	941	-0.0340
19.5	8.75	928	-0.0716
19.5	9.25	568	-0.0082
19.5	9.75	442	0.0136
19.5	10.25	237	-0.0541
19.5	10.75	148	-0.0749
20.5	4.25	138	0.1069
20.5	4.75	258	0.1067
20.5	5.25	382	0.0751
20.5	5.75	574	0.0293
20.5	6.25	662	0.0435
20.5	6.75	726	0.0369
20.5	7.25	800	-0.0341
20.5	7.75	636	0.0378
20.5	8.25	591	-0.0702
20.5	8.75	609	-0.0727
20.5	9.25	388	-0.0107
20.5	9.75	333	-0.0796
20.5	10.25	176	-0.0587

20.5	10.75	163	-0.0800
21.5	4.75	122	0.1661
21.5	5.25	214	0.0711
21.5	5.75	267	-0.0072
21.5	6.25	427	0.0700
21.5	6.75	447	0.1090
21.5	7.25	438	0.0066
21.5	7.75	356	-0.0019
21.5	8.25	348	-0.0346
21.5	8.75	313	-0.0511
21.5	9.25	315	-0.0681
21.5	9.75	281	-0.0355
21.5	10.25	133	-0.1032
21.5	10.75	122	-0.0709
22.5	6.25	164	0.1076
22.5	6.75	203	0.0076
22.5	7.25	254	0.0541
22.5	7.75	163	0.0140
22.5	8.25	229	0.0018
22.5	8.75	196	-0.0597
22.5	9.25	176	-0.1217
22.5	9.75	182	-0.0025
22.5	10.25	115	-0.0585
23.5	7.25	151	0.0512
23.5	8.25	118	-0.0178
23.5	8.75	139	-0.0314
23.5	9.25	103	-0.0432
23.5	9.75	112	-0.0732

radiometer 1
H

0.5	0.75	2529	0.0119
0.5	1.25	10834	-0.0346
0.5	1.75	12567	-0.0503
0.5	2.25	9772	-0.0574
0.5	2.75	4772	-0.0629
0.5	3.25	1810	-0.0558
0.5	3.75	883	-0.0688
0.5	4.25	256	-0.0609
1.5	0.75	3412	0.0675
1.5	1.25	16261	0.0165
1.5	1.75	22390	-0.0085
1.5	2.25	19527	-0.0242
1.5	2.75	11778	-0.0452
1.5	3.25	6184	-0.0403
1.5	3.75	3273	-0.0531
1.5	4.25	1294	-0.0437

1.5	4.75	519	−0.0561
1.5	5.25	190	−0.0884
2.5	0.75	3911	0.0932
2.5	1.25	20456	0.0454
2.5	1.75	31343	0.0149
2.5	2.25	27836	−0.0118
2.5	2.75	18282	−0.0310
2.5	3.25	10356	−0.0354
2.5	3.75	6322	−0.0358
2.5	4.25	2747	−0.0468
2.5	4.75	1240	−0.0513
2.5	5.25	452	−0.0689
2.5	5.75	188	−0.0818
3.5	0.75	5681	0.1153
3.5	1.25	30803	0.0600
3.5	1.75	53004	0.0187
3.5	2.25	44750	−0.0049
3.5	2.75	29622	−0.0346
3.5	3.25	18461	−0.0429
3.5	3.75	10378	−0.0438
3.5	4.25	5103	−0.0512
3.5	4.75	2280	−0.0572
3.5	5.25	1067	−0.0749
3.5	5.75	523	−0.0631
3.5	6.25	197	−0.0361
4.5	0.75	6239	0.1428
4.5	1.25	43420	0.0542
4.5	1.75	84833	0.0225
4.5	2.25	76648	−0.0068
4.5	2.75	48599	−0.0283
4.5	3.25	30027	−0.0490
4.5	3.75	18107	−0.0585
4.5	4.25	9185	−0.0541
4.5	4.75	4565	−0.0433
4.5	5.25	2168	−0.0721
4.5	5.75	923	−0.0685
4.5	6.25	355	−0.0317
4.5	6.75	133	−0.0563
5.5	0.75	4215	0.1938
5.5	1.25	47048	0.0597
5.5	1.75	119159	0.0217
5.5	2.25	114212	−0.0047
5.5	2.75	71991	−0.0242
5.5	3.25	42607	−0.0453
5.5	3.75	25695	−0.0570
5.5	4.25	14482	−0.0476
5.5	4.75	7591	−0.0463
5.5	5.25	3712	−0.0457
5.5	5.75	1693	−0.0241
5.5	6.25	679	−0.0334

5.5	6.75	239	0.0059
6.5	0.75	2001	0.3028
6.5	1.25	36781	0.0751
6.5	1.75	138178	0.0206
6.5	2.25	155823	0.0014
6.5	2.75	94926	-0.0173
6.5	3.25	56813	-0.0404
6.5	3.75	33859	-0.0507
6.5	4.25	21290	-0.0497
6.5	4.75	11691	-0.0426
6.5	5.25	5985	-0.0416
6.5	5.75	2791	-0.0360
6.5	6.25	1125	-0.0337
6.5	6.75	448	0.0268
6.5	7.25	169	0.0218
7.5	0.75	512	0.4060
7.5	1.25	17080	0.1127
7.5	1.75	111985	0.0403
7.5	2.25	174456	0.0062
7.5	2.75	117893	-0.0076
7.5	3.25	69087	-0.0355
7.5	3.75	43173	-0.0464
7.5	4.25	27009	-0.0549
7.5	4.75	15850	-0.0620
7.5	5.25	8967	-0.0658
7.5	5.75	4164	-0.0629
7.5	6.25	2177	-0.0516
7.5	6.75	813	-0.0247
7.5	7.25	325	0.0046
7.5	7.75	106	-0.0207
8.5	1.25	3996	0.1874
8.5	1.75	54522	0.0675
8.5	2.25	142276	0.0267
8.5	2.75	126364	0.0084
8.5	3.25	78560	-0.0236
8.5	3.75	49257	-0.0419
8.5	4.25	32936	-0.0549
8.5	4.75	20071	-0.0699
8.5	5.25	11534	-0.0704
8.5	5.75	6221	-0.0770
8.5	6.25	3110	-0.0743
8.5	6.75	1711	-0.0677
8.5	7.25	712	-0.0491
8.5	7.75	273	-0.0745
9.5	1.25	829	0.3097
9.5	1.75	14782	0.1085
9.5	2.25	75411	0.0437
9.5	2.75	107359	0.0199
9.5	3.25	80597	-0.0029
9.5	3.75	53153	-0.0226

9.5	4.25	36516	-0.0420
9.5	4.75	23868	-0.0547
9.5	5.25	13563	-0.0642
9.5	5.75	8417	-0.0764
9.5	6.25	4637	-0.0857
9.5	6.75	2683	-0.0878
9.5	7.25	1332	-0.0734
9.5	7.75	488	-0.0731
9.5	8.25	141	-0.1197
10.5	1.25	198	0.2883
10.5	1.75	3696	0.1144
10.5	2.25	25512	0.0740
10.5	2.75	60464	0.0330
10.5	3.25	69574	0.0139
10.5	3.75	52350	-0.0056
10.5	4.25	37850	-0.0251
10.5	4.75	25538	-0.0377
10.5	5.25	15950	-0.0451
10.5	5.75	9731	-0.0546
10.5	6.25	5741	-0.0691
10.5	6.75	3321	-0.0639
10.5	7.25	1939	-0.0712
10.5	7.75	782	-0.0900
10.5	8.25	459	-0.1415
10.5	8.75	164	-0.0635
11.5	1.75	1160	0.0873
11.5	2.25	8143	0.0764
11.5	2.75	25654	0.0476
11.5	3.25	44691	0.0255
11.5	3.75	46598	0.0104
11.5	4.25	38245	-0.0128
11.5	4.75	26505	-0.0234
11.5	5.25	17316	-0.0283
11.5	5.75	11403	-0.0385
11.5	6.25	6940	-0.0517
11.5	6.75	3568	-0.0613
11.5	7.25	2571	-0.0602
11.5	7.75	1112	-0.0666
11.5	8.25	619	-0.0796
11.5	8.75	215	-0.0882
11.5	9.25	125	-0.0537
12.5	1.75	407	0.1086
12.5	2.25	3356	0.0797
12.5	2.75	11148	0.0464
12.5	3.25	23425	0.0300
12.5	3.75	32286	0.0161
12.5	4.25	31431	-0.0007
12.5	4.75	25816	-0.0154
12.5	5.25	17938	-0.0160
12.5	5.75	12384	-0.0335
12.5	6.25	7934	-0.0330

12.5	6.75	4689	-0.0336
12.5	7.25	2986	-0.0527
12.5	7.75	1583	-0.0405
12.5	8.25	776	-0.0451
12.5	8.75	386	-0.0729
12.5	9.25	141	-0.0447
13.5	1.75	138	0.1265
13.5	2.25	1216	0.0684
13.5	2.75	4709	0.0558
13.5	3.25	11669	0.0403
13.5	3.75	18523	0.0198
13.5	4.25	22569	0.0070
13.5	4.75	22338	-0.0072
13.5	5.25	17350	-0.0127
13.5	5.75	12165	-0.0255
13.5	6.25	8428	-0.0215
13.5	6.75	5315	-0.0232
13.5	7.25	3532	-0.0176
13.5	7.75	2424	-0.0294
13.5	8.25	1084	-0.0426
13.5	8.75	576	-0.0564
13.5	9.25	228	-0.0495
13.5	9.75	109	-0.0845
14.5	2.25	494	0.1085
14.5	2.75	2053	0.0504
14.5	3.25	5602	0.0449
14.5	3.75	9821	0.0248
14.5	4.25	13711	0.0176
14.5	4.75	14856	-0.0004
14.5	5.25	13262	-0.0043
14.5	5.75	10965	-0.0144
14.5	6.25	7947	-0.0159
14.5	6.75	5770	-0.0315
14.5	7.25	3645	-0.0278
14.5	7.75	2772	-0.0336
14.5	8.25	1487	-0.0602
14.5	8.75	818	-0.0643
14.5	9.25	409	-0.0311
14.5	9.75	139	-0.0727
15.5	2.25	206	0.1143
15.5	2.75	733	0.0840
15.5	3.25	2287	0.0666
15.5	3.75	4835	0.0478
15.5	4.25	7521	0.0300
15.5	4.75	9323	0.0080
15.5	5.25	9659	-0.0088
15.5	5.75	8681	-0.0103
15.5	6.25	7140	-0.0179
15.5	6.75	5602	-0.0235
15.5	7.25	3889	-0.0366
15.5	7.75	2609	-0.0286

15.5	8.25	1694	-0.0414
15.5	8.75	922	-0.0375
15.5	9.25	586	-0.0560
15.5	9.75	146	-0.0152
15.5	10.25	104	-0.0156
16.5	2.75	281	0.0462
16.5	3.25	906	0.0799
16.5	3.75	2239	0.0467
16.5	4.25	3749	0.0463
16.5	4.75	5225	0.0299
16.5	5.25	6016	-0.0023
16.5	5.75	6186	0.0048
16.5	6.25	5735	-0.0138
16.5	6.75	4746	-0.0203
16.5	7.25	3542	-0.0374
16.5	7.75	2302	-0.0209
16.5	8.25	1611	-0.0395
16.5	8.75	1183	-0.0566
16.5	9.25	633	-0.0439
16.5	9.75	239	-0.0292
16.5	10.25	143	-0.0110
17.5	2.75	127	0.0502
17.5	3.25	451	0.0755
17.5	3.75	886	0.0461
17.5	4.25	1593	0.0649
17.5	4.75	2330	0.0276
17.5	5.25	3281	0.0166
17.5	5.75	3884	0.0042
17.5	6.25	3723	0.0044
17.5	6.75	3644	-0.0114
17.5	7.25	2596	-0.0085
17.5	7.75	1974	-0.0274
17.5	8.25	1537	-0.0228
17.5	8.75	1077	-0.0367
17.5	9.25	672	-0.0707
17.5	9.75	379	-0.0348
17.5	10.25	203	-0.0986
18.5	3.25	129	0.1304
18.5	3.75	383	0.0969
18.5	4.25	647	0.0681
18.5	4.75	1036	0.0548
18.5	5.25	1936	0.0430
18.5	5.75	2074	-0.0002
18.5	6.25	2358	0.0082
18.5	6.75	2452	0.0098
18.5	7.25	2000	-0.0105
18.5	7.75	1524	-0.0272
18.5	8.25	1227	-0.0380
18.5	8.75	978	-0.0653
18.5	9.25	694	-0.0538
18.5	9.75	405	-0.0352

18.5	10.25	343	-0.1288
18.5	10.75	123	-0.1024
19.5	3.75	177	0.0940
19.5	4.25	316	0.1014
19.5	4.75	492	0.0980
19.5	5.25	886	0.0817
19.5	5.75	1100	0.0124
19.5	6.25	1335	0.0212
19.5	6.75	1308	0.0085
19.5	7.25	1247	-0.0137
19.5	7.75	1077	-0.0216
19.5	8.25	941	-0.0179
19.5	8.75	928	-0.0537
19.5	9.25	568	-0.0168
19.5	9.75	442	-0.0389
19.5	10.25	237	-0.0810
19.5	10.75	148	-0.1186
20.5	4.25	138	0.1562
20.5	4.75	258	0.1480
20.5	5.25	382	0.0816
20.5	5.75	574	0.0526
20.5	6.25	662	0.0508
20.5	6.75	726	0.0263
20.5	7.25	800	-0.0160
20.5	7.75	636	0.0212
20.5	8.25	591	-0.0483
20.5	8.75	609	-0.0567
20.5	9.25	388	-0.0554
20.5	9.75	333	-0.0419
20.5	10.25	176	-0.1012
20.5	10.75	163	-0.0819
21.5	4.75	122	0.1478
21.5	5.25	214	0.0845
21.5	5.75	267	0.0661
21.5	6.25	427	0.0800
21.5	6.75	447	0.0837
21.5	7.25	438	0.0078
21.5	7.75	356	-0.0133
21.5	8.25	348	-0.0457
21.5	8.75	313	-0.0440
21.5	9.25	315	-0.0437
21.5	9.75	281	-0.0362
21.5	10.25	133	-0.0766
21.5	10.75	122	-0.0664
22.5	6.25	164	0.1243
22.5	6.75	203	0.0260
22.5	7.25	254	0.0351
22.5	7.75	163	-0.0236
22.5	8.25	229	-0.0040
22.5	8.75	196	-0.0413

22.5	9.25	176	-0.0602
22.5	9.75	182	-0.0684
22.5	10.25	115	-0.0704
23.5	7.25	151	0.1087
23.5	8.25	118	-0.0198
23.5	8.75	139	-0.0716
23.5	9.25	103	-0.0212
23.5	9.75	112	-0.0919

radiometer 2
V

0.5	0.75	2279	0.0735
0.5	1.25	10044	0.0203
0.5	1.75	12193	-0.0164
0.5	2.25	8765	-0.0360
0.5	2.75	5044	-0.0589
0.5	3.25	1585	-0.0639
0.5	3.75	838	-0.0552
0.5	4.25	232	-0.0634
1.5	0.75	2594	0.0907
1.5	1.25	14025	0.0496
1.5	1.75	20722	0.0125
1.5	2.25	18314	-0.0146
1.5	2.75	11704	-0.0432
1.5	3.25	6211	-0.0564
1.5	3.75	3197	-0.0563
1.5	4.25	1431	-0.0466
1.5	4.75	464	-0.0533
1.5	5.25	210	-0.1169
2.5	0.75	3218	0.1082
2.5	1.25	18864	0.0685
2.5	1.75	29716	0.0236
2.5	2.25	26915	-0.0115
2.5	2.75	18295	-0.0399
2.5	3.25	11698	-0.0547
2.5	3.75	5900	-0.0672
2.5	4.25	2995	-0.0776
2.5	4.75	1164	-0.0726
2.5	5.25	591	-0.0967
2.5	5.75	269	-0.1220
2.5	6.25	115	-0.0302
3.5	0.75	3998	0.1574
3.5	1.25	26036	0.0796
3.5	1.75	46659	0.0388
3.5	2.25	43758	-0.0038
3.5	2.75	29264	-0.0420
3.5	3.25	19087	-0.0589

3.5	3.75	10799	-0.0816
3.5	4.25	5615	-0.0919
3.5	4.75	2772	-0.0982
3.5	5.25	1245	-0.1108
3.5	5.75	549	-0.1525
3.5	6.25	200	-0.1271
4.5	0.75	4383	0.1585
4.5	1.25	36924	0.0789
4.5	1.75	76317	0.0406
4.5	2.25	70743	0.0052
4.5	2.75	45463	-0.0328
4.5	3.25	29832	-0.0580
4.5	3.75	17807	-0.0834
4.5	4.25	9760	-0.0874
4.5	4.75	5072	-0.0946
4.5	5.25	2350	-0.1232
4.5	5.75	1080	-0.1241
4.5	6.25	409	-0.1346
4.5	6.75	102	-0.0734
5.5	0.75	3030	0.1320
5.5	1.25	43942	0.0626
5.5	1.75	109311	0.0326
5.5	2.25	105268	0.0106
5.5	2.75	67244	-0.0192
5.5	3.25	42254	-0.0517
5.5	3.75	25780	-0.0749
5.5	4.25	14824	-0.0844
5.5	4.75	8130	-0.0899
5.5	5.25	3788	-0.0955
5.5	5.75	1682	-0.1199
5.5	6.25	789	-0.1146
5.5	6.75	325	-0.1018
5.5	7.25	128	-0.1196
6.5	0.75	1536	0.1369
6.5	1.25	34037	0.0737
6.5	1.75	126899	0.0341
6.5	2.25	143065	0.0092
6.5	2.75	88831	-0.0116
6.5	3.25	53336	-0.0393
6.5	3.75	33714	-0.0629
6.5	4.25	20487	-0.0778
6.5	4.75	12137	-0.0892
6.5	5.25	5943	-0.0952
6.5	5.75	2956	-0.1175
6.5	6.25	1152	-0.1408
6.5	6.75	667	-0.1058
6.5	7.25	187	-0.0997
7.5	0.75	471	0.2087
7.5	1.25	15026	0.1039
7.5	1.75	103177	0.0468

7.5	2.25	163641	0.0099
7.5	2.75	106026	0.0003
7.5	3.25	63968	-0.0251
7.5	3.75	40436	-0.0483
7.5	4.25	26738	-0.0710
7.5	4.75	15937	-0.0858
7.5	5.25	8907	-0.1078
7.5	5.75	4073	-0.1230
7.5	6.25	2100	-0.1363
7.5	6.75	874	-0.1212
7.5	7.25	371	-0.1550
7.5	7.75	119	-0.1577
8.5	1.25	3997	0.1143
8.5	1.75	52224	0.0659
8.5	2.25	136469	0.0270
8.5	2.75	115356	0.0116
8.5	3.25	71145	-0.0108
8.5	3.75	44134	-0.0359
8.5	4.25	30292	-0.0549
8.5	4.75	18675	-0.0835
8.5	5.25	11296	-0.1053
8.5	5.75	5982	-0.1246
8.5	6.25	3344	-0.1472
8.5	6.75	1903	-0.1518
8.5	7.25	728	-0.1650
8.5	7.75	208	-0.1638
9.5	1.25	893	0.1189
9.5	1.75	14840	0.0871
9.5	2.25	73984	0.0379
9.5	2.75	101587	0.0145
9.5	3.25	74129	0.0111
9.5	3.75	48219	-0.0148
9.5	4.25	33264	-0.0386
9.5	4.75	21233	-0.0596
9.5	5.25	12242	-0.0871
9.5	5.75	7281	-0.1036
9.5	6.25	4336	-0.1220
9.5	6.75	2490	-0.1009
9.5	7.25	1240	-0.1422
9.5	7.75	547	-0.1707
9.5	8.25	247	-0.1551
10.5	1.25	266	0.2222
10.5	1.75	3695	0.0993
10.5	2.25	25713	0.0525
10.5	2.75	57758	0.0180
10.5	3.25	64957	0.0185
10.5	3.75	47720	0.0028
10.5	4.25	34412	-0.0171
10.5	4.75	23294	-0.0425
10.5	5.25	14244	-0.0508
10.5	5.75	9312	-0.0709

10.5	6.25	5162	-0.0911
10.5	6.75	3014	-0.0975
10.5	7.25	1812	-0.0882
10.5	7.75	882	-0.1150
10.5	8.25	481	-0.1379
10.5	8.75	160	-0.2136
11.5	1.75	1176	0.1004
11.5	2.25	7279	0.0636
11.5	2.75	23423	0.0201
11.5	3.25	42973	0.0280
11.5	3.75	43165	0.0128
11.5	4.25	34657	-0.0053
11.5	4.75	23766	-0.0238
11.5	5.25	16498	-0.0376
11.5	5.75	10702	-0.0435
11.5	6.25	6653	-0.0602
11.5	6.75	4108	-0.0653
11.5	7.25	2408	-0.0854
11.5	7.75	1272	-0.0977
11.5	8.25	696	-0.0718
11.5	8.75	299	-0.1227
12.5	1.75	380	0.0876
12.5	2.25	2702	0.0662
12.5	2.75	10109	0.0265
12.5	3.25	20846	0.0227
12.5	3.75	29567	0.0148
12.5	4.25	29014	0.0040
12.5	4.75	23648	-0.0096
12.5	5.25	17593	-0.0193
12.5	5.75	10932	-0.0281
12.5	6.25	7582	-0.0474
12.5	6.75	4399	-0.0428
12.5	7.25	3055	-0.0520
12.5	7.75	1532	-0.0466
12.5	8.25	973	-0.0614
12.5	8.75	423	-0.0763
13.5	1.75	114	0.2256
13.5	2.25	960	0.1218
13.5	2.75	4176	0.0220
13.5	3.25	10313	0.0146
13.5	3.75	16853	0.0195
13.5	4.25	20573	0.0150
13.5	4.75	20182	0.0022
13.5	5.25	16085	-0.0118
13.5	5.75	11241	-0.0215
13.5	6.25	8003	-0.0407
13.5	6.75	5405	-0.0335
13.5	7.25	3647	-0.0406
13.5	7.75	1983	-0.0424
13.5	8.25	1067	-0.0597
13.5	8.75	610	-0.0488

13.5	9.25	246	-0.0366
14.5	2.25	324	0.1343
14.5	2.75	1557	0.0546
14.5	3.25	4889	0.0232
14.5	3.75	8796	0.0171
14.5	4.25	12894	0.0136
14.5	4.75	14252	-0.0009
14.5	5.25	12419	-0.0013
14.5	5.75	10549	-0.0084
14.5	6.25	7983	-0.0237
14.5	6.75	5224	-0.0308
14.5	7.25	3652	-0.0348
14.5	7.75	2299	-0.0394
14.5	8.25	1365	-0.0561
14.5	8.75	759	-0.0380
14.5	9.25	356	-0.0206
14.5	9.75	192	-0.0669
15.5	2.25	158	0.3077
15.5	2.75	589	0.0370
15.5	3.25	2032	0.0323
15.5	3.75	4499	0.0256
15.5	4.25	6603	0.0270
15.5	4.75	9057	0.0049
15.5	5.25	8814	-0.0024
15.5	5.75	8138	-0.0089
15.5	6.25	6896	-0.0207
15.5	6.75	5041	-0.0256
15.5	7.25	3875	-0.0250
15.5	7.75	2444	-0.0369
15.5	8.25	1508	-0.0584
15.5	8.75	876	-0.0486
15.5	9.25	448	-0.0396
15.5	9.75	253	-0.0893
15.5	10.25	109	-0.0403
16.5	2.75	217	-0.0043
16.5	3.25	870	0.0653
16.5	3.75	2203	0.0352
16.5	4.25	3292	0.0139
16.5	4.75	4485	0.0185
16.5	5.25	5537	-0.0034
16.5	5.75	5722	-0.0111
16.5	6.25	5319	-0.0092
16.5	6.75	4625	-0.0231
16.5	7.25	3393	-0.0122
16.5	7.75	2210	-0.0289
16.5	8.25	1550	-0.0503
16.5	8.75	943	-0.0654
16.5	9.25	589	-0.0170
16.5	9.75	221	-0.0387
16.5	10.25	182	0.0273

17.5	3.25	415	0.0803
17.5	3.75	906	0.0646
17.5	4.25	1705	0.0038
17.5	4.75	2228	0.0191
17.5	5.25	3244	0.0164
17.5	5.75	3438	-0.0088
17.5	6.25	3568	0.0031
17.5	6.75	3241	-0.0177
17.5	7.25	2784	-0.0102
17.5	7.75	2102	-0.0179
17.5	8.25	1492	-0.0097
17.5	8.75	954	-0.0766
17.5	9.25	578	-0.0460
17.5	9.75	318	-0.0161
17.5	10.25	243	-0.0722
18.5	3.25	191	0.0892
18.5	3.75	363	0.0819
18.5	4.25	815	0.0090
18.5	4.75	1029	0.0021
18.5	5.25	1640	0.0058
18.5	5.75	1924	0.0030
18.5	6.25	1967	0.0306
18.5	6.75	1826	-0.0013
18.5	7.25	1929	-0.0298
18.5	7.75	1575	-0.0154
18.5	8.25	1282	0.0029
18.5	8.75	1005	-0.0191
18.5	9.25	647	-0.0276
18.5	9.75	445	-0.0376
18.5	10.25	242	-0.0851
19.5	4.25	276	0.0642
19.5	4.75	456	-0.0084
19.5	5.25	798	0.0254
19.5	5.75	885	0.0191
19.5	6.25	1169	0.0176
19.5	6.75	1156	-0.0053
19.5	7.25	1068	-0.0300
19.5	7.75	1067	0.0144
19.5	8.25	781	0.0015
19.5	8.75	669	-0.0042
19.5	9.25	663	-0.0106
19.5	9.75	514	-0.0075
19.5	10.25	349	-0.0565
19.5	10.75	130	0.0182
20.5	4.25	108	-0.0139
20.5	4.75	210	0.0357
20.5	5.25	382	0.1235
20.5	5.75	400	0.0843
20.5	6.25	615	0.0126
20.5	6.75	600	0.0035
20.5	7.25	692	-0.0186

20.5	7.75	655	-0.0071
20.5	8.25	530	0.0171
20.5	8.75	481	0.0013
20.5	9.25	463	-0.0250
20.5	9.75	346	-0.0428
20.5	10.25	241	-0.0466
20.5	10.75	178	-0.0165
21.5	5.25	141	0.1349
21.5	5.75	171	0.1407
21.5	6.25	265	0.0379
21.5	6.75	315	-0.0310
21.5	7.25	337	-0.0423
21.5	7.75	311	0.0247
21.5	8.25	308	-0.0027
21.5	8.75	312	0.0301
21.5	9.25	241	-0.0385
21.5	9.75	217	-0.0440
21.5	10.25	161	-0.0646
21.5	10.75	145	-0.0410
22.5	6.25	130	0.1802
22.5	6.75	180	-0.0278
22.5	7.25	184	-0.0136
22.5	7.75	152	-0.0174
22.5	8.25	174	-0.0286
22.5	8.75	168	0.0391
22.5	9.25	166	-0.0296
22.5	9.75	110	-0.0864
22.5	10.25	131	-0.0962
23.5	6.75	102	0.0006
23.5	8.25	119	-0.0599
23.5	8.75	114	-0.0353

radiometer 2

H

0.5	0.75	2279	0.0087
0.5	1.25	10044	-0.0417
0.5	1.75	12193	-0.0527
0.5	2.25	8765	-0.0612
0.5	2.75	5044	-0.0646
0.5	3.25	1585	-0.0419
0.5	3.75	838	-0.0482
0.5	4.25	232	-0.0426
1.5	0.75	2594	0.0485
1.5	1.25	14025	0.0221
1.5	1.75	20722	0.0017
1.5	2.25	18314	-0.0119
1.5	2.75	11704	-0.0225

1.5	3.25	6211	-0.0124
1.5	3.75	3197	-0.0176
1.5	4.25	1431	-0.0082
1.5	4.75	464	0.0264
1.5	5.25	210	-0.0382
2.5	0.75	3218	0.0674
2.5	1.25	18864	0.0443
2.5	1.75	29716	0.0121
2.5	2.25	26915	-0.0064
2.5	2.75	18295	-0.0201
2.5	3.25	11698	-0.0191
2.5	3.75	5900	-0.0210
2.5	4.25	2995	-0.0118
2.5	4.75	1164	-0.0073
2.5	5.25	591	-0.0222
2.5	5.75	269	-0.0039
2.5	6.25	115	0.0114
3.5	0.75	3998	0.1114
3.5	1.25	26036	0.0584
3.5	1.75	46659	0.0218
3.5	2.25	43758	-0.0057
3.5	2.75	29264	-0.0293
3.5	3.25	19087	-0.0264
3.5	3.75	10799	-0.0278
3.5	4.25	5615	-0.0191
3.5	4.75	2772	-0.0120
3.5	5.25	1245	-0.0316
3.5	5.75	549	-0.0358
3.5	6.25	200	0.0047
4.5	0.75	4383	0.1534
4.5	1.25	36924	0.0635
4.5	1.75	76317	0.0229
4.5	2.25	70743	-0.0017
4.5	2.75	45463	-0.0288
4.5	3.25	29832	-0.0391
4.5	3.75	17807	-0.0423
4.5	4.25	9760	-0.0369
4.5	4.75	5072	-0.0103
4.5	5.25	2350	-0.0367
4.5	5.75	1080	-0.0234
4.5	6.25	409	0.0111
4.5	6.75	102	0.1038
5.5	0.75	3030	0.1757
5.5	1.25	43942	0.0626
5.5	1.75	109311	0.0262
5.5	2.25	105268	0.0010
5.5	2.75	67244	-0.0256
5.5	3.25	42254	-0.0471
5.5	3.75	25780	-0.0486
5.5	4.25	14824	-0.0448

5.5	4.75	8130	-0.0184
5.5	5.25	3788	-0.0069
5.5	5.75	1682	-0.0193
5.5	6.25	789	-0.0025
5.5	6.75	325	0.0374
5.5	7.25	128	0.0158
6.5	0.75	1536	0.1857
6.5	1.25	34037	0.0703
6.5	1.75	126899	0.0302
6.5	2.25	143065	0.0063
6.5	2.75	88831	-0.0239
6.5	3.25	53336	-0.0477
6.5	3.75	33714	-0.0526
6.5	4.25	20487	-0.0550
6.5	4.75	12137	-0.0402
6.5	5.25	5943	-0.0237
6.5	5.75	2956	-0.0237
6.5	6.25	1152	-0.0187
6.5	6.75	667	-0.0013
6.5	7.25	187	0.0187
7.5	0.75	471	0.2978
7.5	1.25	15026	0.1153
7.5	1.75	103177	0.0420
7.5	2.25	163641	0.0081
7.5	2.75	106026	-0.0122
7.5	3.25	63968	-0.0377
7.5	3.75	40436	-0.0511
7.5	4.25	26738	-0.0601
7.5	4.75	15937	-0.0558
7.5	5.25	8907	-0.0549
7.5	5.75	4073	-0.0568
7.5	6.25	2100	-0.0590
7.5	6.75	874	-0.0321
7.5	7.25	371	-0.0460
7.5	7.75	119	0.0073
8.5	1.25	3997	0.1850
8.5	1.75	52224	0.0689
8.5	2.25	136469	0.0256
8.5	2.75	115356	-0.0015
8.5	3.25	71145	-0.0281
8.5	3.75	44134	-0.0455
8.5	4.25	30292	-0.0529
8.5	4.75	18675	-0.0578
8.5	5.25	11296	-0.0579
8.5	5.75	5982	-0.0535
8.5	6.25	3344	-0.0776
8.5	6.75	1903	-0.0651
8.5	7.25	728	-0.0757
8.5	7.75	208	-0.0611
9.5	1.25	893	0.2673

9.5	1.75	14840	0.1060
9.5	2.25	73984	0.0394
9.5	2.75	101587	0.0080
9.5	3.25	74129	-0.0038
9.5	3.75	48219	-0.0291
9.5	4.25	33264	-0.0432
9.5	4.75	21233	-0.0490
9.5	5.25	12242	-0.0578
9.5	5.75	7281	-0.0530
9.5	6.25	4336	-0.0594
9.5	6.75	2490	-0.0413
9.5	7.25	1240	-0.0615
9.5	7.75	547	-0.0833
9.5	8.25	247	-0.0893
10.5	1.25	266	0.5416
10.5	1.75	3695	0.1220
10.5	2.25	25713	0.0606
10.5	2.75	57758	0.0212
10.5	3.25	64957	0.0053
10.5	3.75	47720	-0.0120
10.5	4.25	34412	-0.0254
10.5	4.75	23294	-0.0393
10.5	5.25	14244	-0.0412
10.5	5.75	9312	-0.0417
10.5	6.25	5162	-0.0531
10.5	6.75	3014	-0.0393
10.5	7.25	1812	-0.0477
10.5	7.75	882	-0.0467
10.5	8.25	481	-0.0707
10.5	8.75	160	-0.0912
11.5	1.75	1176	0.1218
11.5	2.25	7279	0.0657
11.5	2.75	23423	0.0288
11.5	3.25	42973	0.0219
11.5	3.75	43165	0.0028
11.5	4.25	34657	-0.0097
11.5	4.75	23766	-0.0252
11.5	5.25	16498	-0.0294
11.5	5.75	10702	-0.0297
11.5	6.25	6653	-0.0299
11.5	6.75	4108	-0.0289
11.5	7.25	2408	-0.0335
11.5	7.75	1272	-0.0462
11.5	8.25	696	-0.0408
11.5	8.75	299	-0.0695
12.5	1.75	380	0.1593
12.5	2.25	2702	0.0538
12.5	2.75	10109	0.0283
12.5	3.25	20846	0.0223
12.5	3.75	29567	0.0086
12.5	4.25	29014	0.0001

12.5	4.75	23648	-0.0092
12.5	5.25	17593	-0.0174
12.5	5.75	10932	-0.0222
12.5	6.25	7582	-0.0234
12.5	6.75	4399	-0.0224
12.5	7.25	3055	-0.0099
12.5	7.75	1532	-0.0160
12.5	8.25	973	-0.0326
12.5	8.75	423	-0.0322
13.5	1.75	114	0.1921
13.5	2.25	960	0.0431
13.5	2.75	4176	0.0256
13.5	3.25	10313	0.0157
13.5	3.75	16853	0.0189
13.5	4.25	20573	0.0086
13.5	4.75	20182	-0.0022
13.5	5.25	16085	-0.0101
13.5	5.75	11241	-0.0146
13.5	6.25	8003	-0.0144
13.5	6.75	5405	-0.0214
13.5	7.25	3647	-0.0132
13.5	7.75	1983	-0.0079
13.5	8.25	1067	-0.0197
13.5	8.75	610	-0.0057
13.5	9.25	246	-0.0656
14.5	2.25	324	0.0780
14.5	2.75	1557	0.0386
14.5	3.25	4889	0.0259
14.5	3.75	8796	0.0184
14.5	4.25	12894	0.0078
14.5	4.75	14252	0.0028
14.5	5.25	12419	-0.0028
14.5	5.75	10549	-0.0051
14.5	6.25	7983	-0.0175
14.5	6.75	5224	-0.0111
14.5	7.25	3652	-0.0037
14.5	7.75	2299	-0.0119
14.5	8.25	1365	-0.0383
14.5	8.75	759	-0.0405
14.5	9.25	356	-0.0037
14.5	9.75	192	-0.0428
15.5	2.25	158	0.1339
15.5	2.75	589	0.0381
15.5	3.25	2032	0.0370
15.5	3.75	4499	0.0222
15.5	4.25	6603	0.0217
15.5	4.75	9057	0.0072
15.5	5.25	8814	-0.0002
15.5	5.75	8138	-0.0038
15.5	6.25	6896	-0.0109
15.5	6.75	5041	-0.0051

15.5	7.25	3875	-0.0129
15.5	7.75	2444	-0.0244
15.5	8.25	1508	-0.0442
15.5	8.75	876	-0.0335
15.5	9.25	448	-0.0050
15.5	9.75	253	-0.0471
15.5	10.25	109	-0.0095
16.5	2.75	217	0.0453
16.5	3.25	870	0.0565
16.5	3.75	2203	0.0249
16.5	4.25	3292	0.0158
16.5	4.75	4485	0.0144
16.5	5.25	5537	0.0117
16.5	5.75	5722	-0.0030
16.5	6.25	5319	-0.0060
16.5	6.75	4625	-0.0087
16.5	7.25	3393	-0.0089
16.5	7.75	2210	-0.0287
16.5	8.25	1550	-0.0306
16.5	8.75	943	-0.0429
16.5	9.25	589	-0.0133
16.5	9.75	221	-0.0223
16.5	10.25	182	-0.0043
17.5	3.25	415	0.0694
17.5	3.75	906	0.0649
17.5	4.25	1705	0.0245
17.5	4.75	2228	0.0325
17.5	5.25	3244	0.0235
17.5	5.75	3438	-0.0161
17.5	6.25	3568	0.0094
17.5	6.75	3241	-0.0105
17.5	7.25	2784	-0.0141
17.5	7.75	2102	-0.0168
17.5	8.25	1492	-0.0041
17.5	8.75	954	-0.0602
17.5	9.25	578	-0.0181
17.5	9.75	318	-0.0308
17.5	10.25	243	-0.0194
18.5	3.25	191	0.0735
18.5	3.75	363	0.0700
18.5	4.25	815	0.0324
18.5	4.75	1029	0.0327
18.5	5.25	1640	0.0095
18.5	5.75	1924	0.0010
18.5	6.25	1967	0.0169
18.5	6.75	1826	0.0053
18.5	7.25	1929	-0.0135
18.5	7.75	1575	-0.0067
18.5	8.25	1282	0.0148
18.5	8.75	1005	-0.0283
18.5	9.25	647	-0.0183

18.5	9.75	445	-0.0448
18.5	10.25	242	-0.0809
19.5	4.25	276	0.0917
19.5	4.75	456	0.0417
19.5	5.25	798	0.0690
19.5	5.75	885	0.0041
19.5	6.25	1169	0.0083
19.5	6.75	1156	0.0027
19.5	7.25	1068	-0.0138
19.5	7.75	1067	0.0099
19.5	8.25	781	0.0221
19.5	8.75	669	0.0080
19.5	9.25	663	-0.0143
19.5	9.75	514	-0.0550
19.5	10.25	349	-0.0677
19.5	10.75	130	-0.0086
20.5	4.25	108	0.0733
20.5	4.75	210	0.0587
20.5	5.25	382	0.1231
20.5	5.75	400	0.0678
20.5	6.25	615	0.0218
20.5	6.75	600	-0.0060
20.5	7.25	692	0.0128
20.5	7.75	655	0.0139
20.5	8.25	530	-0.0000
20.5	8.75	481	-0.0173
20.5	9.25	463	-0.0299
20.5	9.75	346	-0.0540
20.5	10.25	241	-0.0181
20.5	10.75	178	0.0109
21.5	5.25	141	0.1647
21.5	5.75	171	0.0639
21.5	6.25	265	0.0540
21.5	6.75	315	0.0168
21.5	7.25	337	-0.0065
21.5	7.75	311	0.0055
21.5	8.25	308	-0.0127
21.5	8.75	312	0.0143
21.5	9.25	241	-0.0091
21.5	9.75	217	-0.0545
21.5	10.25	161	-0.0719
21.5	10.75	145	-0.0192
22.5	6.25	130	0.1926
22.5	6.75	180	-0.0112
22.5	7.25	184	0.0133
22.5	7.75	152	-0.0309
22.5	8.25	174	-0.0564
22.5	8.75	168	0.0201
22.5	9.25	166	0.0053
22.5	9.75	110	-0.0277

22.5	10.25	131	-0.0854
23.5	6.75	102	0.0251
23.5	8.25	119	-0.0628
23.5	8.75	114	-0.0298

radiometer 3
V

0.5	0.75	1710	0.0708
0.5	1.25	9757	0.0240
0.5	1.75	10806	-0.0198
0.5	2.25	7128	-0.0509
0.5	2.75	4007	-0.0655
0.5	3.25	1138	-0.0682
0.5	3.75	498	-0.0996
0.5	4.25	103	-0.0759
1.5	0.75	2527	0.0995
1.5	1.25	15314	0.0383
1.5	1.75	22122	0.0145
1.5	2.25	18900	-0.0080
1.5	2.75	12751	-0.0310
1.5	3.25	5903	-0.0343
1.5	3.75	2978	-0.0507
1.5	4.25	1081	-0.0571
1.5	4.75	503	-0.0716
1.5	5.25	129	-0.1073
2.5	0.75	3187	0.1342
2.5	1.25	18992	0.0578
2.5	1.75	30613	0.0235
2.5	2.25	28311	-0.0057
2.5	2.75	19586	-0.0272
2.5	3.25	11203	-0.0435
2.5	3.75	6241	-0.0477
2.5	4.25	3330	-0.0843
2.5	4.75	1387	-0.0928
2.5	5.25	622	-0.0820
2.5	5.75	296	-0.1305
3.5	0.75	3748	0.1609
3.5	1.25	23975	0.0711
3.5	1.75	45803	0.0293
3.5	2.25	42847	-0.0002
3.5	2.75	29014	-0.0324
3.5	3.25	18270	-0.0489
3.5	3.75	10934	-0.0688
3.5	4.25	6126	-0.0714
3.5	4.75	2961	-0.0789
3.5	5.25	1253	-0.0872
3.5	5.75	656	-0.1313

3.5	6.25	206	−0.1408
4.5	0.75	3585	0.1679
4.5	1.25	32818	0.0736
4.5	1.75	68666	0.0394
4.5	2.25	64092	0.0094
4.5	2.75	41955	−0.0289
4.5	3.25	27427	−0.0454
4.5	3.75	17265	−0.0748
4.5	4.25	10370	−0.0844
4.5	4.75	4993	−0.1067
4.5	5.25	2240	−0.1046
4.5	5.75	1124	−0.1009
4.5	6.25	485	−0.1469
4.5	6.75	129	−0.1365
5.5	0.75	2518	0.1348
5.5	1.25	39527	0.0762
5.5	1.75	99116	0.0336
5.5	2.25	95644	0.0102
5.5	2.75	61240	−0.0176
5.5	3.25	37749	−0.0419
5.5	3.75	24236	−0.0692
5.5	4.25	14861	−0.0869
5.5	4.75	7657	−0.1010
5.5	5.25	3684	−0.1025
5.5	5.75	1881	−0.1204
5.5	6.25	741	−0.1408
5.5	6.75	325	−0.1254
5.5	7.25	127	−0.1256
6.5	0.75	1067	0.1555
6.5	1.25	33118	0.0862
6.5	1.75	120611	0.0400
6.5	2.25	136348	0.0098
6.5	2.75	84264	−0.0055
6.5	3.25	49286	−0.0412
6.5	3.75	30478	−0.0591
6.5	4.25	19678	−0.0850
6.5	4.75	11341	−0.1015
6.5	5.25	5626	−0.1133
6.5	5.75	2835	−0.1335
6.5	6.25	1273	−0.1480
6.5	6.75	507	−0.1765
6.5	7.25	192	−0.1300
7.5	0.75	281	0.1851
7.5	1.25	14056	0.0985
7.5	1.75	100754	0.0591
7.5	2.25	157006	0.0151
7.5	2.75	102730	0.0054
7.5	3.25	59953	−0.0250
7.5	3.75	36992	−0.0543
7.5	4.25	24048	−0.0823

7.5	4.75	14629	-0.1002
7.5	5.25	8294	-0.1145
7.5	5.75	4264	-0.1506
7.5	6.25	2024	-0.1531
7.5	6.75	889	-0.1441
7.5	7.25	394	-0.1571
7.5	7.75	114	-0.1458
8.5	1.25	4191	0.1180
8.5	1.75	51197	0.0691
8.5	2.25	133973	0.0291
8.5	2.75	112961	0.0162
8.5	3.25	69102	-0.0066
8.5	3.75	42910	-0.0440
8.5	4.25	27531	-0.0744
8.5	4.75	18044	-0.0934
8.5	5.25	10370	-0.1251
8.5	5.75	5467	-0.1490
8.5	6.25	2936	-0.1532
8.5	6.75	1696	-0.1827
8.5	7.25	780	-0.1740
8.5	7.75	364	-0.1936
9.5	1.25	729	0.1080
9.5	1.75	15370	0.0916
9.5	2.25	73050	0.0384
9.5	2.75	102061	0.0252
9.5	3.25	75012	0.0154
9.5	3.75	47046	-0.0224
9.5	4.25	32625	-0.0573
9.5	4.75	20933	-0.0746
9.5	5.25	12168	-0.0996
9.5	5.75	7238	-0.1204
9.5	6.25	3730	-0.1459
9.5	6.75	2394	-0.1505
9.5	7.25	1283	-0.1673
9.5	7.75	652	-0.1841
9.5	8.25	257	-0.1860
10.5	1.25	187	0.2184
10.5	1.75	3717	0.0833
10.5	2.25	25199	0.0535
10.5	2.75	58919	0.0322
10.5	3.25	65750	0.0275
10.5	3.75	49328	0.0018
10.5	4.25	35095	-0.0309
10.5	4.75	22693	-0.0559
10.5	5.25	14174	-0.0731
10.5	5.75	8860	-0.0953
10.5	6.25	5096	-0.0989
10.5	6.75	3148	-0.1184
10.5	7.25	1878	-0.1457
10.5	7.75	1005	-0.1501
10.5	8.25	405	-0.1584

10.5	8.75	152	-0.2389
11.5	1.75	958	0.1284
11.5	2.25	7133	0.0458
11.5	2.75	23069	0.0374
11.5	3.25	41687	0.0399
11.5	3.75	42450	0.0200
11.5	4.25	33501	-0.0094
11.5	4.75	23546	-0.0389
11.5	5.25	16170	-0.0471
11.5	5.75	10272	-0.0615
11.5	6.25	6737	-0.0722
11.5	6.75	3752	-0.0877
11.5	7.25	2233	-0.1004
11.5	7.75	1255	-0.0985
11.5	8.25	547	-0.1267
11.5	8.75	236	-0.1486
12.5	1.75	284	-0.0501
12.5	2.25	2667	0.0647
12.5	2.75	9583	0.0276
12.5	3.25	20346	0.0365
12.5	3.75	28349	0.0285
12.5	4.25	29182	0.0155
12.5	4.75	23430	-0.0132
12.5	5.25	17799	-0.0322
12.5	5.75	10852	-0.0443
12.5	6.25	7470	-0.0526
12.5	6.75	4968	-0.0629
12.5	7.25	2962	-0.0744
12.5	7.75	1484	-0.0644
12.5	8.25	803	-0.0922
12.5	8.75	369	-0.1041
12.5	9.25	145	-0.1046
13.5	1.75	116	0.0321
13.5	2.25	991	0.1040
13.5	2.75	4240	0.0598
13.5	3.25	9845	0.0310
13.5	3.75	16258	0.0305
13.5	4.25	20441	0.0205
13.5	4.75	19473	-0.0031
13.5	5.25	15666	-0.0229
13.5	5.75	10985	-0.0277
13.5	6.25	7441	-0.0337
13.5	6.75	5658	-0.0517
13.5	7.25	3404	-0.0602
13.5	7.75	2014	-0.0732
13.5	8.25	1167	-0.0873
13.5	8.75	514	-0.0695
13.5	9.25	143	-0.0634
14.5	2.25	281	0.0331
14.5	2.75	1606	0.0484

14.5	3.25	4591	0.0375
14.5	3.75	8431	0.0363
14.5	4.25	12489	0.0178
14.5	4.75	13674	0.0078
14.5	5.25	12800	-0.0089
14.5	5.75	10328	-0.0161
14.5	6.25	7113	-0.0231
14.5	6.75	5676	-0.0365
14.5	7.25	3482	-0.0493
14.5	7.75	1938	-0.0911
14.5	8.25	1450	-0.0541
14.5	8.75	741	-0.0677
14.5	9.25	305	-0.1251
14.5	9.75	138	-0.0778
15.5	2.75	551	0.0709
15.5	3.25	2151	0.0571
15.5	3.75	3987	0.0463
15.5	4.25	6639	0.0379
15.5	4.75	8677	0.0065
15.5	5.25	8805	0.0005
15.5	5.75	8611	-0.0065
15.5	6.25	6508	-0.0189
15.5	6.75	5065	-0.0373
15.5	7.25	3638	-0.0447
15.5	7.75	2624	-0.0279
15.5	8.25	1802	-0.0618
15.5	8.75	957	-0.0552
15.5	9.25	386	-0.0473
15.5	9.75	162	-0.0921
16.5	2.75	177	0.0375
16.5	3.25	819	0.0979
16.5	3.75	1918	0.0677
16.5	4.25	3209	0.0449
16.5	4.75	4741	0.0250
16.5	5.25	5579	0.0138
16.5	5.75	5654	-0.0091
16.5	6.25	4468	-0.0082
16.5	6.75	4007	-0.0338
16.5	7.25	3526	-0.0456
16.5	7.75	2407	-0.0336
16.5	8.25	1661	-0.0685
16.5	8.75	978	-0.0414
16.5	9.25	580	-0.0426
16.5	9.75	374	-0.1156
16.5	10.25	151	-0.1629
16.5	10.75	112	-0.1487
17.5	3.25	323	0.0755
17.5	3.75	827	0.0604
17.5	4.25	1360	0.0381
17.5	4.75	2414	0.0485
17.5	5.25	2912	0.0316

17.5	5.75	3348	0.0119
17.5	6.25	3065	0.0031
17.5	6.75	3043	-0.0307
17.5	7.25	2887	-0.0242
17.5	7.75	1803	-0.0393
17.5	8.25	1506	-0.0506
17.5	8.75	1043	-0.0462
17.5	9.25	595	-0.0637
17.5	9.75	396	-0.0531
17.5	10.25	225	-0.0427
17.5	10.75	159	-0.1724
18.5	3.25	135	0.1293
18.5	3.75	222	0.0620
18.5	4.25	614	0.0514
18.5	4.75	1097	0.0517
18.5	5.25	1588	0.0557
18.5	5.75	1749	0.0183
18.5	6.25	1834	0.0160
18.5	6.75	1868	-0.0077
18.5	7.25	1942	-0.0193
18.5	7.75	1694	-0.0183
18.5	8.25	1264	-0.0388
18.5	8.75	864	-0.0384
18.5	9.25	625	-0.0760
18.5	9.75	507	-0.0615
18.5	10.25	178	-0.0534
18.5	10.75	133	-0.0903
19.5	3.75	101	0.1570
19.5	4.25	184	0.0399
19.5	4.75	449	0.0571
19.5	5.25	616	0.0569
19.5	5.75	971	0.0317
19.5	6.25	1100	0.0183
19.5	6.75	1182	-0.0067
19.5	7.25	1159	-0.0060
19.5	7.75	1033	-0.0104
19.5	8.25	889	-0.0391
19.5	8.75	793	-0.0265
19.5	9.25	562	-0.0576
19.5	9.75	390	-0.0305
19.5	10.25	201	0.0011
19.5	10.75	115	-0.0225
20.5	4.75	187	0.0692
20.5	5.25	253	0.1018
20.5	5.75	499	0.0374
20.5	6.25	602	0.0281
20.5	6.75	604	0.0593
20.5	7.25	691	0.0010
20.5	7.75	693	-0.0181
20.5	8.25	657	-0.0386
20.5	8.75	530	-0.0404

20.5	9.25	490	-0.0262
20.5	9.75	310	-0.0217
20.5	10.25	158	-0.0207
21.5	4.75	104	0.1765
21.5	5.25	154	0.1004
21.5	5.75	201	0.0932
21.5	6.25	285	0.0660
21.5	6.75	286	0.0735
21.5	7.25	356	-0.0362
21.5	7.75	361	-0.0124
21.5	8.25	333	-0.1064
21.5	8.75	335	0.0116
21.5	9.25	290	-0.0036
21.5	9.75	242	-0.0184
21.5	10.25	135	-0.0654
22.5	6.25	149	0.1240
22.5	6.75	181	0.0481
22.5	7.25	248	0.0116
22.5	7.75	148	-0.0087
22.5	8.25	172	0.0071
22.5	8.75	177	0.0262
22.5	9.25	220	-0.0693
22.5	9.75	198	-0.0812
22.5	10.25	125	-0.1306
23.5	6.75	114	-0.0053
23.5	7.25	116	-0.0689
23.5	7.75	112	-0.0284
23.5	9.25	137	0.0479

radiometer 3
H

0.5	0.75	1710	-0.0290
0.5	1.25	9757	-0.0405
0.5	1.75	10806	-0.0499
0.5	2.25	7128	-0.0593
0.5	2.75	4007	-0.0581
0.5	3.25	1138	-0.0233
0.5	3.75	498	-0.0325
0.5	4.25	103	0.0234
1.5	0.75	2527	0.0217
1.5	1.25	15314	0.0027
1.5	1.75	22122	-0.0005
1.5	2.25	18900	-0.0092
1.5	2.75	12751	-0.0097
1.5	3.25	5903	0.0086
1.5	3.75	2978	0.0014
1.5	4.25	1081	0.0308

1.5	4.75	503	0.0851
1.5	5.25	129	0.0407
2.5	0.75	3187	0.0462
2.5	1.25	18992	0.0159
2.5	1.75	30613	0.0100
2.5	2.25	28311	-0.0041
2.5	2.75	19586	-0.0020
2.5	3.25	11203	0.0038
2.5	3.75	6241	0.0030
2.5	4.25	3330	0.0185
2.5	4.75	1387	0.0373
2.5	5.25	622	0.0198
2.5	5.75	296	-0.0112
3.5	0.75	3748	0.0652
3.5	1.25	23975	0.0207
3.5	1.75	45803	0.0070
3.5	2.25	42847	-0.0023
3.5	2.75	29014	-0.0111
3.5	3.25	18270	-0.0060
3.5	3.75	10934	0.0088
3.5	4.25	6126	0.0199
3.5	4.75	2961	0.0499
3.5	5.25	1253	0.0446
3.5	5.75	656	0.0122
3.5	6.25	206	0.0177
4.5	0.75	3585	0.0928
4.5	1.25	32818	0.0217
4.5	1.75	68666	0.0098
4.5	2.25	64092	-0.0046
4.5	2.75	41955	-0.0202
4.5	3.25	27427	-0.0208
4.5	3.75	17265	-0.0060
4.5	4.25	10370	0.0189
4.5	4.75	4993	0.0404
4.5	5.25	2240	0.0594
4.5	5.75	1124	0.0540
4.5	6.25	485	0.0740
4.5	6.75	129	0.0644
5.5	0.75	2518	0.1134
5.5	1.25	39527	0.0350
5.5	1.75	99116	0.0133
5.5	2.25	95644	-0.0001
5.5	2.75	61240	-0.0247
5.5	3.25	37749	-0.0330
5.5	3.75	24236	-0.0239
5.5	4.25	14861	0.0002
5.5	4.75	7657	0.0231
5.5	5.25	3684	0.0308
5.5	5.75	1881	0.0642
5.5	6.25	741	0.0420

5.5	6.75	325	0.0918
5.5	7.25	127	0.1758
6.5	0.75	1067	0.1519
6.5	1.25	33118	0.0529
6.5	1.75	120611	0.0262
6.5	2.25	136348	0.0034
6.5	2.75	84264	-0.0191
6.5	3.25	49286	-0.0415
6.5	3.75	30478	-0.0407
6.5	4.25	19678	-0.0280
6.5	4.75	11341	-0.0103
6.5	5.25	5626	0.0087
6.5	5.75	2835	0.0177
6.5	6.25	1273	0.0018
6.5	6.75	507	0.0182
6.5	7.25	192	0.1024
7.5	0.75	281	0.1282
7.5	1.25	14056	0.0766
7.5	1.75	100754	0.0418
7.5	2.25	157006	0.0134
7.5	2.75	102730	-0.0077
7.5	3.25	59953	-0.0400
7.5	3.75	36992	-0.0501
7.5	4.25	24048	-0.0427
7.5	4.75	14629	-0.0296
7.5	5.25	8294	-0.0166
7.5	5.75	4264	-0.0125
7.5	6.25	2024	-0.0207
7.5	6.75	889	0.0148
7.5	7.25	394	0.0092
7.5	7.75	114	0.0149
8.5	1.25	4191	0.1062
8.5	1.75	51197	0.0535
8.5	2.25	133973	0.0280
8.5	2.75	112961	0.0009
8.5	3.25	69102	-0.0268
8.5	3.75	42910	-0.0530
8.5	4.25	27531	-0.0609
8.5	4.75	18044	-0.0567
8.5	5.25	10370	-0.0487
8.5	5.75	5467	-0.0346
8.5	6.25	2936	-0.0355
8.5	6.75	1696	-0.0354
8.5	7.25	780	-0.0160
8.5	7.75	364	0.0213
9.5	1.25	729	0.1346
9.5	1.75	15370	0.0780
9.5	2.25	73050	0.0351
9.5	2.75	102061	0.0177
9.5	3.25	75012	-0.0073

9.5	3.75	47046	-0.0438
9.5	4.25	32625	-0.0573
9.5	4.75	20933	-0.0549
9.5	5.25	12168	-0.0539
9.5	5.75	7238	-0.0430
9.5	6.25	3730	-0.0409
9.5	6.75	2394	-0.0254
9.5	7.25	1283	-0.0232
9.5	7.75	652	-0.0075
9.5	8.25	257	0.0034
10.5	1.25	187	0.2233
10.5	1.75	3717	0.0738
10.5	2.25	25199	0.0468
10.5	2.75	58919	0.0290
10.5	3.25	65750	0.0144
10.5	3.75	49328	-0.0187
10.5	4.25	35095	-0.0365
10.5	4.75	22693	-0.0447
10.5	5.25	14174	-0.0488
10.5	5.75	8860	-0.0384
10.5	6.25	5096	-0.0398
10.5	6.75	3148	-0.0292
10.5	7.25	1878	-0.0180
10.5	7.75	1005	-0.0624
10.5	8.25	405	-0.0496
10.5	8.75	152	-0.0848
11.5	1.75	958	0.1041
11.5	2.25	7133	0.0449
11.5	2.75	23069	0.0315
11.5	3.25	41687	0.0263
11.5	3.75	42450	0.0048
11.5	4.25	33501	-0.0184
11.5	4.75	23546	-0.0307
11.5	5.25	16170	-0.0343
11.5	5.75	10272	-0.0231
11.5	6.25	6737	-0.0258
11.5	6.75	3752	-0.0228
11.5	7.25	2233	-0.0060
11.5	7.75	1255	-0.0387
11.5	8.25	547	-0.0265
11.5	8.75	236	-0.0253
12.5	1.75	284	0.0391
12.5	2.25	2667	0.0530
12.5	2.75	9583	0.0341
12.5	3.25	20346	0.0256
12.5	3.75	28349	0.0077
12.5	4.25	29182	0.0017
12.5	4.75	23430	-0.0115
12.5	5.25	17799	-0.0177
12.5	5.75	10852	-0.0155
12.5	6.25	7470	-0.0178

12.5	6.75	4968	-0.0188
12.5	7.25	2962	-0.0165
12.5	7.75	1484	-0.0096
12.5	8.25	803	-0.0132
12.5	8.75	369	-0.0083
12.5	9.25	145	0.0191
13.5	1.75	116	0.0616
13.5	2.25	991	0.0847
13.5	2.75	4240	0.0424
13.5	3.25	9845	0.0230
13.5	3.75	16258	0.0112
13.5	4.25	20441	0.0106
13.5	4.75	19473	-0.0087
13.5	5.25	15666	-0.0107
13.5	5.75	10985	-0.0100
13.5	6.25	7441	-0.0088
13.5	6.75	5658	-0.0142
13.5	7.25	3404	-0.0135
13.5	7.75	2014	-0.0079
13.5	8.25	1167	-0.0322
13.5	8.75	514	-0.0073
13.5	9.25	143	0.0268
14.5	2.25	281	0.0636
14.5	2.75	1606	0.0494
14.5	3.25	4591	0.0270
14.5	3.75	8431	0.0230
14.5	4.25	12489	0.0142
14.5	4.75	13674	-0.0057
14.5	5.25	12800	-0.0042
14.5	5.75	10328	-0.0092
14.5	6.25	7113	-0.0158
14.5	6.75	5676	-0.0119
14.5	7.25	3482	-0.0105
14.5	7.75	1938	-0.0324
14.5	8.25	1450	-0.0128
14.5	8.75	741	0.0089
14.5	9.25	305	-0.0313
14.5	9.75	138	-0.0075
15.5	2.75	551	0.0357
15.5	3.25	2151	0.0289
15.5	3.75	3987	0.0337
15.5	4.25	6639	0.0253
15.5	4.75	8677	0.0075
15.5	5.25	8805	0.0032
15.5	5.75	8611	-0.0058
15.5	6.25	6508	-0.0133
15.5	6.75	5065	-0.0230
15.5	7.25	3638	-0.0182
15.5	7.75	2624	-0.0060
15.5	8.25	1802	-0.0200
15.5	8.75	957	-0.0127

15.5	9.25	386	-0.0243
15.5	9.75	162	-0.0174
16.5	2.75	177	0.0713
16.5	3.25	819	0.0644
16.5	3.75	1918	0.0375
16.5	4.25	3209	0.0342
16.5	4.75	4741	0.0158
16.5	5.25	5579	0.0156
16.5	5.75	5654	-0.0006
16.5	6.25	4468	-0.0069
16.5	6.75	4007	-0.0250
16.5	7.25	3526	-0.0276
16.5	7.75	2407	-0.0190
16.5	8.25	1661	-0.0237
16.5	8.75	978	-0.0152
16.5	9.25	580	-0.0236
16.5	9.75	374	-0.0550
16.5	10.25	151	-0.1276
16.5	10.75	112	-0.1324
17.5	3.25	323	0.0537
17.5	3.75	827	0.0409
17.5	4.25	1360	0.0386
17.5	4.75	2414	0.0462
17.5	5.25	2912	0.0304
17.5	5.75	3348	0.0202
17.5	6.25	3065	0.0017
17.5	6.75	3043	-0.0317
17.5	7.25	2887	-0.0180
17.5	7.75	1803	-0.0362
17.5	8.25	1506	-0.0350
17.5	8.75	1043	-0.0271
17.5	9.25	595	-0.0252
17.5	9.75	396	-0.0140
17.5	10.25	225	-0.0647
17.5	10.75	159	-0.1147
18.5	3.25	135	0.1054
18.5	3.75	222	0.0128
18.5	4.25	614	0.0629
18.5	4.75	1097	0.0787
18.5	5.25	1588	0.0430
18.5	5.75	1749	0.0088
18.5	6.25	1834	0.0094
18.5	6.75	1868	-0.0074
18.5	7.25	1942	-0.0246
18.5	7.75	1694	-0.0034
18.5	8.25	1264	-0.0278
18.5	8.75	864	0.0021
18.5	9.25	625	-0.0265
18.5	9.75	507	-0.0633
18.5	10.25	178	-0.0133
18.5	10.75	133	-0.0339

19.5	3.75	101	0.1256
19.5	4.25	184	0.0483
19.5	4.75	449	0.1107
19.5	5.25	616	0.0662
19.5	5.75	971	0.0363
19.5	6.25	1100	0.0140
19.5	6.75	1182	0.0133
19.5	7.25	1159	-0.0034
19.5	7.75	1033	-0.0026
19.5	8.25	889	-0.0379
19.5	8.75	793	-0.0318
19.5	9.25	562	-0.0411
19.5	9.75	390	-0.0304
19.5	10.25	201	-0.0111
19.5	10.75	115	-0.0192
20.5	4.75	187	0.0912
20.5	5.25	253	0.0972
20.5	5.75	499	0.0289
20.5	6.25	602	0.0123
20.5	6.75	604	0.0307
20.5	7.25	691	0.0160
20.5	7.75	693	0.0015
20.5	8.25	657	-0.0240
20.5	8.75	530	0.0025
20.5	9.25	490	-0.0495
20.5	9.75	310	-0.0079
20.5	10.25	158	-0.0069
21.5	4.75	104	0.1684
21.5	5.25	154	0.1318
21.5	5.75	201	0.1056
21.5	6.25	285	0.0550
21.5	6.75	286	0.0268
21.5	7.25	356	-0.0242
21.5	7.75	361	-0.0189
21.5	8.25	333	-0.0504
21.5	8.75	335	0.0428
21.5	9.25	290	-0.0229
21.5	9.75	242	-0.0290
21.5	10.25	135	-0.0674
22.5	6.25	149	0.0672
22.5	6.75	181	0.0244
22.5	7.25	248	0.0187
22.5	7.75	148	-0.0051
22.5	8.25	172	-0.0230
22.5	8.75	177	0.0208
22.5	9.25	220	-0.0304
22.5	9.75	198	-0.0640
22.5	10.25	125	-0.0725
23.5	6.75	114	0.0463

23.5	7.25	116	−0.0158
23.5	7.75	112	−0.0223
23.5	9.25	137	−0.0234